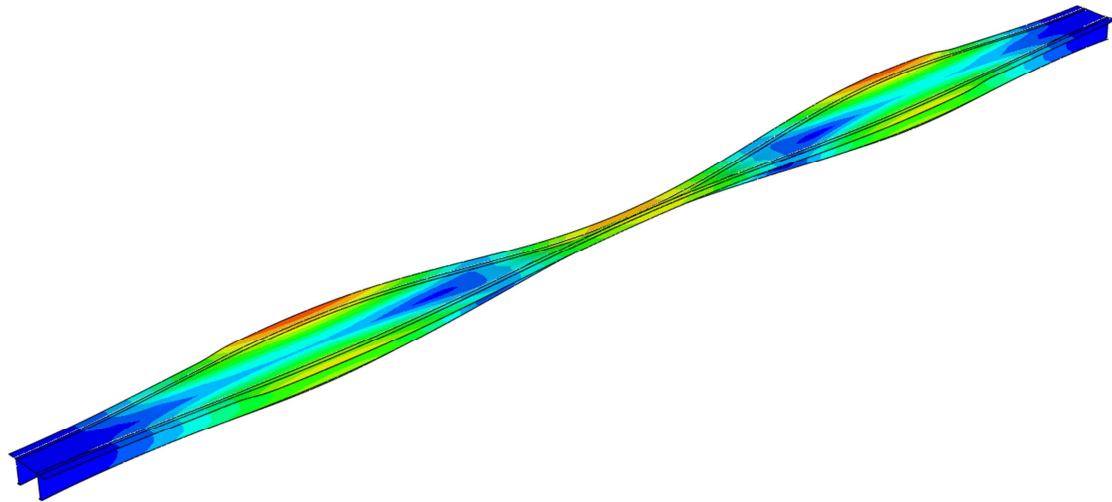


CHALMERS



Towards Pedestrian Graphene Bridges

A dynamic analysis and evaluation

Master's Thesis in the Master's Programme in Structural Engineering and Building Technology

JESÚS ARMESTO BARROS
ANDRÉS SERENA GÓMEZ

Department of Civil and Environmental Engineering
Division of *Structural Engineering*
CHALMERS UNIVERSITY OF TECHNOLOGY
Göteborg, Sweden, 2015
Report No. 2015:118

MASTER'S THESIS 2015:118

Towards Pedestrian Graphene Bridges

A dynamic analysis and evaluation

*Master's Thesis in the Master's Programme in
Structural Engineering and Building Technology*

JESÚS ARMESTO BARROS
ANDRÉS SERENA GÓMEZ

Department of Civil and Environmental Engineering
Division of *Structural Engineering*
CHALMERS UNIVERSITY OF TECHNOLOGY
Göteborg, Sweden 2015

Towards Pedestrian Graphene Bridges. A dynamic analysis and evaluation
*Master's Thesis in the Master's Programme in Structural Engineering and Building
Technology*

JESÚS ARMESTO BARROS

ANDRÉS SERENA GÓMEZ

© JESÚS ARMESTO BARROS, ANDRÉS SERENA GÓMEZ, 2015

Examensarbete 2015:118

Department of Civil and Environmental Engineering

Division of *Structural Engineering*

Chalmers University of Technology

SE-412 96 Göteborg

Sweden

Telephone: + 46 (0)31-772 1000

Cover: Vibration mode of a graphene based bridge.

Chalmers Reproservice / Department of Civil and Environmental Engineering
Göteborg, Sweden 2015

Towards Pedestrian Graphene Bridges. A dynamic analysis and evaluation

Master's Thesis in the Master's Programme in Structural Engineering and Building Technology

JESÚS ARMESTO BARROS

ANDRÉS SERENA GÓMEZ

Department of Civil and Environmental Engineering

Division of *Structural Engineering*

Chalmers University of Technology

ABSTRACT

The use of graphene in pedestrian bridges, where aesthetics and design have an important role, will lead to a revolution in the field. The strength and lightness of graphene will broaden the possibilities in span lengths and slenderness. Together with these possibilities dynamic problems may arise.

This project reviewed the dynamic problems of pedestrian bridges with the intention to check the suitability of graphene on them. This material is known for its lightness, and that may cause a difference in the dynamic behaviour.

72 different bridge models with two different cross-sections and four material combinations were analysed to check their dynamic performance. They were designed for ULS and SLS, and then, their dynamic comfort was checked. These cases combined the use of traditional materials (steel and concrete) and high-performance innovative and futuristic materials (respectively FRP and graphene).

The results showed that graphene performed better than the other materials for short bridges, due to its higher stiffness. However, it also suffered dynamic problems in longer bridges. Frequencies followed clear patterns depending on the length of the bridges, getting lower values when span length increases. Lateral frequencies rose when width was increased, meanwhile vertical frequencies did not show any special trend dependant on width.

The accelerations were calculated according to the latest Guidelines and Eurocodes. The results could not be evaluated as a trend due to the limitations of the load definitions, just defined by the cases where the eigenvalues were in range. However, general material and geometry observations were concluded, such as dependency on damping of the material and influence of the load value.

In conclusion, the evaluation highlighted how graphene had a great dynamic performance and the geometry and material influenced in the dynamic behaviour.

Key words: Bridge, Pedestrian Bridge, Footbridge, Ultra-lightweight Bridge, Lightweight Bridge, Dynamic Analysis, Pedestrian Loading, Pedestrian Load Model, Graphene, FRP, Steel, Concrete, Resonance, Comfort Criteria, Vibrations, Bridge, Finite Element, FEM, Python

Table of contents

Abstract	I
Table of contents	III
Preface	VII
Notations	IX
Abbreviations	X
1 Introduction	1
1.1 Purpose.....	1
1.2 Objectives.....	2
1.3 General Layout.....	3
2 Structural dynamics of footbridges	5
2.1 Structural dynamics theory	5
2.1.1 Equation of motion	5
2.1.2 Natural frequencies and modes for undamped systems.....	6
2.1.3 Damping	7
2.1.4 Resonance.....	8
2.1.5 Response of the system	10
2.1.6 Mass participation	11
2.2 Dynamic loads in pedestrian bridges	12
2.2.1 Load definition	14
2.2.2 Crowds behaviour.....	20
2.3 Dimensioning for comfort.....	25
2.3.1 Receivers	25
2.4 Guidelines	27
3 Materials.....	29
3.1 Graphene	29
3.1.1 Graphene nanoparticles	30
3.1.2 Graphene-based composites	31
3.1.3 Expected mechanical properties in macroscale	33
3.1.4 Design properties for graphene as a construction material.....	35
3.2 Other high-performance materials: Fibre reinforced polymer composites	36
3.2.1 Polymer matrices	36
3.2.2 Fibre reinforcement	37

3.2.3	Use of FRP in construction.....	39
4	Structural types.....	41
4.1	Holländerbrücke.....	42
4.2	Stanislas pedestrian bridge.....	42
4.3	Almuñecar pedestrian bridge.....	43
4.4	King Stormwater Channel Bridge.....	43
4.5	Full orthotropic deck.....	44
4.5.1	Korea road-bridge.....	44
4.5.2	Klipphausen road-bridge.....	44
4.5.3	Hollow-core deck.....	44
5	Methodology.....	45
5.1	Bridge description.....	45
5.2	Static design.....	46
5.3	Dynamic analysis.....	48
5.4	Extraction of results.....	49
5.5	Work flow.....	50
5.6	Limitations.....	52
6	Results.....	53
6.1	Natural frequencies.....	53
6.1.1	Influence of span length.....	53
6.1.2	Influence of width variation.....	56
6.1.3	Materials comparison.....	58
6.2	Accelerations.....	59
6.3	Summary charts.....	60
7	Discussion of the results.....	63
7.1	Study of natural frequencies.....	63
7.1.1	Raw analysis.....	63
7.1.2	Dependency study.....	64
7.2	Accelerations.....	70
8	Conclusions.....	73
9	Further studies.....	75
10	References.....	77

APPENDIX A	Bridge design
APPENDIX B	FE modelling in BRIGADE
APPENDIX C	Results tables from dynamic analysis
APPENDIX D	Accelerations plots

Preface

This Master's Thesis is the result of the cooperation of NCC Construction and the division of Structural Engineering of the Department of Civil and Environmental Engineering at Chalmers University of Technology, in Göteborg (Sweden).

This project could not be possible without the guidance and support of Alexandre Mathern, supervisor from NCC Construction, and Rasmus Rempling, supervisor and examiner from Chalmers University of Technology. Their predisposition for helping on a daily basis has been very enriching.

Thanks as well to Valbona Mara for her support, in not few times, with relation to FRP materials and to David Tarazona Ramos, for his help with the ABAQUS scripting and modelling.

We are grateful for the licenses that Scanscot Technology gave to us in order to use their FE-software BRIGADE Plus that allowed us to develop the FEM modelling.

Andrés would like to especially thank his parents, Andrés and Carmina, for their unconditional support and love. Thanks for believing in me and allowing me, not without great effort, to follow my professional and personal aspirations even if that meant living and studying abroad.

Jesús wants to thank his parents, Jesús and Mercedes, and her sister Sara, for being of a great support always with love and good advice. He also wants to thank to all his friends, both from his home, Galicia, and the ones that live all around the world.

During this adventure abroad we can honestly say that everybody, friend, family, flatmates, classmates, professors, assistants... that has crossed in our way has contributed to make all this possible.

Notations

Roman uppercase letters

C	Viscous damping matrix	[N·s/m]
\hat{C}	Modal damping matrix	[N·s/m]
E	Young's modulus	[N/m ²]
$F(t)$	Force vector	[N]
K	Stiffness matrix	[N/m]
\hat{K}	Modal stiffness matrix	[N/m]
M	Mass matrix	[kg]
\hat{M}	Modal mass matrix	[kg]
N	Number of DOFs of the system	[-]
$P(t)$	Modal force vector	[N]
T_D	Damped natural period	[s]
T_n	Undamped natural period	[s]

Roman lowercase letters

c	Viscous damping coefficient	[N·s/m]
c_{cr}	Critical viscous damping	[N·s/m]
f_D	Damped natural frequency	[s ⁻¹]
f_n	Undamped natural frequency	[s ⁻¹]
f_u	Ultimate normal stress	[N/m ²]
f_y	Yielding normal stress	[N/m ²]
k	Elastic spring stiffness	[N/m]
m	Mass	[kg]
t	Time	[s]
p_0	Amplitude of an applied periodic force	[N]
u	Displacement	[m]
\dot{u}	Velocity	[m/s]
\ddot{u}	Acceleration	[m/s ²]
vol%	Percentage by volume	[%]
wt%	Percentage by mass	[%]

Greek uppercase letters

Φ	Modal matrix	[-]
--------	--------------	-------

Greek lowercase letters

ζ	Viscous damping ratio	[-]
η_r	Displacement in a base formed by the eigenvectors of the problem	[m]
$\dot{\eta}_r$	Velocity in a base formed by the eigenvectors of the	[m/s]

	problem	
$\dot{\eta}_r$	Acceleration in a base formed by the eigenvectors of the problem	[m/s ²]
ν	Poisson's ratio	[-]
ρ	Density	[kg/m ³]
σ	Normal stress	[N/m ²]
ϕ_n	Natural mode of vibration	[-]
τ_u	Ultimate shear stress	[N/m ²]
ω	Generic circular natural frequency	[rad/s]
ω_D	Damped circular natural frequency	[rad/s]
ω_n	Undamped circular natural frequency	[rad/s]

Abbreviations

CNT	Carbon nanotube
DLF	Dynamic load factor
DOF	Degrees of freedom
FE	Finite element
MDOF	Multiple degrees of freedom
MWCNT	Multi-walled carbon nanotube
OPC	Ordinary Portland cement
SDOF	Single degree of freedom
SWCNT	Single-walled carbon nanotube
SLS	Serviceability limit state
ULS	Ultimate limit state
FRP	Fibre reinforced polymer
PAN	Polyacrylonitrile

1 Introduction

Graphene is a one-atom-thick layer of carbon atoms arranged in a honeycomb crystal lattice, the first two-dimensional material. It is the thinnest, strongest, lightest, most flexible and best heat and electricity conducting known material and in combination with different elements it can produce several materials with various superior properties and applications.

The use of this material in civil engineering is still uncertain since the main research has been developed mostly in nanoscale. Despite this lack of specific mechanical properties of the material in a bigger scale, individually or as composite, it is possible to analyse the expected behaviour and problems that would arise. It is therefore interesting to investigate how such a light material would behave in a real structure.

Graphene has been studied for decades, but the term graphene was not introduced until 1985, by Boehm, Setton and Stumpp (Boehm, et al., 1985). Before that, some authors had already studied the theoretical magnificent properties that one isolated layer of graphite could perform. Despite that, its isolation seemed to be impossible for several years, due to the conclusions extracted from some theoretical studies on the thermodynamic stability of two-dimensional crystals. The development of a method for the production of single layer graphene from graphite, known as the scotch tape method, was announced by Geim and Novoselov in 2004 (Novoselov, et al., 2004) which were awarded with the Nobel Prize in Physics in the year 2010 (The Royal Swedish Academy of Sciences, 2010). Since then, universities and industries have been working in developing better ways of producing it, together with investigating its properties and behaviour.

This ultra-light and ultra-resistant material will make possible the construction of ultra-light and slender bridges that may lead to dynamic problems on the structure. There has been a concern about dynamic problems on bridges for many years; that is the reason, for example, why troops break step while crossing. An inflexion point concerning dynamic problems due to footsteps appeared in the year 2000 with the Millennium Bridge in London (Dallard, et al., 2001). The bridge had to be closed a few days after its opening, due to the detection of unexpected vibrations produced by the pedestrian-structure interaction.

Dynamic loads to be taken into account on the calculation of pedestrian bridges are defined in *Eurocode 1- Part 2: Traffic loads on bridges* (CEN, 2003), although they are vaguely described, and it can be unclear for the engineer how to proceed in order to check the dynamic response of structures to avoid these problems.

1.1 Purpose

The purpose of this project was to achieve a clear and framed use of the graphene in the design of bridges, defining structural types and elements in the bridge where this material will suppose an advantage. For that, an increase of the knowledge about the mechanical properties of graphene for the use on the structural analysis needs to be extrapolated from the nowadays reality in graphene research, where almost none real-scale experimental data has been achieved.

Further, establish a rationalised and optimized solution for the use of this material in pedestrian bridges, identifying and defining the problems associated with graphene characteristics, together with the proposed solutions that are needed to fulfil both serviceability and ultimate limit states.

The known characteristics of this material will directly lead to an ultra-lightweight structure; therefore another main purpose of this project is to identify the dynamic problems associated with ultra-light pedestrian bridges. For that a comparison between conventional materials and graphene is developed together with the study of the influence of different geometry cross-sections.

1.2 Objectives

Four main objectives have been identified:

- Gather the knowledge about graphene mechanical properties in order to use the material in the analysis.
 - Establish the state of the art of the use of graphene in civil engineering.
 - Define the assumptions and chosen mechanical properties of the graphene together with recommendations of its adequate use in the different structural elements of the pedestrian bridges.
- Broaden the knowledge of the behaviour of ultra-light pedestrian bridges, based on the hypothetical use of graphene as the reference material.
 - Establish the dynamic theory that will be used for an adequate evaluation of the problem and the pedestrian loads according to the codes and guidelines.
 - Based on the research of both material properties and dynamic behaviour of the pedestrian bridges specify, the structural elements where this material will be used.
- Analyse the dynamic behaviour of different case studies from several structural types under the defined pedestrian loads.
 - Define the parameters to be compared for each case study in order to systematize their evaluation.
 - Calculate for each case study the chosen parameters with the help of appropriate engineering software according to the characteristic of each study case.
 - Compare the achieved results of the different case studies in order to make conclusions of the limits in the use of graphene in each case.
- Gather the conclusions of the previous studies to be able to define an appropriate and optimised conceptual structural type for the use of graphene in pedestrian bridges.

1.3 General Layout

The present study is divided in three different parts, a literature review, the study of several cases and the conclusions.

In Section 0, structural dynamics of footbridges are presented, including a brief introduction in structural dynamics and the definition of the pedestrian loads. In Section 3, graphene and FRP materials are presented. Finally, in Section 4 different structural types currently used in FRP bridge concepts are described.

In Section 5 the methodology followed in the present study is presented and the results of its appliance are gathered in Section 6. Finally the discussion of the results is included in Section 7 with the final conclusions in Section 8. Section 9 presents suggestions for further studies.

Four appendices are included at the end of the document. APPENDIX A and APPENDIX B explain in depth some sub-studies that were needed to be developed along the analysis. APPENDIX C and APPENDIX D present the results of the dynamic analysis.

2 Structural dynamics of footbridges

Structural dynamics is the discipline that studies the behaviour of structures over time. Loads vary in time producing variations in the deflection of the structure. These effects are of importance in bridges, where pedestrians, vehicles, wind or earthquakes can start a dynamic response of the structure that needs to be checked in terms of the Service Limit State (SLS) and Ultimate Limit State (ULS).

The dynamic response of the structure is sometimes decisive in the calculations of a pedestrian bridge, as dimensioning regarding ULS and SLS take them to a high point of slenderness where the dynamic problem may appear.

The variable loads applied are collected from guidelines recently published that aim to define this problem in a proper and accurate way. They model extreme cases for the dynamic problems such as the crowd behaviour over the structures. When these loads are applied on the model, they produce a response on the way of displacements and accelerations that need to be limited to achieve a certain level of comfort, as it will be explained in this section.

2.1 Structural dynamics theory

The approach to calculate the behaviour of a system subjected to a dynamic loading is derived starting from a simple system, to then get the response of a more complex finite element system, which can represent in a good manner a real structure.

Dynamic analysis of pedestrian bridges is directly related with moving loads. Models for this matter are based on the integration over time of the dynamic equations under the pedestrian loads. This problem can be approached by developing the whole integration with multiple degrees of freedom (MDOF) systems or reducing the equations with modal analysis, which can be done by numerical approximated calculations of the vibrations modes or, if possible, obtaining the analytical solution.

Analytical calculation can only be obtained for simple structures such as simply supported beams and some statically indeterminate structures. However, for more complex structures commercial software allows to calculate the normal modes for the approximated integrations of the dynamic equations following the FE-method.

2.1.1 Equation of motion

The theory behind structural dynamics can be understood easier starting from a simple degree of freedom (SDOF) model, to extrapolate it later to MDOF systems. As shown in Figure 2.1, SDOF systems can be represented by a mass attached in parallel to a spring and a damper. This mass is subjected to a general force $F(t)$, and is located at $u(t)$.

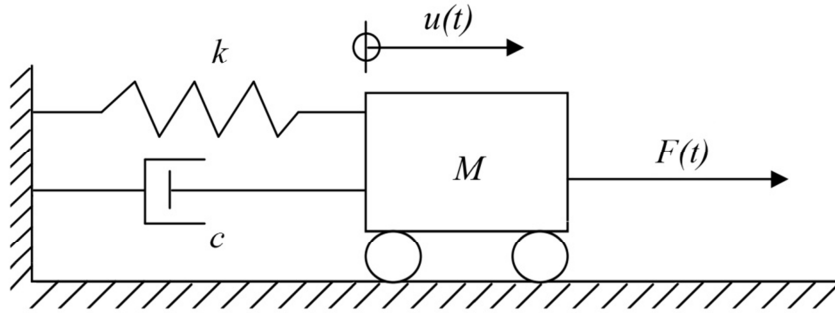


Figure 2.1. SDOF system with a mass m attached to a spring of stiffness k and a damper with viscosity c , subjected to a force $F(t)$ and placed at $u(t)$.

The equation of motion for the model can then be derived using Newton's 2nd Law or Lagrange equations (Craig Jr & Kurdila, 2006), to obtain:

$$m \cdot \ddot{u} + c \cdot \dot{u} + k \cdot u = F(t) \quad (2.1)$$

The exact solution of this differential equation exists only for certain $F(t)$, therefore for most of the cases, the use of numerical methods is needed in order to get an approximation of the solution for the problem.

MDOF systems can be modelled in an equivalent way, using matrices and vectors instead of scalar variables. The derivation is done again using either Newton's 2nd Law or Lagrange equations (Craig Jr & Kurdila, 2006) and results in the following equation of motion:

$$\mathbf{M} \cdot \ddot{\mathbf{u}} + \mathbf{C} \cdot \dot{\mathbf{u}} + \mathbf{K} \cdot \mathbf{u} = \mathbf{F}(t) \quad (2.2)$$

Matrices in Equation (2.2) are of dimension $N \times N$, and vectors are of dimension $N \times 1$, N being the number of degrees of freedom (DOF) defined for the model.

2.1.2 Natural frequencies and modes for undamped systems

Vibration of the structure is produced when the frequency reaches its natural value. When this phenomenon is produced the structure acquires the shape of the corresponding natural mode.

For their calculation, it is needed to calculate the solution for the free vibrations case, i.e. taking $\mathbf{F}(t) = \mathbf{0}$ in Equation (2.2). If an undamped system is used here, the solution can be achieved by solving an eigenvalue problem (Craig Jr & Kurdila, 2006) with the following characteristic equation:

$$[\mathbf{K} - \omega_n^2 \cdot \mathbf{M}] \cdot \mathbf{u} = \mathbf{0} \quad (2.3)$$

The characteristic equation for this system is then:

$$\det(\mathbf{K} - \omega_n^2 \cdot \mathbf{M}) = 0 \quad (2.4)$$

Equation (2.4) has N roots, which are the eigenvalues ω_n , associated with the frequencies at which the structure will vibrate, getting the natural frequencies f_n and periods of vibration T_n of the structure as:

$$f_n = \frac{\omega_n}{2 \cdot \pi} \quad (2.5)$$

$$T_n = \frac{2 \cdot \pi}{\omega_n} \quad (2.6)$$

And the natural modes of vibration are the eigenvectors ϕ_n obtained directly from the eigenvalue problem defined by equation (2.3). This is done by finding non-zero solutions for \mathbf{u} , for each of the calculated ω_n .

2.1.3 Damping

In real life, the free vibrations of the systems to analyse are reduced with time; this is what is known as damping. So far, a system without damping has been studied in order to get the natural frequencies of the structure; however, to get a more accurate result of its behaviour, damping of the structure has to be added to the variables considered.

The main factors that cause damping in structures are (Chopra, 1995):

- The transformation of energy due to the thermal effect of repeated straining of the material.
- The loss of energy due to internal friction of particles.
- Other factors that have less influence, but that may be accounted, such as the friction at steel connections, the opening and closing of concrete micro-cracks, or the friction between structural and non-structural components.

The evaluation of damping is not easy and damping factors are usually calculated with empirical methods and idealized as linear viscous dampers (Chopra, 1995). Thus, the expression $\mathbf{C} \cdot \dot{\mathbf{u}}$ is used for this matter in equation (2.2).

In such case, a new variable important for the problem is defined, the viscous damping ratio, ζ (Chopra, 1995):

$$\zeta = \frac{c}{c_{cr}}; \quad c_{cr} = 2 \cdot \sqrt{k \cdot m} \quad (2.7)$$

Depending on the value of ζ , the system can be in any of these three different situations:

- Overdamped, when $\zeta^2 - 1 > 0$ or $c > c_{cr}$. These systems, once excited, return to equilibrium without vibrating.

- Critically damped, when $\zeta^2 - 1 = 0$ or $c = c_{cr}$. The behaviour is the same as for overdamped systems.
- Underdamped, when $\zeta^2 - 1 > 0$ or $c > c_{cr}$. In this case, the structure vibrates with exponentially decreasing amplitude. In this case, a different frequency and period will appear, compared with the undamped problem:

$$\omega_D = \omega_n \cdot \sqrt{1 - \zeta^2} \quad (2.8)$$

$$f_D = \frac{1}{T_D} = \frac{\omega_D}{2 \cdot \pi} \quad (2.9)$$

Damping ratio values are collected in Table 2.1 for different common construction materials. The selected damping ratio for the different materials used in this thesis are defined in Section 2.3.1.2.

Table 2.1. Damping ratios for different materials and construction types for serviceability conditions (Heinemeyer, et al., 2009).

Material / Construction Type	Damping ratio (Minimum ζ)
Reinforced concrete	0.8 %
Pre-stressed concrete	0.5 %
Composite steel-concrete	0.3 %
Steel	0.2 %
Timber	1.0 %
Stress-ribbon	0.7 %

2.1.4 Resonance

2.1.4.1 Undamped systems

When applying a cyclic force as (2.10) over an undamped structure with a frequency ω equal to a natural frequency of the structure ω_n , resonance will appear, as shown below. Thus, it is interesting to know the natural frequencies and modes of the structure from the point of view of structural comfort and avoiding ULS situations.

$$F(t) = p_0 \cdot \sin(\omega_n \cdot t) \quad (2.10)$$

In such a case, the solution for the equation of motion in a SDOF problem would follow an equation of the form of (2.11) (Chopra, 1995). This solution is derived for a case with initial conditions $u(0) = 0$ and $\dot{u}(0) = 0$.

$$u(t) = -\frac{1}{2} \cdot \frac{p_0}{k} \cdot (\omega_n \cdot t \cdot \cos(\omega_n \cdot t) - \sin(\omega_n \cdot t)) \quad (2.11)$$

It is interesting to plot this function with normalized axes, over p_0/k for displacements and over T_n for time. As it can be observed in Figure 2.2, resonance causes an amplification on

the amplitude of $u(t)$, that would lead to failure of a brittle structure, or to yield in the structure if it is ductile. In this last case, the stiffness of the structure would decrease and its natural frequency would change, becoming then different from the frequency of excitation ω , and escaping from resonance (Chopra, 1995).

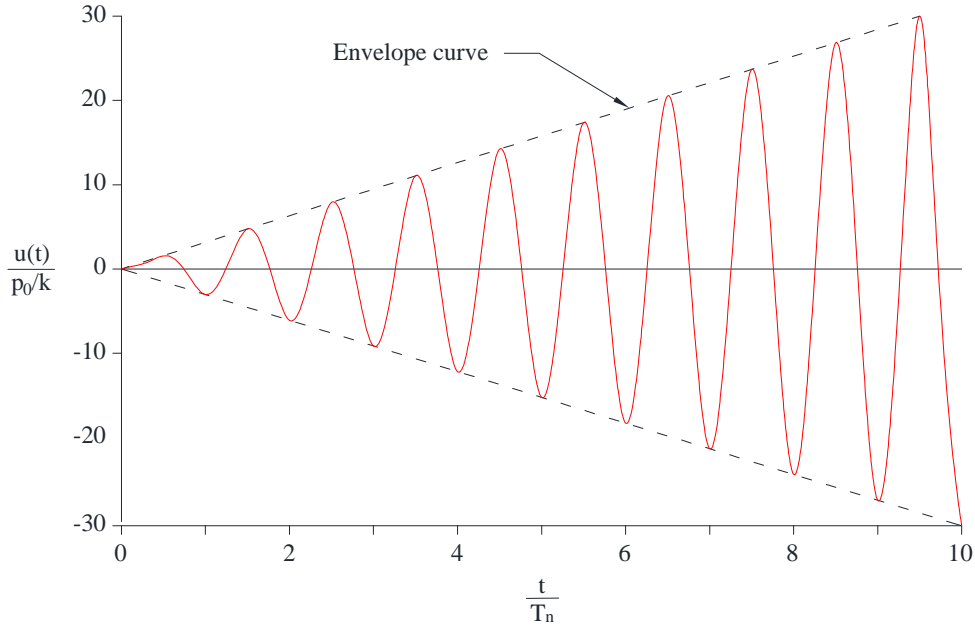


Figure 2.2. Response of undamped structure for the resonance problem.

The goal is therefore to get a structure that has natural frequencies different from the frequency of the expected dynamic excitations during service life, such as wind flutter, pedestrian or vehicles loads. This can be achieved by varying different parameters as the stiffness of the structure, its mass, adding dampers in strategic points, etc.

2.1.4.2 Damped systems

When taking into account damping, the equation of motion of the structure becomes as in equation (2.12) (Chopra, 1995).

$$u(t) = \frac{1}{2\zeta} \cdot \frac{p_0}{k} \cdot \left[e^{-\zeta \omega_n t} \left(\cos(\omega_D \cdot t) + \frac{\zeta}{\sqrt{1-\zeta^2}} \sin(\omega_D \cdot t) \right) - \cos(\omega_n \cdot t) \right] \quad (2.12)$$

The result of equation (2.12) for $\zeta = 0.05$ and starting from rest (i.e. with $u(0) = 0$ and $\dot{u}(0) = 0$) is depicted in the following figure:

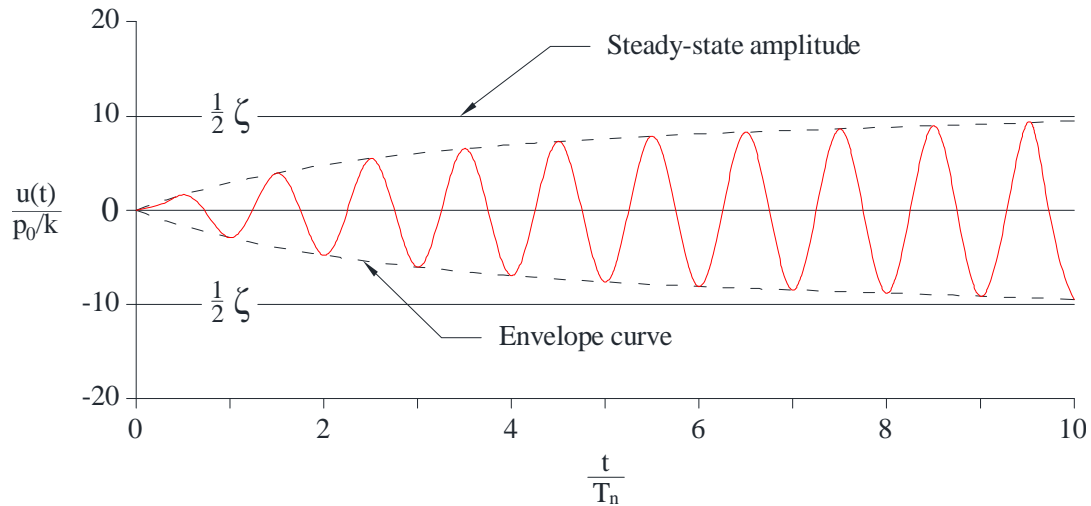


Figure 2.3. Response of damped system to resonance frequency $\omega = \omega_n$ for $\zeta = 0.05$, starting from rest, i.e. with $u(0) = 0$ and $\dot{u}(0) = 0$ (Chopra, 1995).

From Figure 2.3 it is observed that a damped system, under a cyclic force with frequency $\omega = \omega_n$, will increase its amplitude until a certain limit, which occurs when the energy supplied to the system by the external force equals the energy dissipated by the damping effect. This means that the vibration will increase its amplitude to a certain value at which it reaches the steady state. The velocity at which this happens depends on the damping factor ζ . The bigger ζ is, the faster the steady-state is reached, and the lower the amplitude is (Chopra, 1995). Therefore, depending on the damping factor, resonance can be avoided, as one could limit the amplitude to a limit which represents no hazard to the structural integrity of the system. For small damping factors, however, amplitudes bigger than the allowable limit may be reached.

2.1.5 Response of the system

When all the parameters previously studied are known, the dynamic response of the structure for a certain problem can be calculated using the mode superposition method. This is based in transforming the problem to a base formed by the eigenvectors, where one can obtain N uncoupled equations easier to solve (Craig Jr & Kurdila, 2006). Once the response is known in this base, it can easily be transformed back to the original base to get the solution for the problem.

Starting from the MDOF problem defined in Equation (2.2), eigenfrequencies ω_n and eigenvectors ϕ_n are calculated. With them, the principle coordinates Φ are introduced using the eigenvectors:

$$\Phi = [\phi_1 \quad \phi_2 \quad \cdots \quad \phi_N] \quad (2.13)$$

Then, the problem is reformulated as:

$$u(t) = \sum_{r=1}^N \phi_r \cdot \eta_r(t) \quad (2.14)$$

The uncoupled system in the new base is:

$$\widehat{\mathbf{M}} \cdot \ddot{\boldsymbol{\eta}} + \widehat{\mathbf{C}} \cdot \dot{\boldsymbol{\eta}} + \widehat{\mathbf{K}} \cdot \boldsymbol{\eta} = \mathbf{P}(t) \quad (2.15)$$

Where the modal matrices for the system are:

$$\begin{aligned} \widehat{\mathbf{M}} &= \boldsymbol{\Phi}^T \cdot \mathbf{M} \cdot \boldsymbol{\Phi} \equiv \text{modal mass matrix} \\ \widehat{\mathbf{C}} &= \boldsymbol{\Phi}^T \cdot \mathbf{C} \cdot \boldsymbol{\Phi} \equiv \text{modal damping matrix} \\ \widehat{\mathbf{K}} &= \boldsymbol{\Phi}^T \cdot \mathbf{K} \cdot \boldsymbol{\Phi} \equiv \text{modal stiffness matrix} \\ \mathbf{P}(t) &= \boldsymbol{\Phi}^T \cdot \mathbf{F}(t) \equiv \text{modal force vector} \end{aligned} \quad (2.16)$$

From these formulas N uncoupled equations easier to solve can be derived. Once the result is obtained in the transformed base, the result for the original base is achieved using Equation (2.14). Now it is a matter of choosing the right force vector, which has to be modelled depending on the force that excites the structure. This is studied in deep in the Section 2.2 of this document.

2.1.6 Mass participation

Modal effective mass, Equation (2.18), is an important factor in order to know if enough vibration modes are being considered in the simulation. It indicates how strong is the representation of the motion is for a certain direction from each mode calculated.

$$\Gamma_{ai} = \frac{1}{m_\alpha} \cdot \boldsymbol{\phi}_\alpha^N \cdot \mathbf{M}^{NM} \cdot \mathbf{T}_i^M \quad (2.17)$$

$$m_{\alpha i}^{eff} = (\Gamma_{ai})^2 \cdot m_\alpha \quad (2.18)$$

where:

- $m_{\alpha i}^{eff}$: effective mass for mode α in direction i .
- Γ_{ai} : modal participation factor for mode α in direction i .
- m_α : generalized mass of the structure for mode α .
- $\boldsymbol{\phi}_\alpha^N$: eigenvector for mode α .
- \mathbf{M}^{NM} : mass matrix of the structure.
- \mathbf{T}_i^M : magnitude of the rigid body response of a degree of freedom.

If all effective masses are added, the mass of the structure is obtained; therefore, if the summation gives a low value, important modes in order to define motion of the structure will be missing in the calculations.

The mass participation ratio is the percentage of effective mass over total mass of the structure. The number of modes used should be such that the mass participation ratio of them together is over 90% (López & Cruz, 1996) and (Priestley, et al., 1996).

2.2 Dynamic loads in pedestrian bridges

As it was explained in Section 2.1.3, the dynamic problems of pedestrian bridges appear when a vibration is produced near one or more modes of vibration of the structure. This happens due to the coincidence of the range of natural frequencies (vertical or lateral) of the footbridge with the dominant frequencies of the human-induced load (Heinemeyer, et al., 2009), that can end up in a resonance problem.

There are different activities that can produce a dynamic loading in the system, such as sitting, walking, running, jumping, etc. Depending on the intensity, they can cause a bigger or smaller effect on it. When the intensity is relatively low, it can cause an SLS problem, i.e. discomfort and emotional reactions on the pedestrians. High-intensity loads, such as vandal synchronised jumping, can lead to ULS problems (Pedersen, 2009).

Quantifying the intensity of dynamic loadings due to pedestrians is hard, as it is rather difficult to predict how many pedestrians will be there and how they will exactly behave in terms of length or frequency of the step. This is therefore a stochastic case with a high dependency in the random variables and therefore needs to be empirically determined with big samples (Bødker & Christensen, 2010). However, the collapse of structures due to human-induced dynamic problems has occurred very rarely, as the determining parameters are normally ULSs, however, a high intensity loading like bouncing, swaying body horizontally, shaking stay cables, etc. can lead to ultimate limit problems (Heinemeyer, et al., 2009).

The way humans walk is very complex to analyse due to the dependence on many factors. According to Harper, et al. (1961) and Harper (1962) the force of a single-human gait changes with the velocity. This leads to the increase of period and amplitude peak of the load. Lot of research has been done for different values of these factors that affect the load, being the most important: pacing frequency speed, step length or increasing walking speed with variation in vertical and lateral forces of successive steps.

All the mentioned variations were gathered by Wheeler (1980) and (1982) concluding that the increment of step frequencies ended with increasing of the peak amplitude, stride length, velocity and decreasing the contact time as depicted in Figure 2.4.

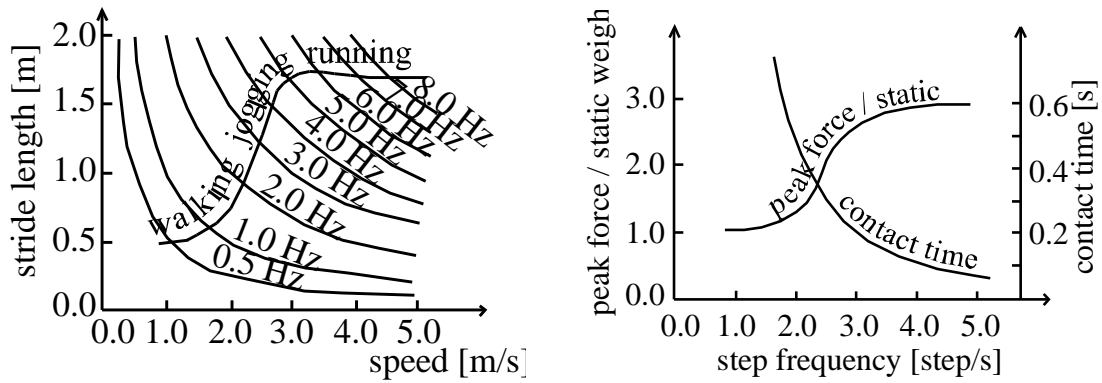


Figure 2.4. (a) Dependence of stride length and velocity for different activities with their corresponding frequencies (walking: 0.5-1.5 Hz, jogging: 1.5-3.5 Hz and running: >4.5 Hz). (b) Dependence of peak force and contact time on different pacing rates (step frequency) (Živanović, et al., 2005).

Measuring the continuous walking forces and overlapping the right and left foot steps lead to a behaviour that can be assumed periodic as it can be seen in Figure 2.5, with a period equal to the reciprocal value of the step frequency (Živanović, et al., 2005).

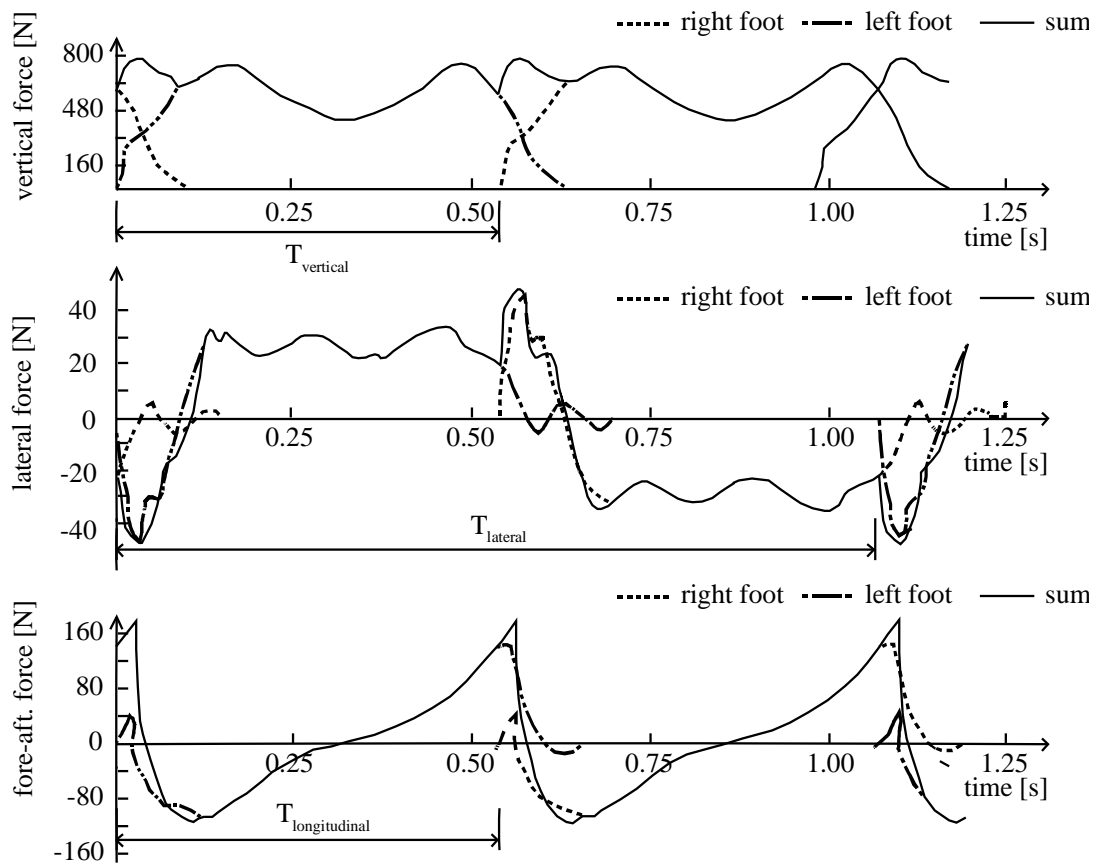


Figure 2.5. Periodic walking time histories in vertical, lateral and longitudinal directions (Živanović, et al., 2005).

Živanović et al. (2005) gathered the research of the analysis of the pedestrian-induced forces from a statistic approach, concluding that it followed a normal distribution with the frequency ranges on Table 2.2 for the different activities.

Table 2.2. Typical frequencies ranges for different pedestrian activities (Živanović, et al., 2005).

Activities	Mean frequencies (Hz)
Running	2.0 – 3.5
Bouncing	1.5 – 3.0
Walking	1.6 – 2.4
Jumping	1.8 – 3.4
Horizontal body swaying	0.4 – 0.7

2.2.1 Load definition

There are different models that try to reflect -in an accurate manner- the real distribution of the pedestrian forces. New construction methods, material and design trends lead to bigger spans and lighter structures that increase the dynamic problems of structures and therefore the necessity of a more accurate definition of this phenomenon.

The uncertainty on the definition of the different parameters and the lack of larger researches focused on this field makes it very difficult to determine this definition.

There are two main approaches according to the definition criteria, time domain (force as function of time) and frequency domain (force as function of frequency) (Zivanovi & Pavic, 2011).

These methods, see Table 2.3, are typically based on semi-empirical relationships of the pedestrian loads while in reality the parameters affecting the phenomenon are stochastic, i.e. depend on random variables (da Silva, et al., 2007).

Table 2.3. Existing procedures for the pedestrian load approach.

Time Domain	Frequency Domain
ISO 10137, Annex A (ISO, 2005)	Hivoss, Butz (Butz, 2008)
French Setra Guideline (Sétra, 2006)	Ingolfsson et al (Ingólfsson, et al., 2008)
FIB, Guidelines for design of footbridges (Federation internationale du beton, 2006)	
EC 1, UK Annex (CEN, 2003)	
EC 5, Annex B (CEN, 2003)	

Time domain approaches are usually based in periodic forces whose parameters can be defined as deterministic or probabilistic. With deterministic parameters the model is generally defined in accordance with different activities, meanwhile using probabilistic parameters the model takes into account the randomness of most parameters affecting the human forces, i.e. body weight and walking frequencies.

Frequency domain models assume the structure as a linear or linearized system and are based on the representation of the random processes according with their power spectral density.

Probabilistic models are based on the stochastic reality of human walking loading as it directly depends on the weight, pacing rate, velocity or time delay between people crowds. This problem can be approached defining each variable from large sample experiments and transforming them into a probabilistic distribution.

The problem of this method is the necessity of large experiments that allow an accurate definition of each variable. For instance, the fact that large crowds sometimes adjust their step according to the movement of the rest of the people is almost unknown and it is taken into account by increasing the safety factors or by placing over-dimensioned dampers (Živanović, et al., 2005).

2.2.1.1 Vertical load

Despite the mentioned probabilistic distribution of different elements affecting the load distribution (as one or more persons walking or running, with the addition of the model synchronization behaviour between people due to the movement of structures as it was experienced in the Millennium bridge) codes are based on time domain deterministic models trying to fit the load distribution of one single person (see Figure 2.5) and based on the assumption that the same force is produced by both feet, i.e. periodic distribution (Živanović, et al., 2005) (Heinemeyer, et al., 2009)

$$F_{p,v}(t) = m_p \cdot g + \sum_{i=1}^n m_p \cdot g \cdot \alpha_{i,v} \cdot \sin(2 \cdot \pi \cdot i \cdot f_s \cdot t - \varphi_{i,v}) \quad (2.19)$$

where:

- m_p : mass of the body
- g : gravity acceleration
- $\alpha_{i,v}$: Fourier coefficient for the i^{th} harmonic (Dynamic load factor, DLF)
- f_s : activity rate
- t : time
- φ_i : phase shift
- n : Total number of harmonics considered

The DLF depends on several parameters such as step frequency (walking pace) (S. Yao, 2002,), people velocity (Rainer, et al., 1988), frequency of the activity (Yoneda, 2002) and the surface of the interaction between humans and low-frequency structures (S. Yao, 2002,) and (S. Yao, 2003). For the case of footbridges the resonant vertical 1st and 2nd harmonics are lower than those on rigid surfaces.

As consequence of the reasons mentioned above, it can be concluded that the DLF is the biggest issue regarding the definition of the pedestrian-induced force in the structure.

The periodic force is affected by the speed of the pedestrians, i.e. is not stationary, from the result of the SYPNEX project, the relationship between the step frequency (from 1.3 to 1.8 Hz) and walking speed is $v_s = 1.271 \cdot f_s - 1$.

Therefore, lot of uncertainty still exists on the definition of the parameters that affect the pedestrian load. Actually, in the European Guideline these values are gathered according to different authors without establishing the most accurate ones. In Equation (2.20) the values of the DLF and phase shift for the walking activity from the recent European research project SYPNEX (Butz, et al., 2008) are shown.

$$\begin{aligned}
 & - \alpha_1 = 0,0115f_s^2 + 0,2803 f_s - 0,2902 \\
 & - \varphi_1 = 0 \\
 & - \alpha_2 = 0,0669f_s^2 + 0,1067 f_s - 0,0417 \\
 & - \varphi_2 = -99,76f_s^2 + 478,92 f_s - 387,8 [^\circ] \\
 & - \alpha_3 = 0,0247 f_s^2 + 0,1149 f_s - 0,1518 \\
 & - \varphi_3 = \\
 & \quad -150,88 f_s^3 + 819,65 f_s^2 - 1431,35 f_s + 811,93 [^\circ] \quad \text{If } f_s < \\
 & \quad 2,0 \text{ Hz} \\
 & - \varphi_3 = 813,12 f_s^3 - 5357,6 f_s^2 + 11726 f_s - 8505,9 [^\circ] \quad \text{If } f_s \geq \\
 & \quad 2,0 \text{ Hz} \\
 & - \alpha_4 = -0,0039 f_s^2 + 0,0285 f_s - 0,0082 \\
 & - \varphi_4 = 34,19 f_s - 65,14 [^\circ]
 \end{aligned} \tag{2.20}$$

The summation on Equation (2.19) aims to reflect the actual behaviour of the peaks of pedestrian loads with a sinusoidal wave-shape. This double hump is the result of the impact with the ground of the heel (first one) and the push off of the foot (second one).

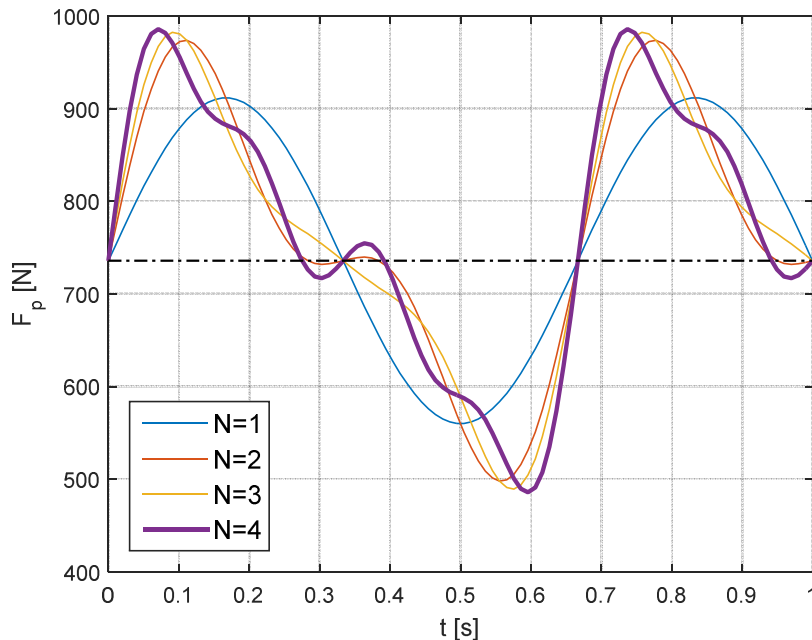


Figure 2.6. Pedestrian induced force from Formula (2.19) and (Bachmann & Ammann, 1986) for $m = 75 \text{ kg}$, $f_s = 1.5 \text{ Hz}$ and $\varphi_i = 0$.

As shown in Figure 2.7, the activity rate is another important factor that influences the dynamic induced pedestrian load (Anon., 2005).

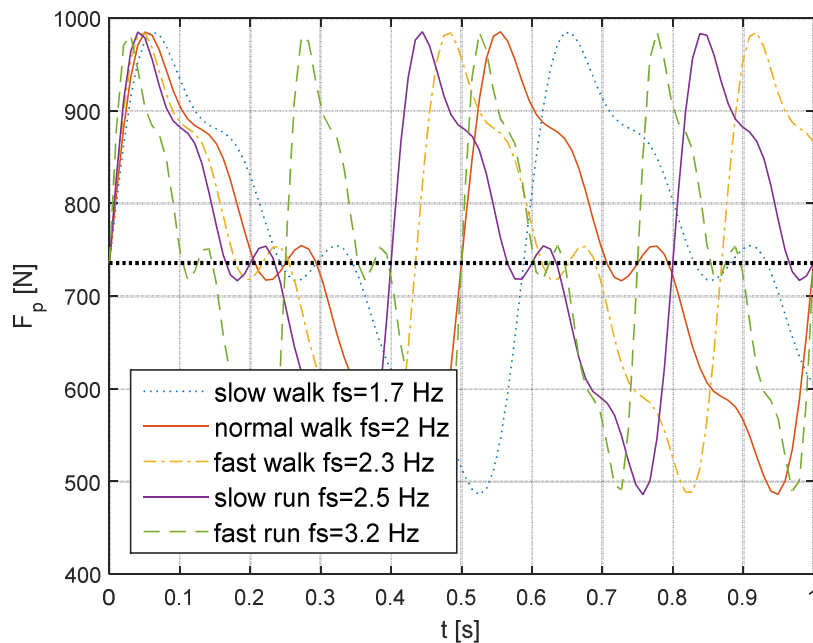


Figure 2.7. Pedestrian load for different activity rate values f_s according to Equation (2.19) and (Anon., 2005).

2.2.1.2 Lateral load

The gravity centre of a person changes its position while walking, inducing a lateral dynamic force with a lateral frequency of about 1 Hz (Nakamura & Kawasakib, 2006) which is around half of the value of the vertical and longitudinal load. This phenomenon can therefore lead to a resonance problem for the bridge element with a frequency close to this value.

Walking of pedestrian in living bridges, i.e. oscillating floors, significantly varies from the fixed floors due to the unconscious gait modification while trying to maintain balance (Ricciardelli, et al., 2014).

From Nakamura & Kawasakib (2006) it was found that when pedestrian deliberately sidestepped with a lateral frequency close to the lateral frequency of the bridge deck just a small crowd could get to the design load of the structure, i.e. few people could easily set the whole bridge to vibrate. However, randomly walking pedestrians' gaits with different phases compensate each other.

This phenomenon is produced due to the synchronization of the pedestrian's gait and the bridge vibration. When walking in a long flexible surface, people tend to spread their legs apart, changing their step frequency, synchronizing their phase step with the floor (McRobie, et al., 2003). This synchronization of the gait and bridge is not more away of 0.1 Hz from the lateral vibration of the structure (Butz, 2006), (Nakamura, et al., 2008) and (Sun & Yuan, 2008).

However when pedestrian feel an uncomfortable vibration they change their behaviour reducing their time step or holding the girder deck leading to a steady-state vibration, i.e. without an increase in the vibration (Nakamura & Kawasakib, 2006).

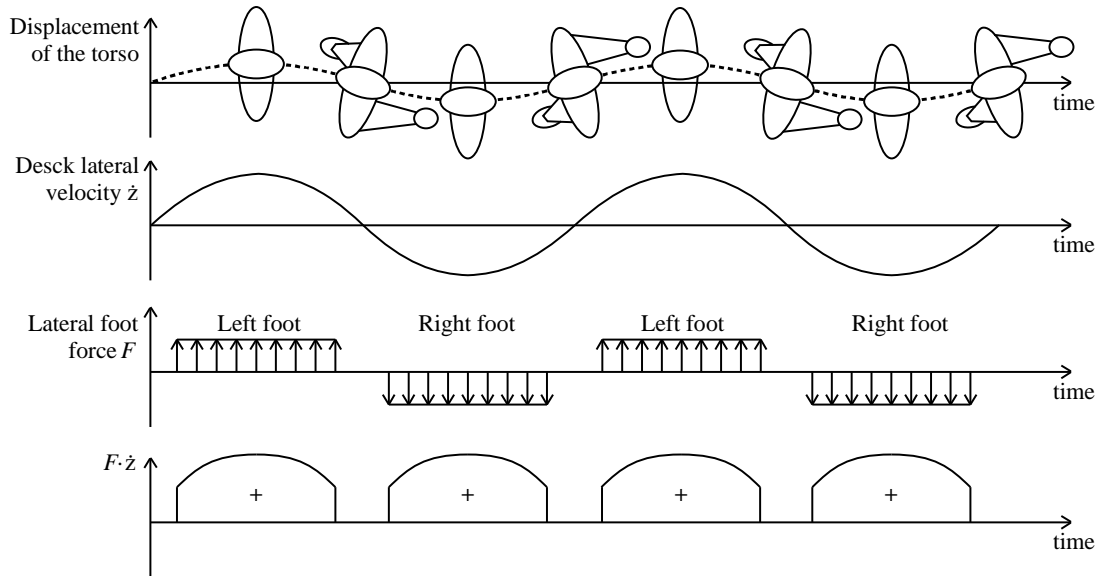


Figure 2.8. Schematic representation of pedestrian-structure synchronization after (Butz, et al., 2008).

The pedestrian gait in flexible footbridges can be understood as the interaction between two oscillators that work as a one-way interaction when the motion of the pedestrian is not affected by the footbridge motion, or as a two way interaction and potentially non-linear when it is affected. This can lead to the synchronization of these two oscillators (Ricciardelli, et al., 2014).

This model system is agreed by studies of different authors that mean that the walkers behave as autonomous dynamic systems interacting with the footbridge and therefore the loading model needs to reflect this interaction between the vibration of the pedestrian and the structure (McRobie, et al., 2003), (Nakamura, et al., 2008), (Macdonald, 2009) and (Ingólfsson, et al., 2011). It can then be defined the Equation (2.21), assuming the lateral force to be a periodic function (Venuti & Bruno, 2009).

$$F_{p,l}(t) = \sum_{i=1}^n m_p \cdot g \cdot \alpha_i \cdot \sin\left(2 \cdot \pi \cdot i \cdot \frac{f_s}{2} \cdot t - \varphi_i\right) \quad (2.21)$$

where:

- m_p : mass of the body
- g : gravity acceleration
- $\alpha_{i,l}$: Fourier coefficient for the i^{th} harmonic (Dynamic load factor, DLF)
- f_s : activity rate
- t : time
- φ_i : phase shift
- n : Total number of harmonics considered

One can note that the period of the function due to the frequency of the vertical and longitudinal loads, Equations (2.19) and (2.22), is double compared to the lateral, Equation (2.21), as it was already mentioned, matching the reflected in the experimental data showed in Figure 2.5.

Using the values proposed by Bachmann & Ammann (1986), Figure 2.9 is plotted. It can be seen how the conclusions made by these authors of limiting the necessity of using just the first five harmonics are correct, as the variation between the last two is minimum.

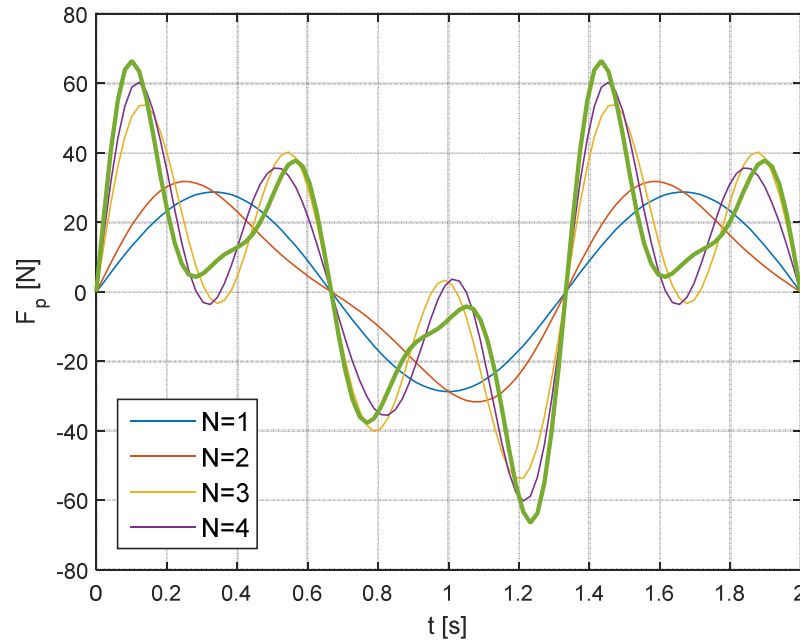


Figure 2.9. Pedestrian induced force from Equation (2.21) and (Bachmann & Ammann, 1986) for $m = 75 \text{ kg}$, $f_s = 1.5 \text{ Hz}$ and $\varphi_i = 0$.

2.2.1.3 Longitudinal load

The longitudinal load induced by a pedestrian, as presented in Section 2.2, can be defined as a deterministic model with a sinusoidal function. The research on the longitudinal load has not been developed as well as vertical and lateral loadings (Živanović, et al., 2005) due to its lower magnitude and importance for the dynamic behaviour of the structure.

Differently to what was presented for the vertical and lateral forces, the longitudinal force has a minimum variability at a normal walking speed (Masani, et al., 2002) and the frequency is the same as the vertical load that is depicted in Figure 2.5.

The characterization of the force is caused by the lateral oscillation of the body and is mainly represented as a Fourier's series assuming a time domain description (Heinemeyer, et al., 2009) .

$$F_{p,long}(t) = \sum_{i=1}^n m_p \cdot g \cdot \alpha_{i,long} \cdot \sin(2 \cdot \pi \cdot i \cdot f_s \cdot t - \varphi_i) \quad (2.22)$$

where:

- m_p : mass of the body
- g : gravity acceleration
- $\alpha_{i,long}$: Fourier coefficient for the i^{th} harmonic (Dynamic load factor, DLF)
- f_s : activity rate
- t : time
- φ_i : phase shift
- n : Total number of harmonics considered

2.2.1.4 Vandal load

Vandal loading is difficult to model and does not occur often in practice. Although intentional vibration would not fulfil the comfort criteria, the stresses produced on the structure should not make it collapse (Heinemeyer, et al., 2009).

This scenario needs to be especially treated when considering light structures which can be excited relatively easy (Živanović, et al., 2005) as it was found by Nakamura et al. (2008) where just 30 persons achieved to vibrate the whole T-bridge (Japan).

2.2.2 Crowds behaviour

The problems related with crowds' behaviour can be studied with different approaches depending on the scale of the observation of the system: single pedestrian, for a small scale, and crowd-structure interaction and response of the structure, for a large scale (Venuti, et al., 2007).

The mathematical modelling of crowd dynamics can also be developed following three different frameworks (Bellomo & Dogbé, 2008):

- Microscopic scale, the contribution of each individual is taken into account for the crowd behaviour definition, as a continuous hydrodynamic model deriving the equations as a continuous flow, with its obvious limitations regarding the possible spaces between pedestrians (Venuti, et al., 2007)
- Mesoscopic scale, statistical distribution based on the microscopic scale (Venuti & Bruno, 2009)
- Macroscopic scale, state of ensemble of individuals with averaged quantities, which is the usual description in the experimental measurements regarding crowd density, velocity and flow (Venuti & Bruno, 2009).

Following the macroscopic scale, the crowd affects the pedestrian velocity while increasing its density, i.e. the higher the density the lower the pedestrian velocity. The fundamental relation between these values is:

$$q = \rho \cdot v \tag{2.23}$$

where:

- q : flow, pedestrian passing a cross-section of an area in a unit of time [$ped/(m \cdot s)$]
- ρ : crowd density [ped/m^2]
- v : average walking velocity [m/s]

The generalized flow-density diagram, also dependant on the parameters presented at the individual level, can be observed in Figure 2.10.

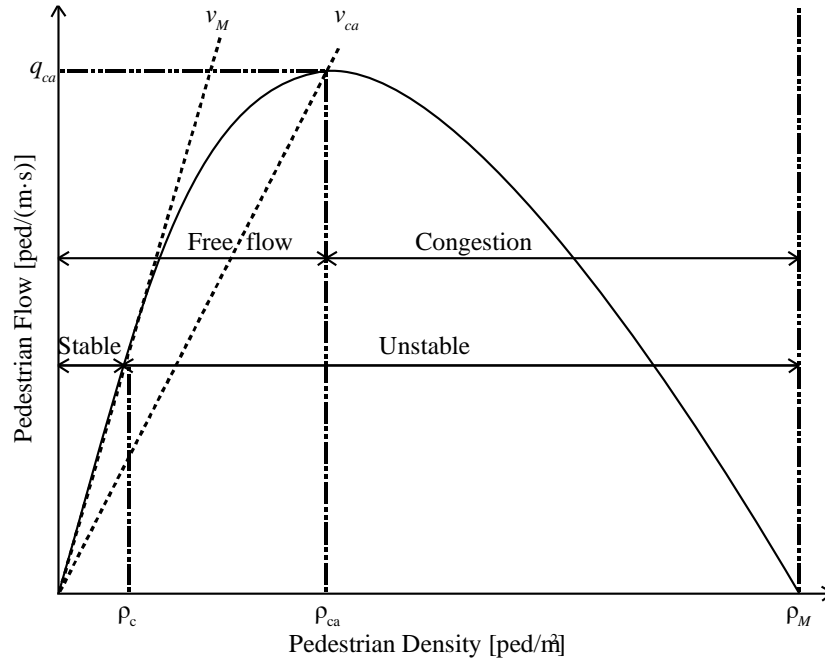


Figure 2.10. Flow-density fundamental diagram (Daamen, 2004).

where:

- v_M : Velocity of a single undamped pedestrian. Slope of the curve when $\rho = 0 \frac{ped}{m^2}$ and $q = 0 \frac{ped}{m \cdot s}$.
- ρ_c : Critical density. Density between *stable* (unconstrained free walking) and *unstable region*.
- $\rho < \rho_c$: constant free speed $v = v_M$
- $\rho \geq \rho_c$: speed decreases with the increasing of density
- v_{ca} : Capacity Velocity, for ρ_{ca} and q_{ca}
- ρ_{ca} : Capacity density. Density between the *free flow* and *congestion region*
- q_{ca} : Maximum pedestrian flow. $q_{ca} = \rho_{ca} \cdot v_{ca}$
- ρ_M : Jam density. Maximum admissible ρ , when $q = 0 \frac{ped}{m \cdot s}$

A different maximum pedestrian density has been estimated according to the minimum average body surface (Buchmueller & Weidmann, 2006) and the buffer zone “area required by the pedestrians for perception, evaluation and reaction” (Seyfried, et al., 2005).

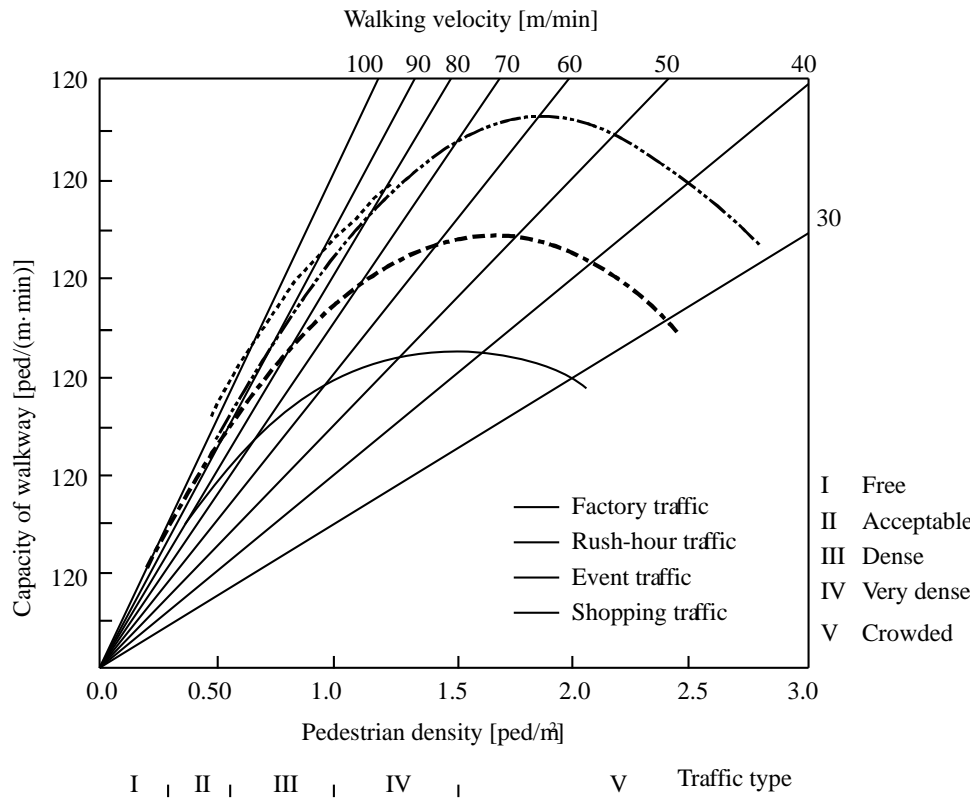


Figure 2.11. Relationship between bridge capacity, pedestrian density and their velocity, after (Oeding, s.f.).

The relation between speed and density cannot be determined including all the parameters dependant on the pedestrian behaviour, therefore a specific law should be used for each crowd condition that is defined for each footbridge capacity and traffic situation. Moreover, the fundamental diagrams, depicted in Figure 2.11, are only valid for steady-state conditions and therefore not suitable for conditions out of the equilibrium (Venuti & Bruno, 2009). Different models tried to present this phenomenon, as “turbulent behaviour” in panic conditions (Helbing, et al., 2007) and (Colombo & Rosini, 2005) and high-density situations (Seyfried, et al., 2005).

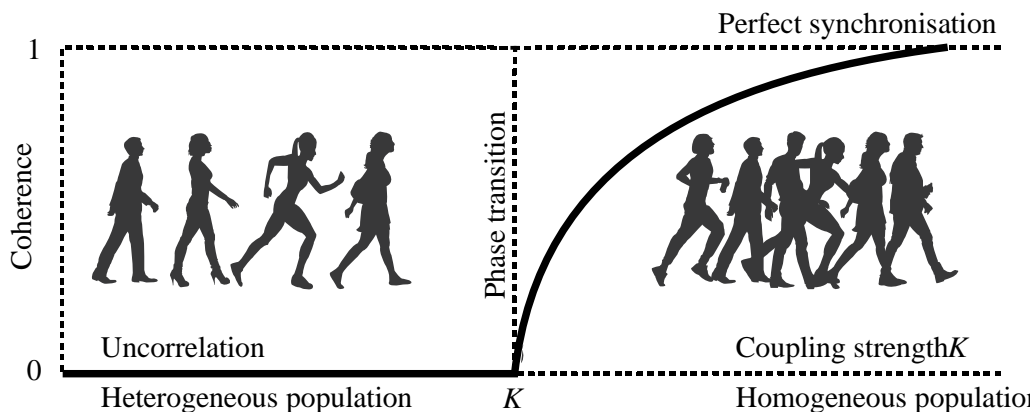


Figure 2.12. Schematic representation of the Winfree's model after Pizzimenti (2005).

It can be observed in Figure 2.12 how the phase transition changes from the uncorrelation phase till the perfect synchronisation as the people become more coherent (as the pedestrian

locks to a common frequency, in contrast with the inevitable differences on the natural frequency of each individual when not coupled) (Strogatz, et al., 2005). This phenomenon was observed in the London Millenium Bridge when, first, small groups of pedestrians started to synchronise and, when the amount of pedestrian increased a critical value, most of them were captured in the synchronisation phenomenon (Pizzimenti, 2005).

In general, codes treat the crowd issue describing different typical traffic situations depending on the amount of pedestrians per square meter of deck (Heinemeyer, et al., 2009).

2.2.2.1 Crowd-structure interaction

The movement of lively footbridges influences the behaviour of the pedestrians, and that is why a human-structure interaction occurs. This interaction is more likely to be produced in the lateral motions as pedestrians are more influenced by unconscious synchronization of their lateral frequency with the moving surface, as presented in Section 2.2.1.2. This phenomenon can be easily observed in the case of people standing or walking on moving boats or floating piers.

Furthermore, this phenomenon is greater with pedestrian crowds as they increase the effect of the pedestrian-structure synchronization (Ricciardelli, et al., 2014) and (Venuti, et al., 2005). However, the synchronization of pedestrians has been observed to diminish the vibration phenomenon in the vertical direction due to their inability to synchronize their gait to the vertical movement of the surface (Willford, 2002) and (Brownjohn, et al., 2008).

This phenomenon is reflected in the guidelines as the *Lock-in of pedestrian crowds*, which reflects pedestrian lateral synchronization limit due to the human-structure interaction. Above this limit, a sudden amplified response arises due to a vanishing of the overall damping and resonance phenomenon (Sétra, 2006) and (Heinemeyer, et al., 2009).

$$N_{crit} = \frac{8 \cdot \pi \cdot \xi \cdot m^* \cdot f}{K} \quad (2.24)$$

where:

- ξ : structural damping ratio
- m^* : modal mass
- f : natural frequency
- k : constant (300 Ns/m for 0.5 – 1.0 Hz)

Another approach is to define the trigger acceleration amplitude when the lock-in phenomenon begins:

$$- a_{lock-in} = 0.1 \text{ to } 0.15 \text{ m/s}^2$$

For activities such as running, groups of people also produce lower DLFs than when jumping alone for higher harmonics (lower harmonic leads to almost the same than for a single person). The average vertical DLFs per person in a group tend to decrease while

increasing the number of persons as the synchronism between them decreases (S. Yao, 2002,) and (S. Yao, 2003).

2.2.2.2 Force models

The crowd models are also based on the same definition criteria as presented in the introduction part of Section 2.2.1.

Using the time domain model for the description of the synchronisation among pedestrians and between pedestrians and structure, most of the force models are based on the multiplication of an equivalent number of pedestrian's single pedestrian forces. These models are based on the following assumptions (Venuti & Bruno, 2009):

- The crowd-footbridge is modelled as an oscillator with the crowd as imposed load (rather than dynamic system).
- The structural response is defined by one mode.
- The crowd is uniformly distributed along the footbridge span.
- The force is considered periodic according to Equations (2.19), (2.21) and (2.22).

There are several new models trying to define the stream of pedestrian load in footbridge, nevertheless any of them are able to include all the factors affecting the behaviour and interaction between human beings in pedestrian bridges. Venuti and Bruno (2009) have gathered different pedestrian models.

In order to take into consideration the statistical effect, several computer simulations were performed. These simulations are explained in the *Technical guide. Footbridges* (Sétra, 2006). Latest codes, as *Design of Lightweight Footbridges for Human Induced Vibrations* (Heinemeyer, et al., 2009), include this effect and define the modelling of a pedestrian stream of n random pedestrians as a stream with n' : perfectly synchronized pedestrians among themselves, in phase, walking at the natural frequency of the footbridge and evenly distributed along it. Both streams are supposed to cause the same effect.

The equivalent pedestrians' stream is:

$$n' = k_{eq} \cdot \sqrt{n \cdot \xi_i} \quad (2.25)$$

where:

- n' : equivalent number of pedestrians.
- $k_{eq} = \frac{z_i}{z'_i} \sqrt{\frac{n}{\xi_i}}$: equivalent coefficient according to Table 2.4

Table 2.4. Equivalent coefficient k_{eq}

Case	Value
Spare or dense crowd (random phases and frequencies with gaussian distribution)	$\frac{10.8}{S}$
Very dense crowd (random phases and all pedestrians at the same frequency)	$\frac{1.85}{S}$

2.3 Dimensioning for comfort

2.3.1 Receivers

Receivers on footbridges are both walking people and standing people. Their reaction is a very subjective issue where each human being reacts differently. Moreover, each person can react differently depending on the day (Griffin, 1996). Also the location and appearance of the footbridge might affect the assessment and perception of motion (HIVOSS, 2008).

The European research project HIVOSS (2008) mentions the following aspects that affect the assessment of vertical and horizontal vibration:

- Number of people walking on the bridge.
- Frequency of use.
- Height above ground.
- Position of human body (sitting, standing, walking).
- Harmonic or transient excitation characteristics (vibration frequency).
- Exposure time.
- Transparency of the deck pavement and the railing.
- Expectancy of vibration due to bridge appearance.

Lots of researchers have studied this phenomenon and widely accepted that the acceleration is the vibration parameter that should be used, even though there are situations where other parameters such as velocity can be used (Živanović, et al., 2005).

2.3.1.1 Comfort classes

The typical criterion for the assessment of comfort classes is represented as limiting the acceleration of the footbridge. Different national and international standards differ in their limits but coincide in the same band width (HIVOSS, 2008). According to Heinemeyer, et al. (2009) four comfort classes are recommended, defined in Table 2.5.

Table 2.5. Defined comfort classes with common acceleration ranges.

Comfort class	Degree of comfort	Vertical a_{limit}	Lateral a_{limit}
CL 1	Maximum	$< 0.5 \text{ m/s}^2$	$< 0.10 \text{ m/s}^2$
CL 2	Medium	$0.5 - 1.00 \text{ m/s}^2$	$0.10 - 0.30 \text{ m/s}^2$
CL 3	Minimum	$1.00 - 2.50 \text{ m/s}^2$	$0.30 - 0.80 \text{ m/s}^2$
CL 4	Unacceptable	2.5 m/s^2	0.80 m/s^2

2.3.1.2 Traffic classes

Typical traffic situations are present in Table 2.6 and depicted in Figure 2.13 according to the Guideline *Design of Lightweight Footbridges for Human Induced Vibrations* for each number of pedestrians, group size and traffic density as defined in Equation (2.23).

Table 2.6. Traffic classes

Traffic class	Density $d (P/m^2)$	Description	Characteristics
TC 1	$15 P/(B \cdot L)$	Very weak	B=width of deck L=length of deck
TC 2	0.2	Weak	Comfortable and free walking. Overtaking is possible Single pedestrians can freely choose pace.
TC 3	0.5	Dense	Still unrestricted walking. Overtaking can intermittently be inhibited.
TC 4	1.0	Very dense	Freedom of movement is restricted. Obstructed walking. Overtaking is no longer possible.
TC 5	1.5	Exceptionally dense	Unpleasant walking. Crowding begins. One can no longer freely choose pace.

Comfort requirements are mainly determined by the owner and expected pedestrian traffic should be discussed in order to specify the potential need for damping measures (HIVOSS, 2008). *Eurocode 0 – Basis of structural design* (CEN, 2002) deals with the traffic situation as different design situation loads depending on the frequency of exceeding a certain limit of comfort, defining them as:

- Persistent design situations, which refer to the conditions of permanent use.
- Transient design situations, which refer to temporary conditions.
- Accidental design situations, which refer to exceptional conditions.

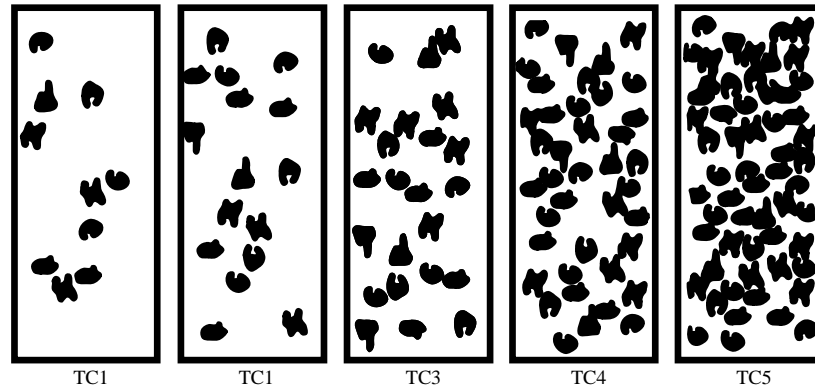


Figure 2.13. Representation of traffic classes.

2.4 Guidelines

The reference guideline for this project is the *Design of Lightweight Footbridges for Human Induced Vibrations* (Heinemeyer, et al., 2009) which is going to be taken as a base for further development of the Eurocodes. This guideline is the consequence of two previous European studies, HIVOSS (2008) and Butz, et al. (2008).

Table 2.7. Critical ranges for natural frequencies f_i of footbridges with pedestrian excitation.

Resonance by i^{th} harmonic	Direction of vibration		
	Vertical	Longitudinal	Lateral
1st harmonic	$1.25 \text{ Hz} \leq f_i \leq 2.3 \text{ Hz}$.		$0.5 \text{ Hz} \leq f_i \leq 1.2 \text{ Hz}$.
2nd harmonic ¹	$1.25 \text{ Hz} \leq f_i \leq 4.6 \text{ Hz}$.		Not affected

Defined load models consider a uniformly distributed harmonic load equivalent to the stream pedestrian load as:

$$p(t) = P \cdot \cos(2 \cdot \pi \cdot f_s \cdot t) \cdot n' \cdot \Psi \quad (2.26)$$

where:

- P : force component due to a single pedestrian with a walking step frequency f_s .

Table 2.8. Critical ranges for natural frequencies f_i of footbridges with pedestrian excitation.

P [N]		
Vertical	Longitudinal	Lateral
280	140	35

- f_s : step frequency, which is assumed equal to the footbridge natural frequency under consideration.
- n' : equivalent number of pedestrians on the loaded surface S according to Table 2.9

¹ A vertical vibration excitation by the second harmonic of pedestrian forces might take place. Until now there is no hint in the literature that significant vibration of footbridges due to the second harmonic of pedestrians has occurred.

Table 2.9. Equivalent number n' of pedestrian on the loaded surface S

$$\begin{aligned} \text{TC1 to TC3 } (d < 1.0 \text{ P/m}^2) \quad n' &= \frac{10.8\sqrt{\xi \cdot n}}{S} \text{ (m}^{-2}\text{)} \\ \text{TC4 and TC5 } (d \geq 1.0 \text{ P/m}^2) \quad n' &= \frac{1.85\sqrt{n}}{S} \text{ (m}^{-2}\text{)} \end{aligned}$$

- ξ : structural damping ratio
- n : number of pedestrians on the loaded surface

$$n = S \cdot d \tag{2.27}$$

- S : area of the loaded surface.
- d : pedestrian density
- ψ : reduction coefficient taking into account the probability that the footfall frequency approaches the critical range of natural frequencies under consideration.

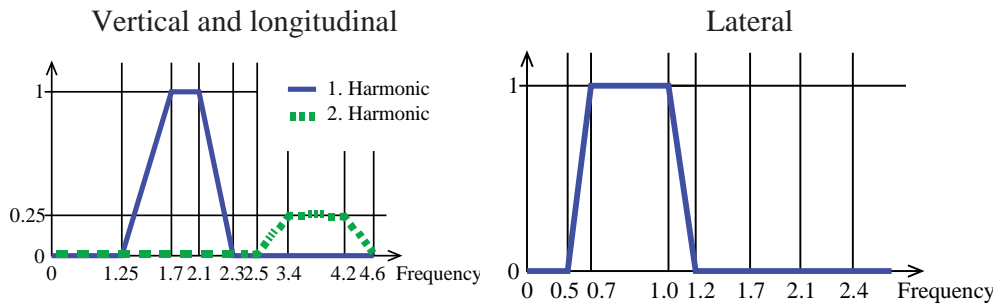


Figure 2.14. Reduction coefficient ψ

The load models depend on the considered traffic class TC1 to TC5 defined in the Section 2.3.1.2.

The latest Guideline for the modelling of pedestrian bridges suggest to accurately calculate the dampers according to the dynamic response and after building the structure measure the real values and accordingly with the real response install the needed dampers (Heinemeyer, et al., 2009)

3 Materials

3.1 Graphene

Although, the term graphene has been widely used since 2004, when Novoselov and Geim announced that they managed to isolate this monolayer material (Novoselov, et al., 2004), the story of graphene goes back to the 19th century, when some scientist already studied the wonderful properties of some graphite-based materials (Brodie, 1859). During the following decades, there was not so much research developed on this field, due to the limited tools of that time, and yet one can find important works as the ones made by Wallace (1947), McClure (1956) or Slonczewski and Weiss (1958), in which graphite-based materials, nowadays referred as graphene, were found to be able to achieve wonderful properties. However it was not until the last decade of the 20th century when the research on carbon-based materials exploded due to the development of new techniques that made easier the experimentation with nanoparticles. It was then in 2004, when Novoselov and Geim isolated a single layer of graphene with the scotch tape method, for what they were awarded the Nobel Prize in Physics in 2010 (The Royal Swedish Academy of Sciences, 2010).

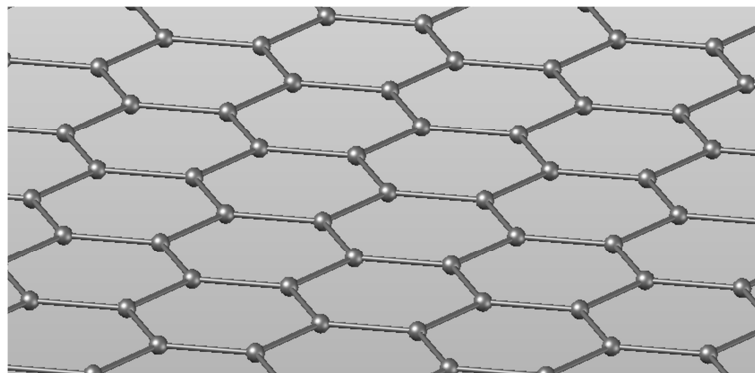


Figure 3.1. Representation of a mono-layer graphene sheet.

As mentioned before, the term graphene was not used in the beginning and was introduced by Boehm, Setton and Stumpp (1985) together with some other designations related with graphite intercalation compounds. Graphene terminology shall be used according to the authors for the material that is defined as follows:

The ending -ene is used for fused polycyclic aromatic hydrocarbons, even when the root of the name is of trivial origin, e.g., naphthalene, anthracene, coronene, ovalene. A single carbon layer of the graphitic structure would be the final member of infinite size of this series. The term graphene layer should be used for such a single carbon layer.

Graphene is therefore the flat monolayer form of the graphitic structure, which is composed of carbon atoms tightly packed into a two-dimensional honeycomb lattice (Geim & Novoselov, 2007). Graphene can be found in different forms, such as 0D fullerenes, 1D CNTs (carbon nanotubes), the basic 2D monolayer sheet or 3D graphite. CNTs are nanoparticles formed by one or several layers of graphene rolled together.

According to Monthieux and Kuznetsov (2006), CNTs were discovered by Iijima (1991), in the form of MWCNTs (multiwall carbon nanotubes). There are records that show that these particles were produced before in other experiments, but the credit for the discovery is given to Iijima due to the fact that he was the first one identifying them. Two years later, a team lead by Iijima and Ichihashi (1993) and other lead by Bethune (1993) announced with a month of difference that they produced SWCNTs (single wall carbon nanotubes).

Since the discovery of the different forms of carbon materials previously mentioned, there has been a growing research to try to develop them into materials suitable for the day life, in the form of new electronic devices as microprocessors, ultra capacity fast-charging batteries, flexible screens; new biotechnological products such as body sensors or regenerative tissue. There is also a big research to develop it into a stronger new construction material, with big efforts in the aerospace industry, as it fits very well its needs of a lighter, stronger and more environmental friendly material.

However, there has not been enough development as material usable in civil engineering. There have been some projects to use it to strengthen geopolymers or composite polymer matrices, but it has not been possible yet to see it in a more pure way with the amazing mechanical properties promised.

In this section, mechanical properties of the different mentioned forms of graphene are gathered and an extrapolation of these properties into the macroscale is presented.

3.1.1 Graphene nanoparticles

As explained in the introduction of this section, graphene can appear in different forms as a monolayer structure, or in more complex forms as fullerenes, CNT, or graphite.

There have been a lot of experimental researches in order to find the properties of monolayer graphene and CNT. However, results tend to vary a lot, due to the different measuring techniques and measured samples. The latter varies mainly in thickness and defects in monolayer graphene (Lee, et al., 2008), or in thickness, diameter, number of layers and defects in the case of CNT (Ávila & Lacerda, 2008) and (Palaci, et al., 2005).

Apart from the experimental measures, computational simulations allow to predict the properties for these allotropes. This technique yields similar results to the experimental ones.

Table 3.1 shows representative values for monolayer graphene and for SWCNTs that show the magnitude range of them in nanoscale. It is important to mention that CNTs' properties are highly dependent on its structure (Xiao, et al., 2005), which reflects the great variation in the range of properties of CNTs.

Table 3.1. Mechanical properties for monolayer graphene of 0.335 nm thickness (Lee, et al., 2008) and SWCNT of 0.335 nm thickness (Ávila & Lacerda, 2008).

Material property	Monolayer graphene	SWCNT
E (TPa)	1.0 ± 0.1	0.994 ± 0.031
G (TPa)	0.43 ± 0.04^2	0.41 ± 0.01^2
ν (-)	0.165	0.22 ± 0.07
f_u (GPa)	130 ± 10	

On one hand, the presence of defects, that may appear randomly in a large-size production make these properties only valid in the nanoscale right now. On the other hand, when used in a composite polymer, the poor interaction between graphene elements and the polymer matrix produces a critical reduction in the final properties of the materials. Therefore, the properties of composites based on graphene and an extrapolation of properties to a macroscale are studied in Section 3.1.2 and 3.1.3.

3.1.2 Graphene-based composites

The two major types of composite materials made with graphene and interesting for civil engineering are polymer nanocomposites and graphene-reinforced geopolymers. According to Potts, et al. (2011), it is in the shape of polymer nanocomposites where most of the promising applications of graphene will be done.

Polymer composites use graphene in two possible ways. The first one is using graphene as filler in a polymeric matrix (Potts, et al., 2011). The other one uses graphene to reinforce the matrix trying to enhance mechanical properties of other composites that exist nowadays (Gibson, 2010).

However, none of this yield much higher properties compared with other carbon-based materials currently produced. It is true that mechanical properties as the E-modulus, fracture toughness, fatigue strength or buckling resistance have been reported to increase, but the values achieved that can be seen in Table 3.2 are in the range of those analysed in Section 3.2. This is due to a poor interaction between graphene and the other materials involved in the polymer (Potts, et al., 2011), so there is still a lot of work to be done in this direction to achieve higher properties that resemble the ones of graphene in the nanoscale. Moreover, this interaction between an elastic matrix and rigid filler often produces a decline in tensile strength.

² Derived from the other properties using the expression: $G = \frac{E}{2 \cdot (1 + \nu)}$.

Table 3.2. Properties for different graphene-based composites collected by Potts, et al. (2011)

Composite	Property	Value
Suspended chemically modified graphene platelets	E (TPa)	0.208
Thermally expanded graphite oxide	E (TPa)	0.070
Reduced graphene oxide (5 vol%) / poly(vinyl alcohol)	f_u (MPa)	43
Graphene / Poly(methyl methacrylate)	τ_u (MPa)	2.3
CNT / polymer composites	τ_u (MPa)	47

Geopolymers are inorganic polymers similar to fly ash, which are used as concrete additions substituting OPC (ordinary Portland cement), achieving a properties-improved and more eco-friendly mixture. Geopolymers show an excellent resistance to acid and sulphate attack when compared to OPC, but, on the other hand, they have the same problems as OPC when it comes to tensile strength and fracture toughness, what makes it a brittle material. Usually, this problem is corrected using micro and nano fibres of different materials. Here is where CNTs are being studied to be used in reinforcing concrete (Saafi, et al., 2015).

The tests made by Saafi, et al. (2015), consisting of breaking 50x50x350 mm beam samples, show an increase in the stiffness and load-carrying capacity of the beams due to the addition of reduced graphene oxide sheets. Table 3.3 shows the results obtained for a graphene content of 0.5 wt%. The authors compare the increase in flexural strength, Young's modulus and flexural toughness with the increase in reduced graphene oxide in the composition. These tests showed that flexural strength and Young's modulus increase a lot until a 0.35 wt%, when the improvement starts to be small. Meanwhile the flexural toughness increases until 0.35 wt% to be reduced again after that, when increasing the graphene content to a 0.5 wt%. Figure 3.2 shows these variations for the different graphene contents analysed.

Table 3.3. Mechanical properties for a beam subjected to four-point bending tests, made with concrete reinforced with an addition of 0.5 wt% of reduced graphene oxide (Saafi, et al., 2015).

Material property	Value
Flexural strength (MPa)	7.4
E (GPa)	2.5
Flexural toughness (kJ/m ³)	1.6

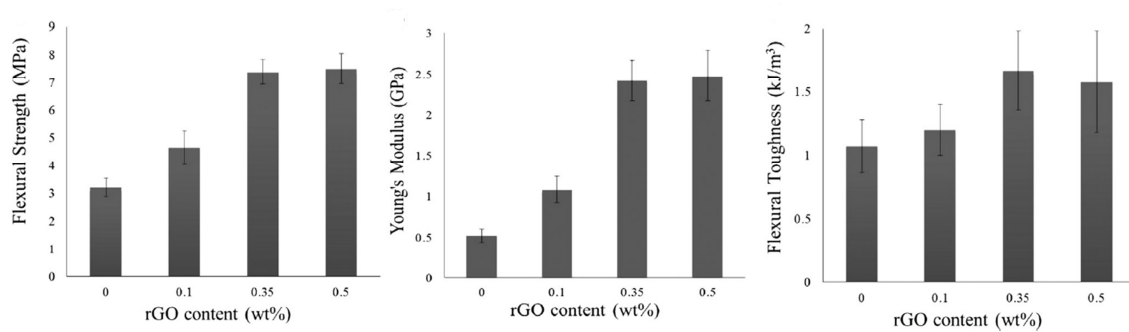


Figure 3.2. Mechanical properties for the beam tested by Saafi, et al. (2015), subjected to four-point bending tests, comparing results using concrete without additions and concrete reinforced with additions of 0.3, 0.35 and 0.5 wt% of reduced graphene oxide (rGO).

These are the first attempts of bringing graphene to the macroscale. However, properties of graphene-based composite materials are still far from its performance at the nanoscale. These results do not show any big improvement to be used in this study, and therefore another approach to mechanical properties is defined in the following section.

3.1.3 Expected mechanical properties in macroscale

The properties shown before are rather at a nanoscale in the case of Section 3.1.1 or for composite materials in Section 3.1.2, which do not show a great improvement on the mechanical properties of current construction materials such as concrete or polymer composite materials.

For this project, a further development in graphene properties is required, taking as a reference the point where the material could get in several years, when materials based in graphene, carbon nanotubes or carbon nanofibers reach properties as wonderful as they perform in the nanoscale.

Nicola M. Pugno proposes statistic approaches in order to derive the strength of graphene at macroscale, giving a value for the yielding strength of 10 GPa (Carpinteri & Pugno, 2008) and a value for the ultimate strength of 35 GPa (Pugno, 2013).

The approach made by Carpinteri & Pugno (2008) to calculate the yielding strength is based on a numerical simulation on four different size levels, from nanocomponents to the macroscale material, as it is depicted in Figure 3.3. For that, they use a spring-based model in which CNTs are used directly in the first level, with E-modulus 1 TPa (Lee, et al., 2008) and strength randomly distributed according to a Weibull distribution (Pugno & Ruoff, 2006). The result in terms of yielding stress is used as an input for the following level, and so on.

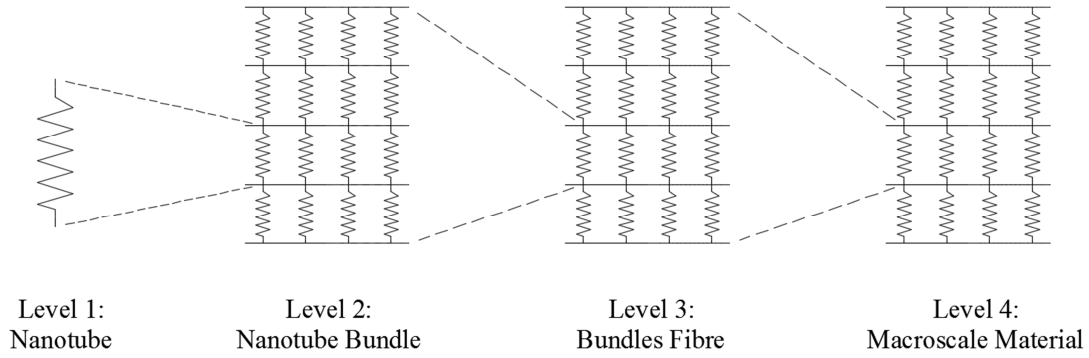


Figure 3.3. Levels approach to calculate yielding stress at macroscale. Adapted from Pugno, et al. (2008).

The authors then compare the results with an analytical model according to the multi-fractal scaling law that can be seen in Equation (3.1), proposed by Carpinteri (1994) and improved by Pugno (2006), which showed a perfect fit with the numerical simulation.

$$\frac{\sigma_f}{\sigma_{macro}} = \sqrt{1 + \frac{l_{ch}}{L + l_0}} \quad (3.1)$$

where:

σ_f : failure stress

σ_{macro} : strength at macroscale

L : structural characteristic size

l_{ch} : characteristic internal length

l_0 : defined by: $\sigma_{macro} \cdot \sqrt{1 + \frac{l_{ch}}{l_0}} = \sigma_{nano}$, σ_{nano} being the nanostrength

Thus, the result previously mentioned of 10 GPa for the yielding strength of graphene is achieved.

The ultimate strength of the material at a macroscale is approached as well by Nicola M. Pugno (2013) by means of the Quantized Fracture Mechanics theory developed by the same author. This theory combines fracture energy theory for nanocracks development with the probability of finding defects in the material at macroscale to finally determine the previously mentioned value of 35 GPa.

The E-modulus is derived by Pugno (2008) in a similar way as the yielding strength, performing multiscale simulations at different levels, to consider the presence of defects in the lattice. In this model, a scale-invariant approach is used applying a constant length/width ratio. The failure strength is distributed again using a Weibull function.

From these simulations, it is concluded that the stiffness is reduced by 22% for a randomly distributed 10% void content (Pugno, et al., 2008). Therefore, for the values from Table 3.1,

E-modulus has a reduced value of 0.78 TPa in the macroscale. It is important to notice that this reduction is not as remarkable as the one suffered by the strength of the material, which is reduced by a 73%, but it has to be taken into account.

The information available for Poisson's ratio is scarce, so establishing a value for this property is more difficult. Finding an approximation like the ones used by Pugno and his colleagues to extrapolate the other mechanical properties of graphene was not possible.

Several options were considered then. First of all, one could take raw values straight from nanoscale, but the accuracy of this is rather uncertain, as the behaviour of the material in a macroscale can be different. Taking into account what the Poisson's ratio means (i.e. the relation between transverse and axial deformation when a force is applied in one of the directions), it can be quite intuitive to think that the behaviour of a pure sheet of 2D graphene or a single CNT would not be the same when a lot of these structures were joined in a 3D continuous structure or "glued" somehow as a composite together, as there would be other mechanisms that could be more decisive when talking about these correlated deformations.

The second option considered, is to use a Poisson's ratio taken from an actual carbon-based composite material as the ones mentioned in Section 3.2. Following the previous argumentation, if one thinks about a bigger mechanism that would cause Poisson's effect, larger than the one produced at nanoscale, then it makes sense to think that it can be similar to other actual carbon-based materials, and therefore this is assumed as the most accurate way to determine it based on the information available.

At last, the chosen density for the calculations is the one used by Nicola M. Pugno in his studies about the space elevator (Pugno, 2006), which is chosen to be of $1\,300\text{ kg/m}^3$ for a low carbon density. This is interesting for this study, as we want the bridge to be as light as possible, in order to magnify the dynamic problems that may appear.

All the values previously mentioned in this section are collected in the following table:

Table 3.4. Expected graphene properties at macroscale.

Material property	Value
E (TPa)	0.78
ρ (kg/m^3)	1 300
f_y (GPa)	10
f_u (GPa)	35

3.1.4 Design properties for graphene as a construction material

Along this chapter, actual and expected properties of graphene at different levels and in different forms were collected. Graphene shows a great performance when isolated in its 2D monolayer shape, or in the form of CNTs. However, it has been seen that these properties stand only at the scale of the particles and they are reduced when put together. This is due to the presence of defects or not knowing exactly how to glue them together with good bonds.

One can expect the properties to be improved, but these problems will always be present (and only reduced), so they have to be taken into account.

The most promising form in which graphene can be used right now in the construction industry is in the way of reinforcement for geopolymers. This is ready to be used, and presents a good cement replacement technique with enhanced properties and better for the environment. However, properties of this mixture are too far from the magnificent ones of graphene in nanoscale, and therefore this was discarded to be the material used in the study.

On the other hand, the graphene-based composite materials developed until now do not show a big improvement compared with other carbon-based composite materials that are in use right now. This is why it was decided not to use this type of graphene in the analysis. It was considered better to use material properties extrapolated from actual composite materials, well tested and with a known behaviour that can yield more realistic results.

Properties shown in Table 3.4 have been decided to be our design properties for a graphene-based material. They do not represent a material that can be used nowadays, but show in a rational way where graphene can be taken in the following years, presenting an ultra-lightweight material, with high stiffness and resistance that takes the analyses of this thesis to a more extreme point, in order to magnify dynamic problems in the footbridges to analyse.

3.2 Other high-performance materials: Fibre reinforced polymer composites

Fibre reinforced polymer (FRP) composites consists of one or more discontinuous phases (reinforcement) embedded in a continuous phase (matrix) with an interface between them acting as bond (Estrada & Lee, 2014).

Matrices are mainly formed by polymers (thermosets or thermoplastics) in construction materials, but in other applications, composites can also be formed by metal (high-temperatures) and ceramics (ultra-high temperatures) (Estrada & Lee, 2014). The matrices transfer the loads to the fibres and protect them.

The properties of the reinforcement are highly dependent on their type and geometry. Two main families can be found: fibre-reinforced (or fibrous reinforced) and particulate-reinforced, which depend on if the composites have their properties derived from the reinforcement or the matrix respectively. (Estrada & Lee, 2014). Only fibrous reinforced composites will be discussed, due to their high performance properties and a great demand in civil engineering. Fibre reinforcement composites are typically glass, carbon and aramid.

3.2.1 Polymer matrices

Polymers matrices can be classified depending on if their reaction with heat is permanent, thermosets, or temporary, thermoplastics. In Table 3.5 the advantages and disadvantages of polymer matrices are reflected (Estrada & Lee, 2014).

Table 3.5. Advantages and Disadvantages of Polymer matrices.

Advantages	Disadvantages
Low cost	Low strength and stiffness
Ease of processing	Low operating temperature
Low density	Deterioration due to ultraviolet radiation exposure
Good chemical resistance	Degradation of mechanical properties due to moisture absorption

There are three main types of thermosetting resin polymers (Bank, 2006).

- Polyester (Orthophthalic, Isophthalic or Terephthalic):
 - Adequate for structural purposes
 - Low cost
- Epoxy:
 - Mostly for adhesive purposes or for tendons
 - Excellent to corrosion
 - Low shrinkage
 - High cost
- Vinyl ester:
 - Hybrid between polyester and epoxy
 - Durability in alkali conditions

3.2.2 Fibre reinforcement

3.2.2.1 Glass fibres

There can be found different types of glass fibres depending on their performance and composition (Estrada & Lee, 2014) (Bank, 2006).

- E-Glass (electrically non-conductive).
- A-Glass (alkaline resistant). Used as main material for glass windows.
- S-Glass (High strength and stiffness). Mostly used in aerospace industry.
- C-Glass (corrosion resistant). Used in structural engineering.
- R-Glass (High strength and stiffness).
- D-Glass.

3.2.2.2 Carbon fibres

Carbon fibres have a great performance for structural engineering strengthening sheets, fabrics, strips, tendons or cables. Graphite fibres are the ones formed by 90% or more elemental carbon and carbon fibres are formed by 80%-90% of elemental carbon (Estrada & Lee, 2014).

3.2.2.3 Aramid Fibres

Aramid fibres are one of the best organic fibres. Mainly used for impact and ballistic protection due to their high toughness (Estrada & Lee, 2014). Their properties make them of poor performance for structural engineering.

3.2.2.4 Comparison of fibres.

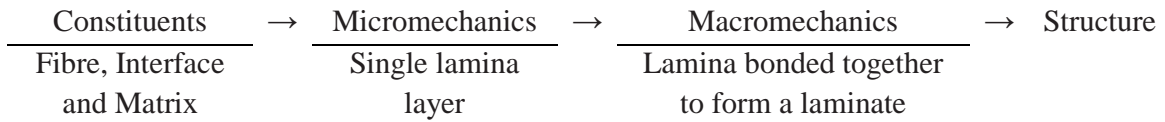
In Table 3.6 a list of advantages and disadvantages for the mentioned reinforcement are reflected.

Table 3.6. Advantages and Disadvantages different kind of fibres (Estrada & Lee, 2014).

Component	Advantages	Disadvantages
Glass fibres	<ul style="list-style-type: none"> Low cost High strength Hardness Corrosion resistance Chemical inertness 	<ul style="list-style-type: none"> Low modulus of elasticity Poor abrasion resistance (lowering strength, need of protective coatings) Poor adhesion with matrix, especially in the presence of moisture (need of chemical coupling agents such as silane)
Carbon fibres	<ul style="list-style-type: none"> High specific strength High specific stiffness Resistance to hot and moisture Resistance to fatigue 	<ul style="list-style-type: none"> High cost
Aramid fibres	<ul style="list-style-type: none"> High toughness Low-density High strength-to-weight ratio High stiffness-to-weight ratio 	<ul style="list-style-type: none"> Low compressive strength Susceptibility to creep Moisture absorption Sensitivity to UV light Temperature-dependant mechanical properties High cost

3.2.3 Use of FRP in construction

Three different levels for the characterization of the structural behaviour of FRP can be defined from the primary elements previously defined.



Each lamina constitutive matrix for transversely isotropic material, i.e. lamina oriented in principle direction of orthotropy, is described in Equation (3.2).

$$\begin{Bmatrix} \sigma_1 \\ \sigma_2 \\ \tau_{12} \end{Bmatrix} = \begin{bmatrix} Q_{11} & Q_{12} & 0 \\ Q_{12} & Q_{22} & 0 \\ 0 & 0 & Q_{66} \end{bmatrix} \begin{Bmatrix} \varepsilon_1 \\ \varepsilon_2 \\ \gamma_{12} \end{Bmatrix} \quad (3.2)$$

where:

- σ_1, σ_2 : normal stresses
- τ_{12} : shear stress
- $\varepsilon_1, \varepsilon_2$: shear strain
- $Q_{11} = \frac{E_1}{1-\nu_{12}\cdot\nu_{21}}, Q_{12} = \frac{\nu_{21}\cdot E_1}{1-\nu_{12}\cdot\nu_{21}}, Q_{22} = \frac{E_2}{1-\nu_{12}\cdot\nu_{21}}, Q_{66} = G_{12}$

Fibres can be aligned at an angle θ to the structural axis, so the principle direction of orthotropy may not coincide with the structural coordinates. The piling of different lamina that forms the laminate can be fibre-orientated with different angles, and therefore will form an orthotropic material with three principal axes (1,2, and 3 in Figure 3.4).

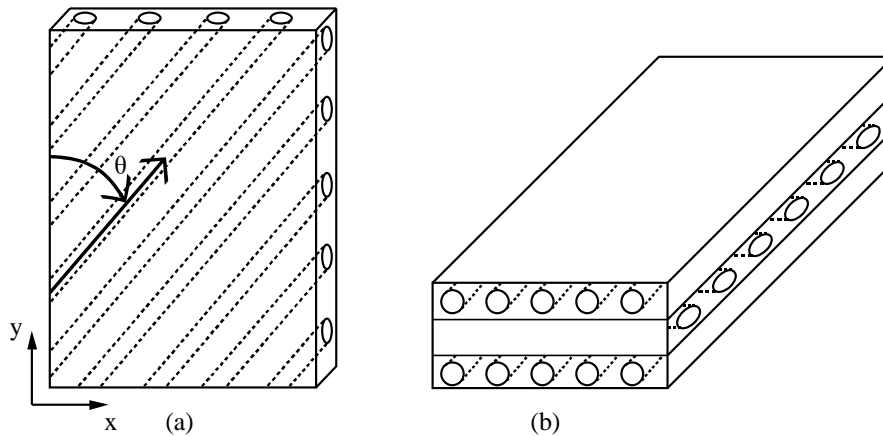


Figure 3.4. a) Composite plate with fibre alignment θ b) Laminate configuration (Estrada & Lee, 2014)

However, as the behaviour in transverse and vertical axes (2 and 3 in Figure 3.4) is nearly equal, the system is not a fully 3-D orthotropic material but a transversely isotropic system. Applying the corresponding transformations (Estrada & Lee, 2014) the strain relations for a lamina of arbitrary orientation can be obtained.

According to the Fiberline Desing Manual (2003), used as reference in the present study, FRP properties are represented in Table 3.7. Fiberline profiles are formed by a matrix of

low-profile quality of either isophthalic polyester or vinyl ester with overlay veil reinforced with E-glass roving with woven and complex mattings.

Table 3.7. Typical dry properties of FRP (Fiberline Composites A/S, 2003).

Property	Symbol	Value	Units
Flexural strength, 0°	$f_{b,0^\circ}$	240000	kN/m^2
Flexural strength, 90°	$f_{b,90^\circ}$	100000	kN/m^2
Tensile strength, 0°	$f_{t,0^\circ}$	240000	kN/m^2
Tensile strength, 90°	$f_{t,90^\circ}$	50000	kN/m^2
Compressive strength, 0°	$f_{c,0^\circ}$	240000	kN/m^2
Compressive strength, 90°	$f_{c,90^\circ}$	70000	kN/m^2
Shear strength	f_τ	25000	kN/m^2
Pin-bearing strength, longitudinal direction	$f_{CB,0^\circ}$	150000	kN/m^2
Pin-bearing strength, transverse direction	$f_{CB,90^\circ}$	70000	kN/m^2
Modulus of elasticity	E_{0°	23000000/28000000	kN/m^2
Modulus of elasticity	E_{90°	8500000	kN/m^2
Modulus in shear	G_{0°	3000000	kN/m^2
Poisson's ratio	$\nu_{0^\circ,90^\circ}$	0.23	-
Poisson's ratio	$\nu_{90^\circ,0^\circ}$	0.09	-

4 Structural types

To define a conceptual bridge, different structural types have to be taken into account in order to analyse their structural behaviour.

A graphene-based footbridge concept could be defined based on several structural types due to the already presented properties. The case of study is a single span where a combination of different lengths, widths, boundary conditions and material configurations are analysed for different cross-section types. For the selection of the cross-section types different experiences in FRP-based pedestrian bridges are studied taking into account their dynamic behaviour.

The main problem of these structures is the vibrations produced under pedestrian loads, and the best variable to quantify that effect is the acceleration. The cross-section geometries are selected according to rough calculations in ULS and the possibility of increasing the frequency of vibration of the structure.

The vibrations of the structure are a consequence of the application of a load with a frequency of vibration close to one natural frequency of the structure. The load frequencies applied by pedestrians are rather low, see Table 2.2, and therefore higher natural frequencies of vibration of the structure are desired. The natural frequencies calculation can be obtained from the simplified formula (Sétra, 2006).

$$f_n = \frac{\lambda_n}{2\pi L^2} \cdot \sqrt{\frac{EI}{\rho S}} \quad (4.1)$$

where:

- $\sqrt{\frac{E}{\rho}}$: material dependant factor, with:
 - E : Poisson's moduli
 - ρ : Density of the material
- $\sqrt{\frac{I}{S}}$: section geometry factor, with:
 - I : moment of inertia
 - S : Area of the cross-section
- λ_n : shape-of-beam factor, according to Table 4.1.

Table 4.1. Influence of the boundary conditions on the natural vibration frequencies. (CECM, 1989)

λ_n	$n = 1$	$n = 2$	$n = 3$	$n = 4$	$n = 5$	$n > 5$
Simply supported	9.87	39.5	88.9	158	247	$[n \cdot \pi]^2$
Double fixed	22.4	61.7	121	200	298	$\left[(2 \cdot n + 1) \cdot \frac{\pi}{2}\right]^2$

Therefore, to reduce the acceleration on a footbridge, the geometry of the cross-section should have a high moment of inertia with reduced area.

4.1 Holländerbrücke

This pedestrian bridge is a replacement structure in Reinbek near Hamburg, in FRP with several short-length spans. The elements of the orthotropic deck, FBD300, made of glass-FRP with a height of 80 mm. The deck elements are not bonded to the steel girders. The steel beams have a separation of 1.8 m and are stiffened by support spans of 1.3 m to increase the stiffness and load-bearing capacity of the structure (Sobek & Trumpf, 2008).

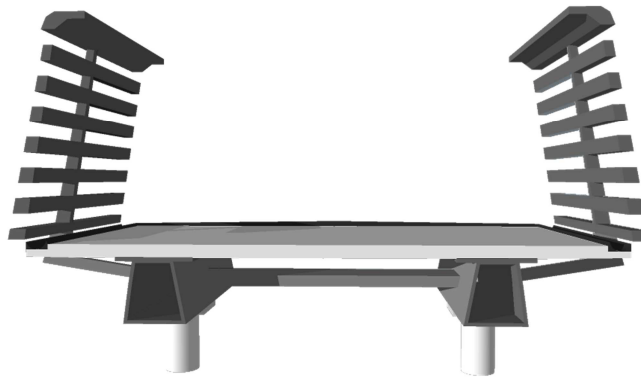


Figure 4.1. Representation of the Holländerbrücke.

This bridge is an adaptation of a bridge concept developed by FiberLine Composites based on an orthotropic deck with a set of beams in the deck depending on the width of the bridge considered (Sobek & Trumpf, 2008).

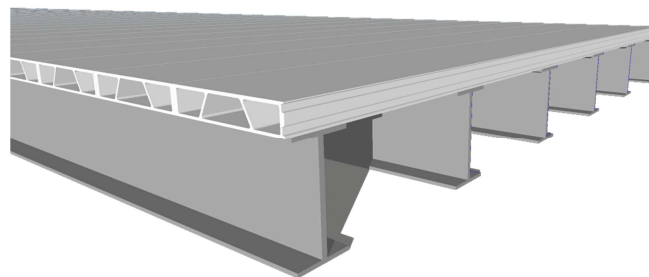


Figure 4.2. Representation of the bridge concept.

4.2 Stanislas pedestrian bridge

This pedestrian bridge located in Delft was built in 2007 by Lightweight Structures B.V. to substitute a concrete and steel old bridge. It has a total length of 44 m with a maximum span of 13.5 m and width of 1.5 m. Both deck and girder are made of Glass-FRP .

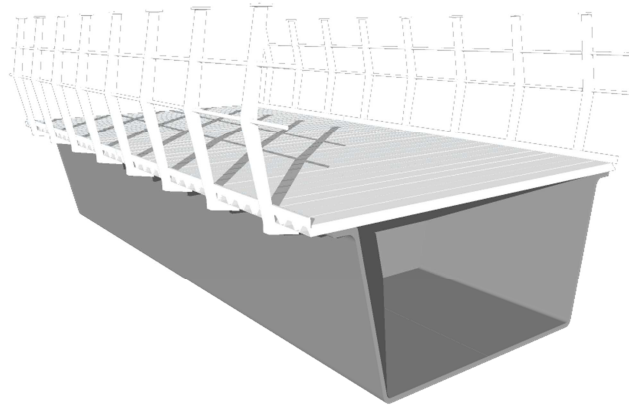


Figure 4.3. Representation of the Stanislas pedestrian bridge in Delft.

4.3 Almuñecar pedestrian bridge

Built in 2010 with a total length of 44 m, it is currently the longest span built with FRP. It is made of resin infusion with carbon fibres and a thickness of 50 mm. It is provided with longitudinal and transversal stiffeners along the bridge (Acciona infraestructuras, 2013).

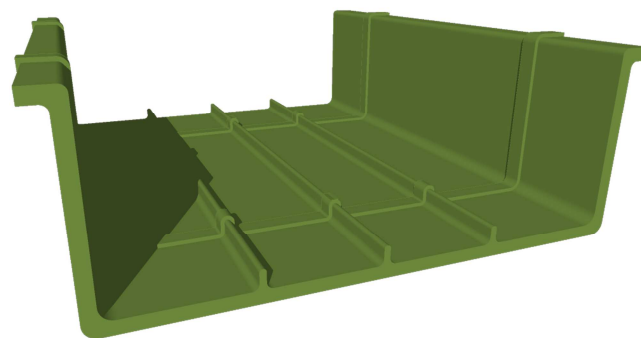


Figure 4.4. Representation of Almuñecar pedestrian bridge in Madrid.

4.4 King Stormwater Channel Bridge

Built in the year 2000 in California, USA, this continuous road-bridge of two spans of 10 m length each and 13 m width, is composed of six Carbon-FRP tube-beams filled with concrete and an orthotropic deck of E-Glass FRP (Canning, 2014).

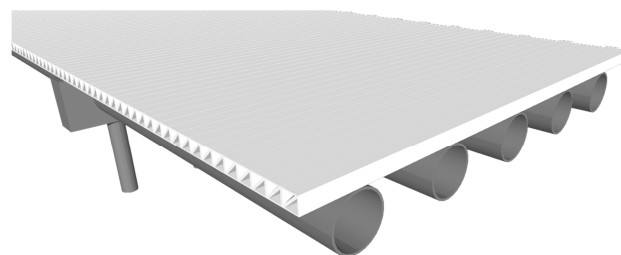


Figure 4.5. Representation of the King Stormwater Channel Bridge in California

4.5 Full orthotropic deck

4.5.1 Korea road-bridge

This cross-section type is part of a Korean bridge deck superstructure completely built with composite materials. The whole deck is made of Glass-FRP. The elements are made of sandwich structures with corrugated cores. This provides a high stiffness per unit weight ratio (Hyo, et al., 2010).

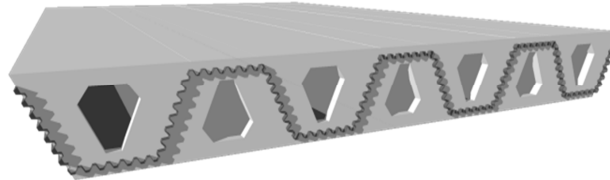


Figure 4.6. Representation of the full orthotropic bridge in Korea.

4.5.2 Klipphausen road-bridge

First German's composite bridge built in Dresden area in 2004. Made of Glass-FRP by Fiberline[®]. The cellular profile are spanning longitudinally with FDB600 ASSET profile. The bridge has a total length of 6.6 m and a width of 6 m (Canning, 2014).

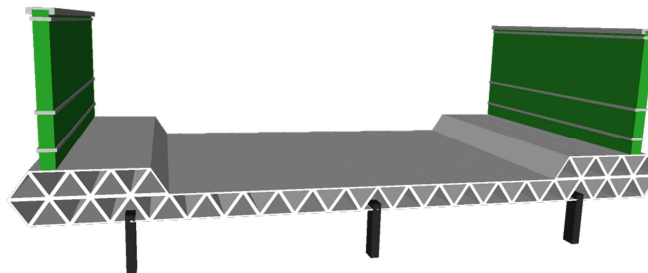


Figure 4.7. Representation of the full orthotropic deck in Dresden

4.5.3 Hollow-core deck

This cross-section has a longitudinal behaviour similar to a series of I-beams and transverse behaviour similar to a castellated beam. The webs are made of fly-ash filled with resin and the top and bottom parts are made of Glass-FRP. The webs provide shear and torsional resistance and carry the loads to the supports (W. Davey, et al., 2001).

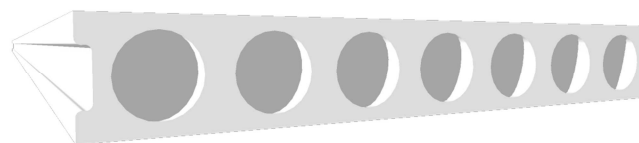


Figure 4.8. Representation of the Hollow Core Deck concept.

5 Methodology

The aim of this process was to evaluate the variation trend for different cases without specifically focusing on the solution of each individual bridge. Therefore the strategy used during this study was to analyse a great number of bridges, varying dimensions, cross-sections and materials in order to compare the change produced in their dynamic behaviour.

NCC provided this study with a bridge concept to use as a reference and to validate the set-based design of the geometries. The bridge consisted of two stainless steel beams with varying height and a concrete deck, 35 m long and 5 m wide.

When designing a bridge, the engineer could follow two different paths in order to design the structure, design for static analysis and adapt the solution so that it fulfils the dynamic requirements or vice versa. Consequently, it could have been decided to design the structure so that it first fulfils the dynamic requirements, as it is the main scope of this work, but this is not how it is done usually and would not yield comparable results. From that point of view, it was considered more interesting to follow the first procedure: first doing the static design and then checking if the dynamic comfort criteria are fulfilled, as this is a more common procedure.

Therefore, the structures simulated in this project were designed to fulfil ULS and SLS in the most optimal way for each case. Then, those geometries were analysed according to the dynamic criteria to check if they fulfilled the comfort requirements from the Eurocodes, as described in the Guideline (Heinemeyer, et al., 2009). At this stage the level of performance under dynamic excitations was evaluated and the behaviour of the structures concluded according to the comfort criteria.

In order to find the optimal configuration that fulfils the limit states, a set-based design approach was carried out. This procedure enabled the geometries to be obtained in a realistic and objective manner. As explained later in this section, loading cases and checks were simplified, as it is not the scope of this study and this whole procedure just aims to provide consistent geometries to be compared in dynamic analysis.

5.1 Bridge description

The structure to analyse consisted of a one span bridge fixed at both ends. The geometry of the cross-section varied as depicted in Figure 5.1. The geometry is intended to be adapted to the shape of the moment distribution for the type of boundary conditions and loads considered.

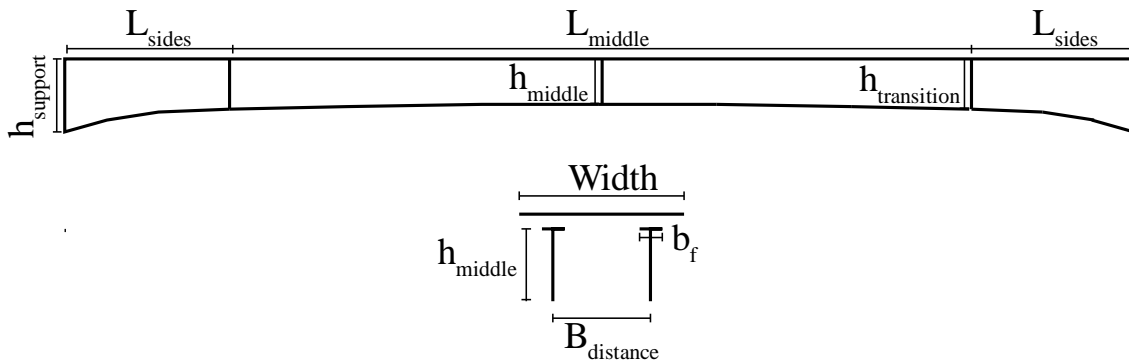


Figure 5.1. General longitudinal profile sketch of the studied bridges.

Span lengths in this study started from the NCC reference case of 35 m, and were ranged from 50 m to 300 m with an increment of 50 m.

Three different widths, 2.5 m, 5 m and 10 m were studied for each span case. They tried to represent three specific bridge cases: pedestrian bridges with low traffic (2.5 m), commonly built in places with a low population density; pedestrian bridges with medium traffic (5 m), typical in urban areas; and pedestrian bridges with high traffic (10 m), which are usual in the centre of big cities. With this range, it is the intention to cover all the different situations that may be designed.

In order to evaluate the influence of the geometry in the dynamic response, two different types of cross-sections were evaluated to consider the effect of the sectional stiffness, comparing an open section, hereafter referred to as II-beams, and a closed section, referred to as Box girder.

The II-beams case matched the NCC concept, used to validate the design process. This model was also used to make some assumptions in order to fix the relations between some parameters of the cross-section. The details of each cross-section are presented in APPENDIX A.4

All these combinations produced enough results to evaluate the aimed dynamic behaviour trend of the studied cases.

5.2 Static design

As mentioned before, a set-based design procedure was used to design the bridges under static loads. For that, a MATLAB code was developed in order to check all the possible combinations for a range of values. The optimal section, defined as the one both maximising the slenderness and minimising the weight, was then automatically selected, as depicted in Figure 5.2. This criterion was selected as it was believed to give the most interesting geometries to evaluate the dynamic behaviour of the structures.

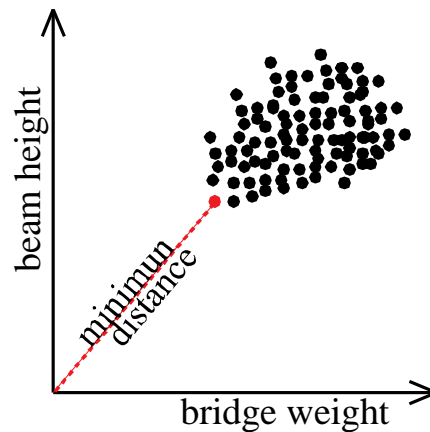


Figure 5.2. Bridge optimization criterion from set-base design process.

Static loading cases follow the rules and limits required in Sweden for bridge design by Trafikverket, reflected in TVRK Bro 11 and Eurocodes 0 and 1. For simplicity, only loading after construction of the structure is considered, taking into account self-weight, a dead weight of non-structural elements of 5 kN/m^2 and the pedestrian variable load.

The design of the steel beams with concrete deck was done according to Eurocodes 2, 3 and 4. In order to calculate FRP and graphene sections, a guideline from Fiberline Composites A/S (2003) was used.

The ULS checks were done in the critical sections for the studied bridges, i.e. at the support, transition and middle span and SLS was checked only for deflection. Steel girders were assumed of cross section class 1 or 2 as high bending capacity and low beam height were desired, thus plastic theory applies (CEN, 2006). For FRP and Graphene girders elastic theory had to be used (Fiberline Composites A/S, 2003).

Full interaction between the girder and the deck was concluded as the most optimal for all studied cases. This case is obvious for all cases but the steel girder and orthotropic deck were a combination between plastic and elastic theory applies, in Section A.4.2.1 all the details are explained.

A limitation of the study was the evaluation of global buckling of the structure. However, this assumption is not believed to influence the results of this study as the global dynamic behaviour of the structures should not be affected.

The bridge geometry was calculated from *fixed* and *variable parameters* to avoid large computation time and achieve comparable geometries. Geometry limitations and fixed parameters were settled as a result of an analysis of geometry relations from IPE profiles. These simplified the problem and avoided solutions with unreasonable geometry. In Section A.2 and Section A.3 these parameter definitions are detailed and justified. Therefore, the considered geometry is the following:

- Fixed parameters
 - Bridge length
 - Bridge width

- Height-to-flange thickness relationship according to what showed in Section A.2.1
- Variable parameters
 - Beam height at the support
 - Web thickness at the middle and the sides' part
 - Flange thickness:
 - Same at the sides and the middle.
 - Same at top and bottom for the II-beams bridge and different for the Box girder.
 - Deck thickness
 - Checked for transversal direction for all cases.
 - Checked for longitudinal direction for Concrete bridges.
 - For the concrete deck the minimum thickness was set to 0.2 m to let enough room for the rebars.
 - For the orthotropic deck the variation was proportional with the deck flanges that were considered the resistant parts as presented in Section A.4.3.2.
- Geometry limitations consequent of IPE relationship analysis
 - Web thickness-to-beam height.
 - Flange thickness-to-web thickness.

5.3 Dynamic analysis

The process was automatized by the creation off three python scripts in order to ease the procedure and avoid human mistakes in the handling of that amount of data. This is further described in Section 5.5.

The dynamic study was performed using the geometries generated with the static design tool. The eigenfrequencies and modes of vibrations were then obtained from BRIGADE for each case. Later, each bridge case was processed so that the dynamic load case could be properly applied when the natural frequencies were within the range defined by Eurocode 1. The sinusoidal time-varying pedestrian loads were applied according to what is reflected in Section 2.4 so that the different traffic classes and comfort classes were included. These were defined following the recommendations stated in the Guideline (Heinemeyer, et al., 2009) and reflected in Table 5.1

Table 5.1. Selected traffic and comfort classes.

Traffic Class	Density $\left(\frac{p}{m^2}\right)$	Comfort Class	Vertical acceleration $\left(\frac{m}{s^2}\right)$	Lateral acceleration $\left(\frac{m}{s^2}\right)$
TC2	0.2	CL1	0.5	0.1
TC3	0.5	CL2	1.0	0.3
TC4	1.0	CL3	2.5	0.8

It is important to remind that each dynamic load was applied following the shape of the vibration mode, as it was presented in Section 2.4. An example of this is depicted in Figure 5.3.

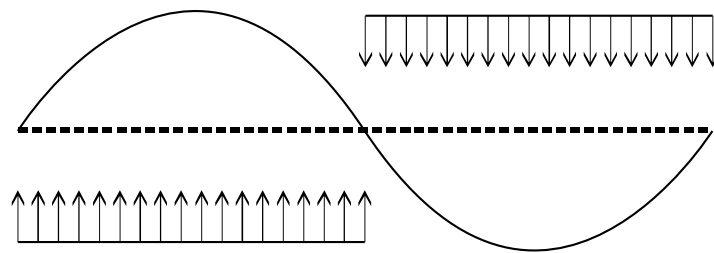


Figure 5.3. Example of a 2nd harmonic of vibration with pedestrian loads direction matching the mode shape.

5.4 Extraction of results

Accelerations were obtained in two different points at middle span. One located at the middle of the bridge width and the other one at the side, as depicted in Figure 5.4.

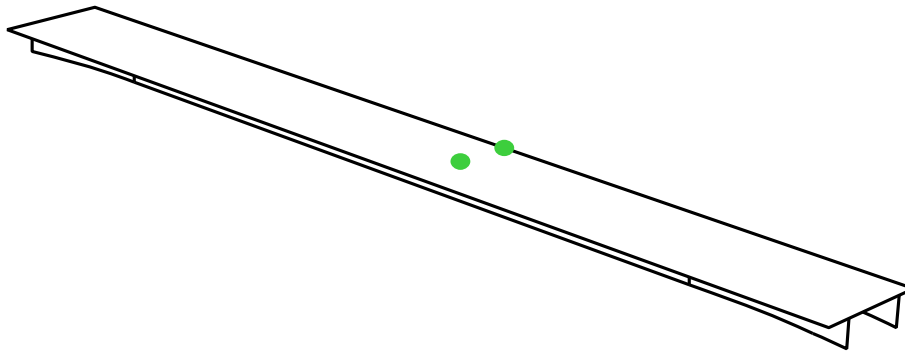


Figure 5.4. Location of analysed accelerations in the bridge deck.

These points were selected as middle span is the worst case for the fixed boundary conditions and taking into account that depending on the vibration mode and type of loading the worst case could be located at any of these two spots.

Accelerations were calculated with the mode superposition method, as explained in Section 2.1.5. According to what was presented in Section 2.1.6, the number of modes to be used in this summation method had to give, at least, a mass participation of 90% for the displacements in each direction (linear or rotational). For some big models, this condition needed a high number of eigenvalues to be used in the longitudinal direction increasing the computation time too much. Thus, it was disregarded for these cases, as the response in the longitudinal direction was negligible due the characteristics of the loads and boundary conditions.

The calculations were carried out for a simulation time of 150 s, as it was observed that at this point, the structure response was already damped. This simulation time had to be predefined before the calculations were done and further checked that the damping phenomenon was really achieved, as depicted in Figure 2.3.

5.5 Work flow

All the process carried out in BRIGADE was scripted in python in order to create an automatized workflow that would save time and avoid accidental mistakes while creating all the bridge geometries, applying loads and obtaining the results.

The process had to be divided in three steps: *Pre-processing*, *Pedestrian loads* and *Post-processing*. Each step loaded some parameters that were either inputs for each step or results from previous steps, with those parameters; it defined geometries and job definitions that were afterwards run by the user.

The Pre-processing step, summarized in Figure 5.5, defined all parameters that needed to be input by the user to be used in the whole analysis. It generated the bridge with the considerations defined in APPENDIX A. The self-weight step was defined, in order to check that the model behaved properly. The eigenfrequencies extraction case was also implemented.

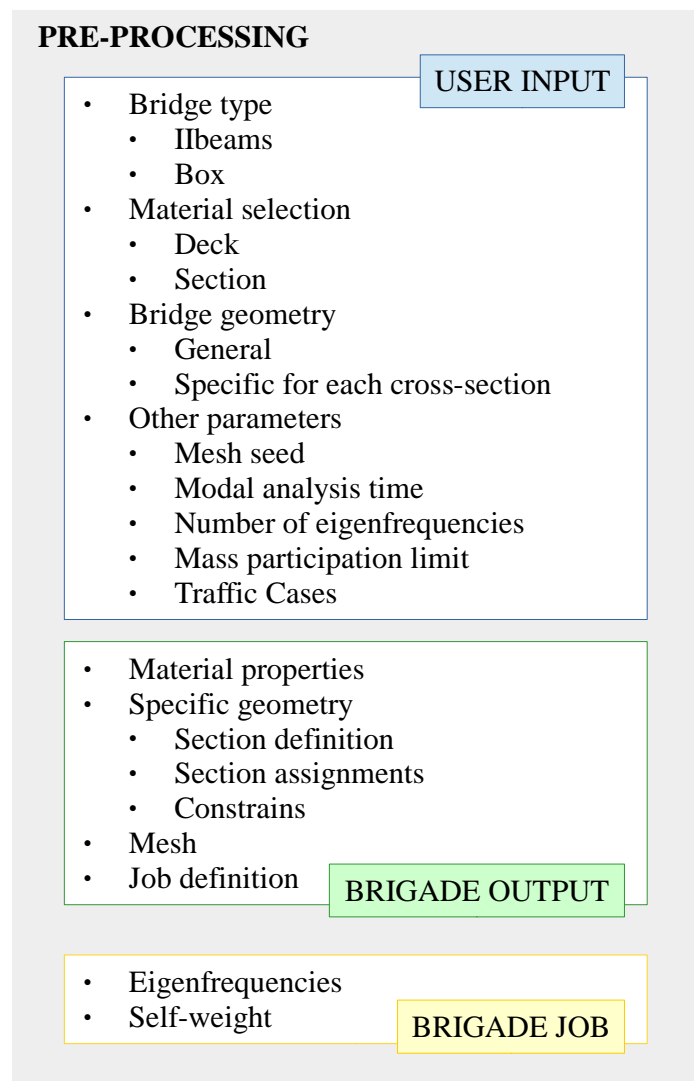


Figure 5.5. Pre-processing workflow chart.

The second script to run, after the previous job was concluded, was the Pedestrian Load script, summarized in Figure 5.6. From the eigenfrequencies calculated before, the dynamic loads were applied to the model, if a dynamic analysis was necessary, according to the Guideline and what was explained in Section 5.3.

At this stage, the user had to check here if the load had a harmonic mode of vibration greater than one and thus, had to be adapted to the mode shape, according to what was explained in Section 5.3. The step with the pedestrian loads was then created by the script.

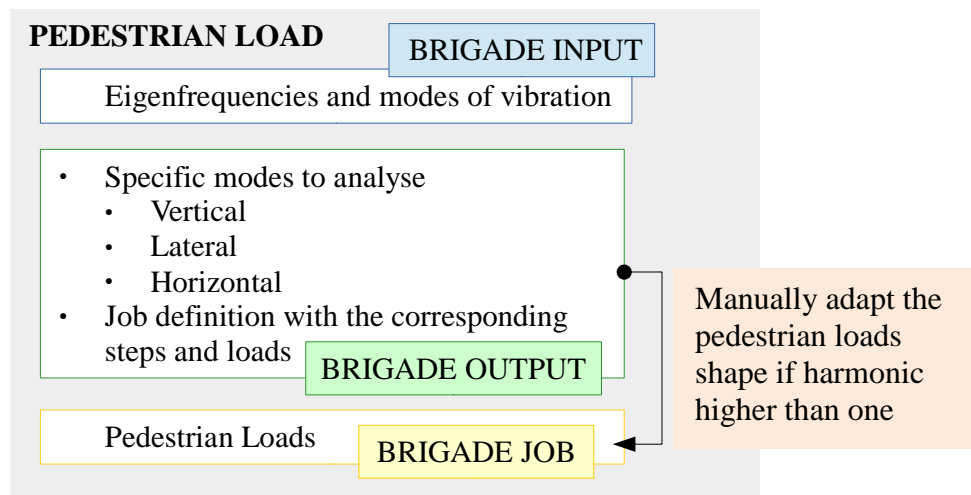


Figure 5.6. Pedestrian Load workflow chart.

The Post-processing phase, summarized in Figure 5.7, used a last script to create an output file, with the desired results. This results were formatted by an excel macro to show them in a more intuitive way.

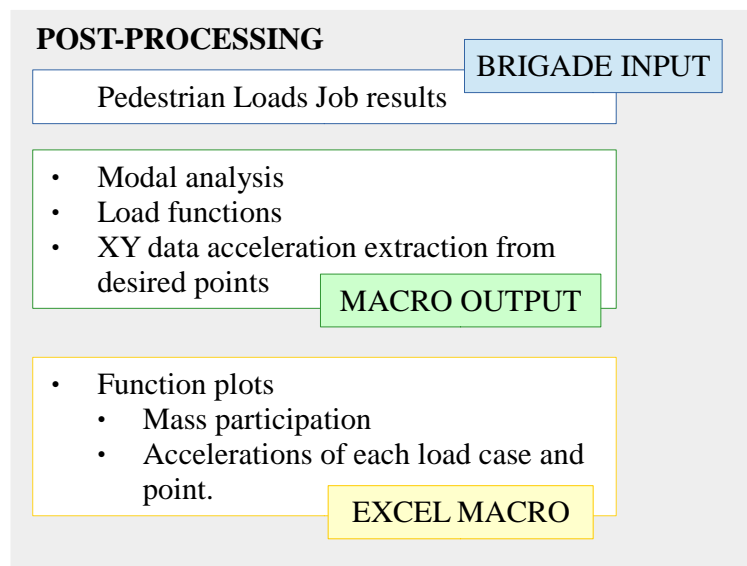


Figure 5.7. Post-processing work flowchart.

Moreover splitting the process in three different steps made possible to visualise some intermediate results that could be interesting for the discussion part.

5.6 Limitations

The limitations of the present study are both the ones given by the codes and the ones that were assumed during the present document:

- Several limitations were used to find the geometries in the set-base design. Only basic ULS and SLS checks were used as mentioned in this section and detailed in APPENDIX A.
- Pedestrian loads were simplified according to the Guideline. Therefore the limitations that are stated in the Guideline were assumed.
- The appliance of the load according to the mode of vibration was done matching the harmonic just in the longitudinal direction as it is reflected in the examples of the Guideline.
- Some material properties had to be assumed due to lack of studies or contradictions between references. Specially, graphene properties came from numerical predictions.
- An equivalent orthotropic deck had to be used, as the more detailed one created a big number of elements, enlarging the analysis time.

6 Results

In this section some results are presented to exemplify and analyse the performance of the studied bridge cases. These results are presented isolating different variables, in order to analyse the influence of span length, bridge width or the behaviour of the different materials. A collection of tables with all the results, with eigenfrequencies and accelerations for each case, is presented in APPENDIX C.

Eigenfrequencies and accelerations have been studied in order to come up with conclusions. The first are analysed as a behaviour trend in order to extrapolate the performance and influence of each parameter while the latter are the results of the cases that, according to Eurocode 1, had to be analysed.

It can be observed that two dotted horizontal lines are included in the charts presented in Section 6.1. These lines mark the limits for the frequency ranges defined in Eurocode 1: 0.5 – 1.2 Hz for lateral vibrations and 1.25 – 2.3 Hz for vertical vibrations. Hence, accelerations were calculated for the frequencies within these ranges.

These results should be interpreted not only by comparing if modes have an increase or decrease in their natural frequencies, but also in the location of them close to the previously mentioned limits.

6.1 Natural frequencies

6.1.1 Influence of span length

Eigenfrequencies are plotted against length in Figure 6.1, Figure 6.2 and Figure 6.3. They all show what it seems to be a hyperbolic decreasing pattern while length increases. Two or three families of eigenfrequencies clearly appear in each case, which correspond to different modes of vibration. Each of them follows the same trending line and has approximately the same mass participation factor. In some specific situations, modes of these families seem to be divided in two different frequencies, which have a sum of mass participation ratios equal to the rest of the family. This is exemplified in Figure 6.1.

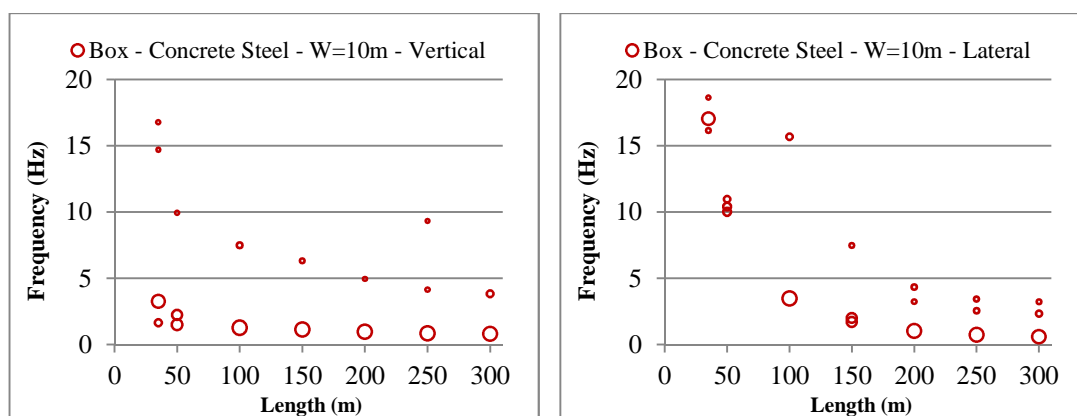


Figure 6.1. Example of mode families. The area of the bubbles is proportional to the mass participation factor.

Figure 6.2 shows a plot of eigenfrequencies for the four different material cases and one width, plotted against bridge length, for vertical modes. It can be observed that Concrete-Steel, FRPSteel and FRP cases show a similar pattern, while eigenfrequencies for Graphene bridges have usually higher values. The difference in the eigenfrequencies between the studied cases is greater for shorter bridges while for larger ones they tend to closer values.

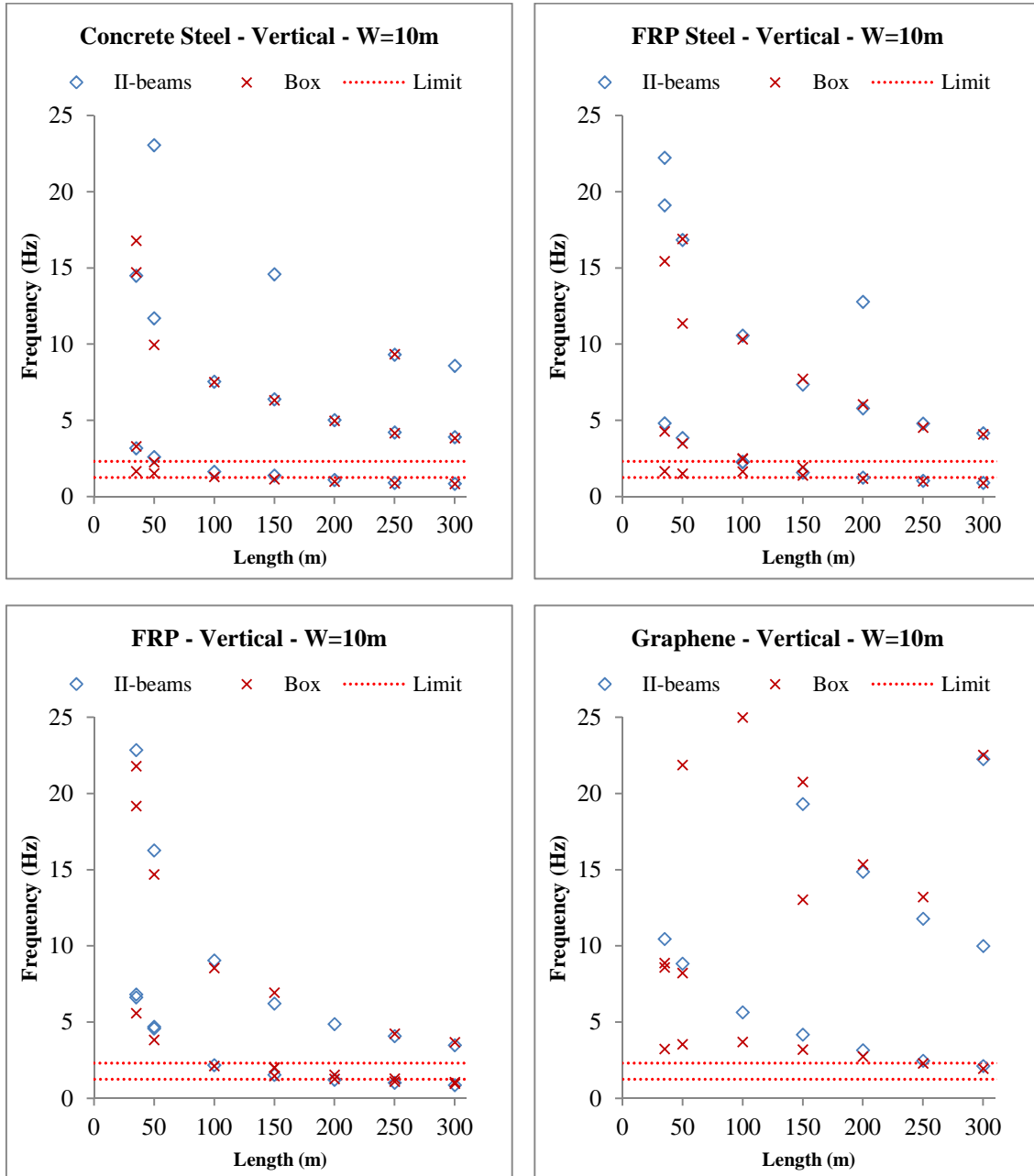


Figure 6.2. Frequency-Length plots for vertical modes and W = 10 m.

The plots for the lateral modes of the eigenfrequencies are shown in Figure 6.3. Here it is observed how the three existing materials gave similar results, while Graphene, once again, proved to have higher frequencies, especially for short bridges.

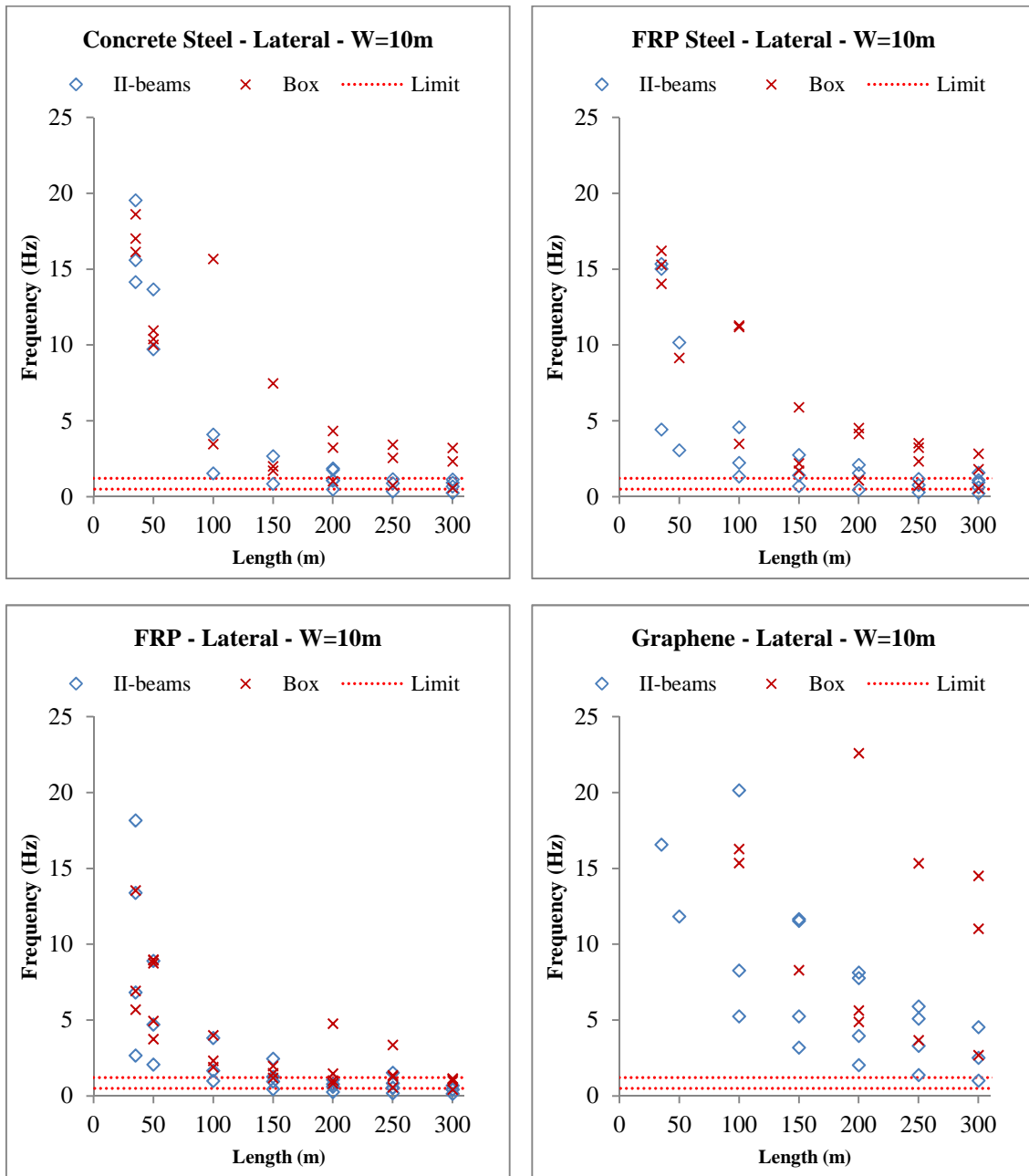


Figure 6.3. Frequency-Length plots for lateral modes.

6.1.2 Influence of width variation

The variation of frequencies for vertical modes did not follow any recognizable pattern when increasing the width. As an illustration of this, Figure 6.4 depicts 35 m long bridges for all the material combinations and cross-sections.

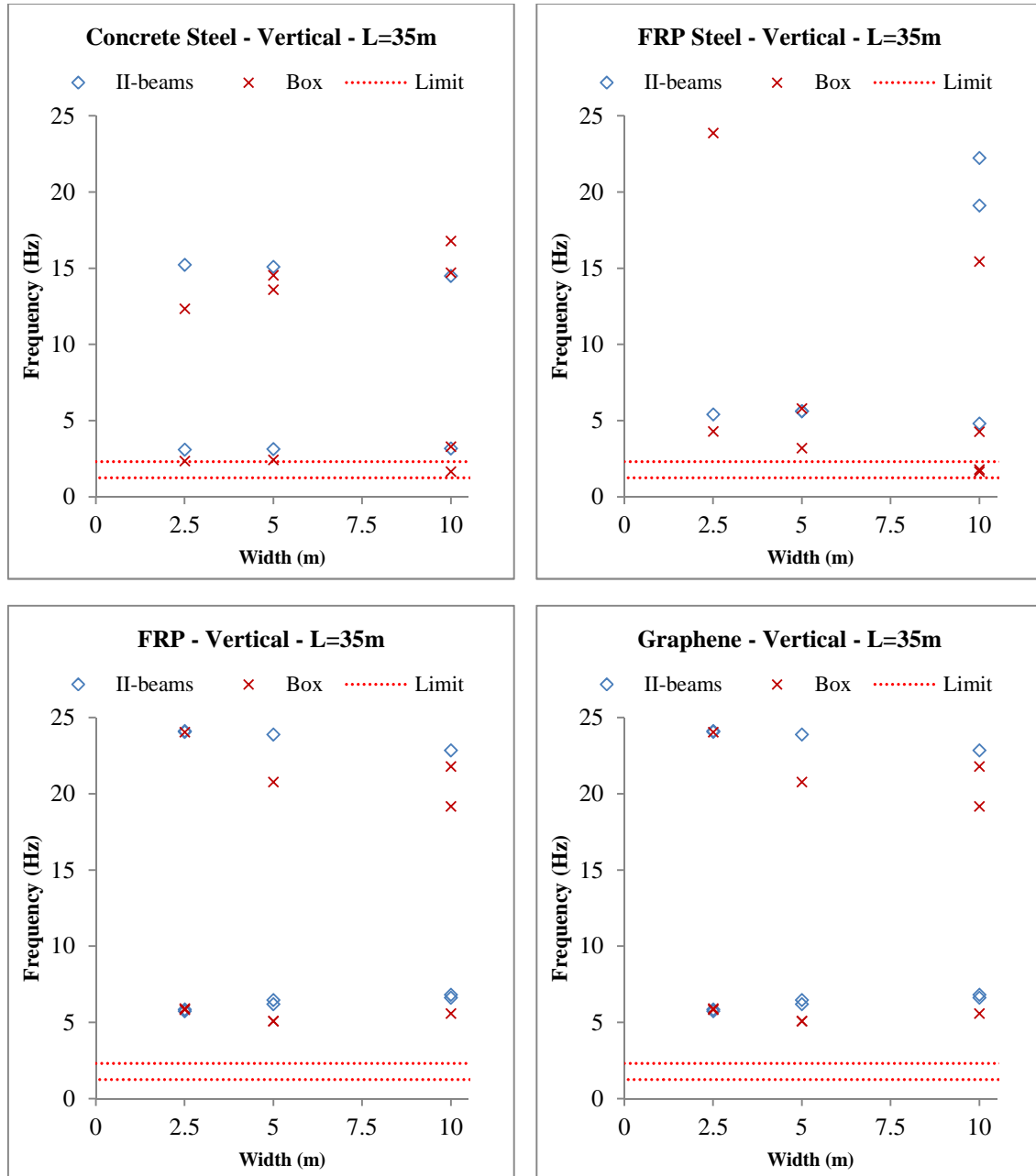


Figure 6.4. Frequency-Width plots for vertical modes for L=35m.

Figure 6.5 collects some of the frequency-width charts for lateral modes. The left column shows these graphs for Concrete-Steel and the right column for Graphene, both for 50 m, 150 m, and 250 m. They serve as examples for the rest of the cases, which can be checked in detail in APPENDIX C. Unlike vertical modes, these ones show a rising trend for wider bridges.

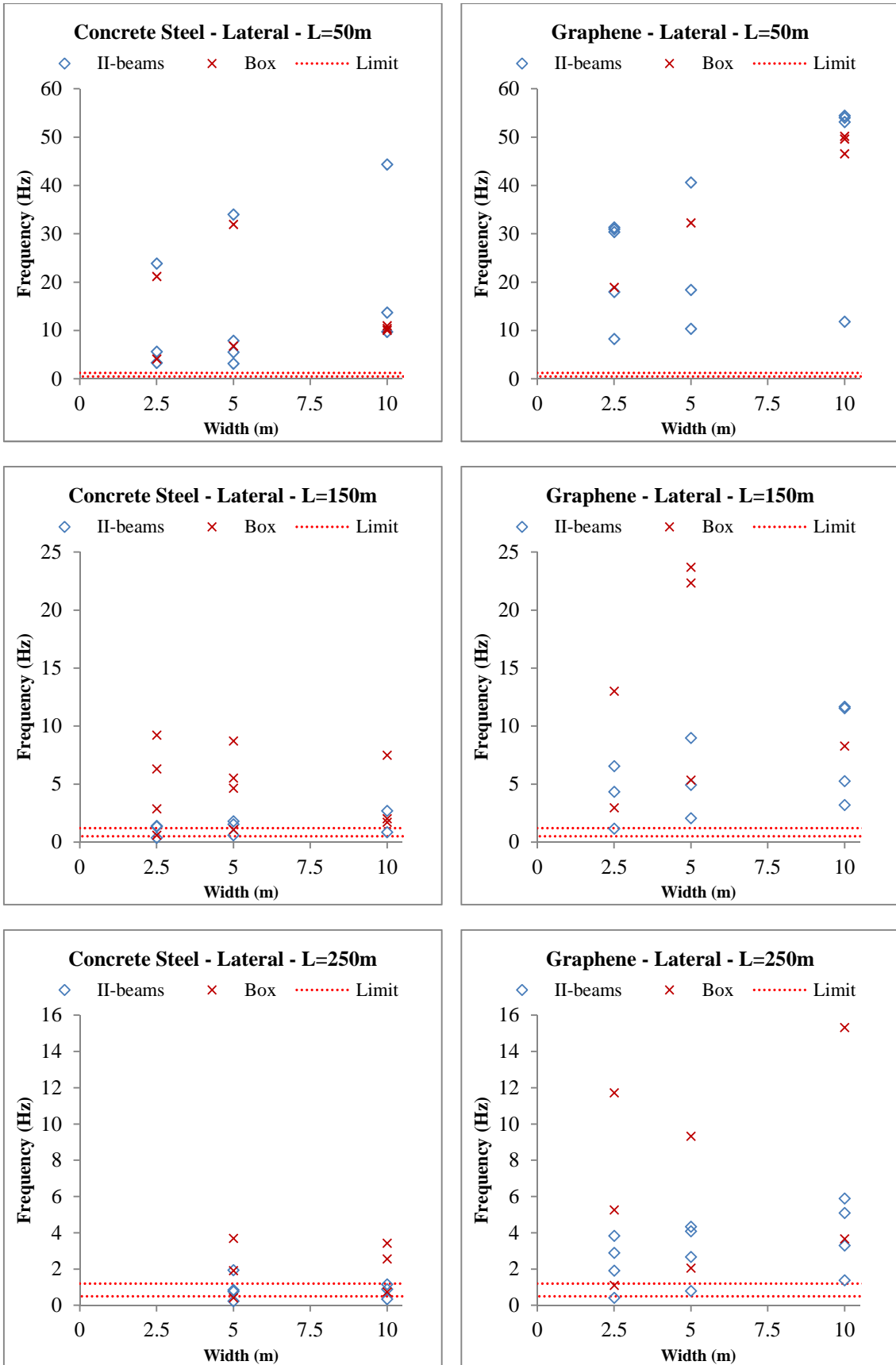


Figure 6.5. Frequency-Width plots for lateral modes for lengths 50 m, 150 m and 250 m (notice that plots have a different vertical scale for each length).

6.1.3 Materials comparison

The influence of the material used is isolated in the charts presented in Figure 6.6 and Figure 6.7. Vertical modes are presented in the left column and lateral modes in the right one.

Graphene shows higher eigenfrequencies when compared with Concrete-Steel, FRP-Steel and FRP. The same was pointed while analysing the influence of the length, in Section 6.1.1. However, among the latter materials a behaviour pattern could not be observed from these results.

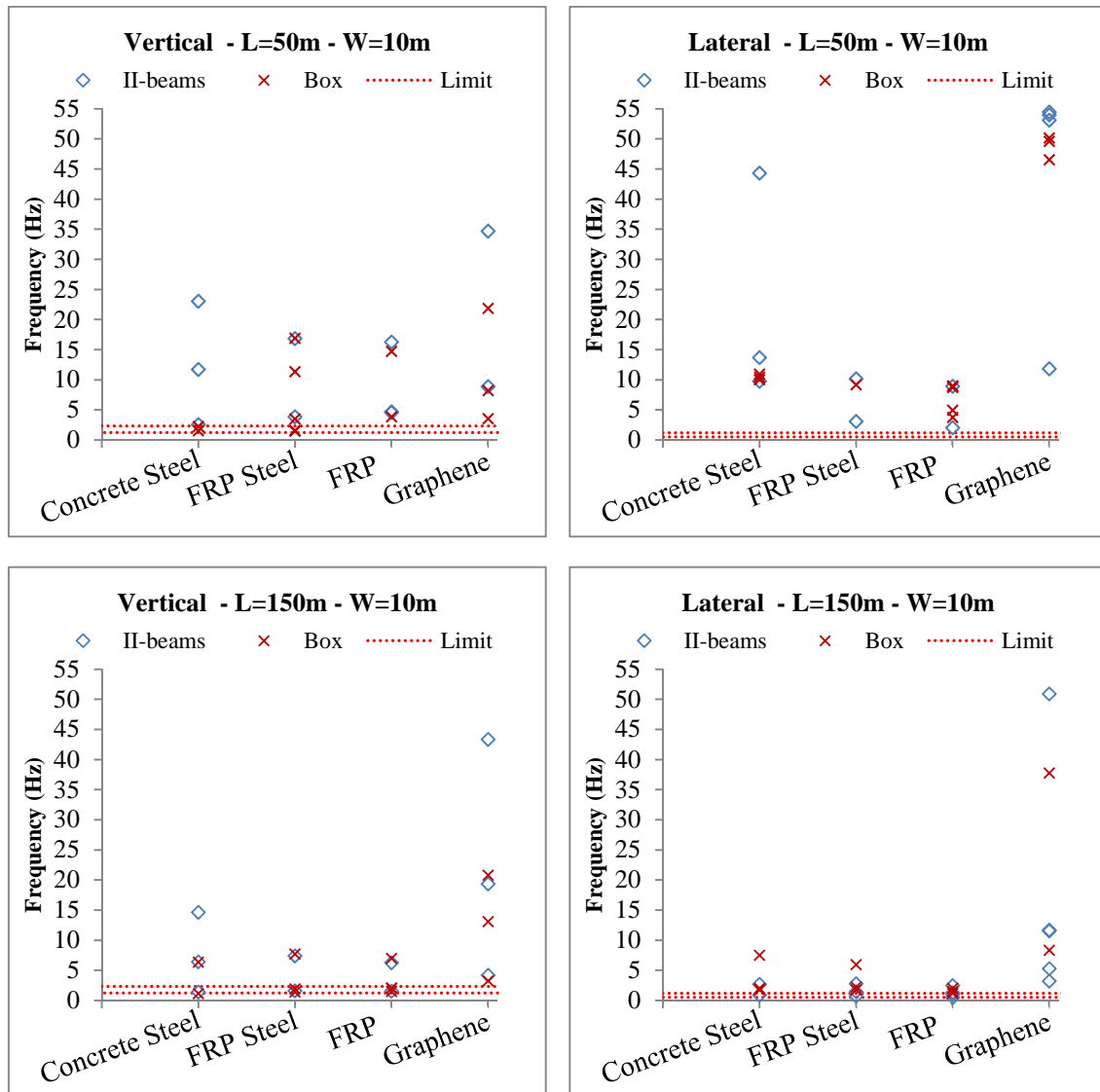


Figure 6.6. Frequency-Material plots for lengths 50 m and 150 m, and width 10 m.

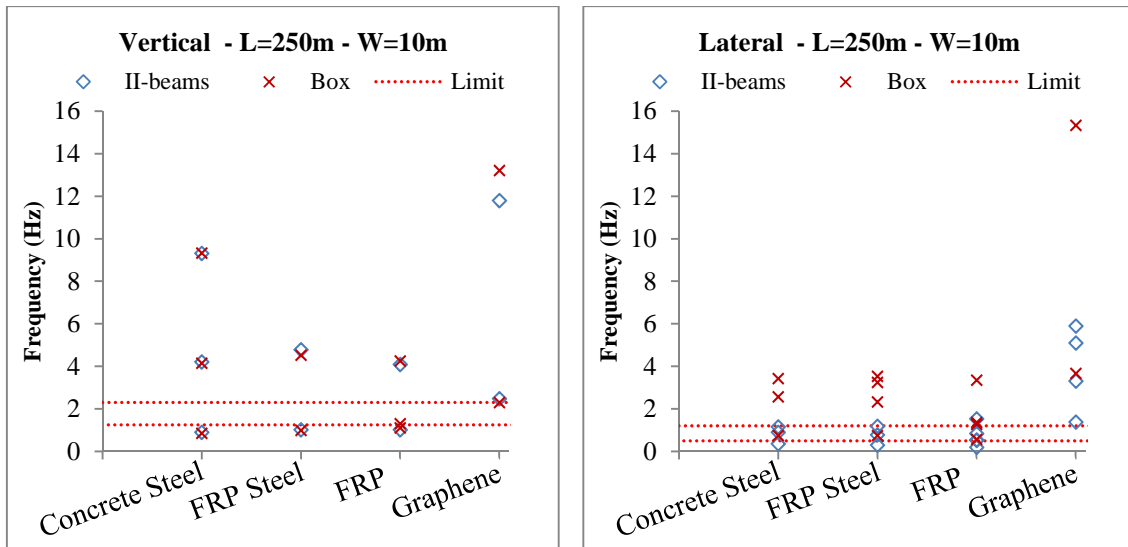


Figure 6.7. Frequency-Material plots for lengths and 250 m and width 10 m.

6.2 Accelerations

The accelerations were calculated for the cases where the eigenfrequencies were in the range stated by Eurocode 1, according to the loads recommended by the Guideline, as explained in Section 2.4. Therefore, they were a consequence of the bridge cases considered in the present study.

The results were plotted in order to be able to analyse them and try to find pattern behaviours. The accelerations are presented in APPENDIX C together with the rest of the results, and plots can be found in APPENDIX D. The main interest on the acceleration is the relation between the oscillation direction and the general behaviour of each bridge, more than the global magnitude.

In Figure 6.8³ the vertical accelerations for the Concrete-Steel bridge with box girder are plotted. There it can be easily found that for the cases where the three widths had to be evaluated the biggest accelerations were found for the narrowest case.

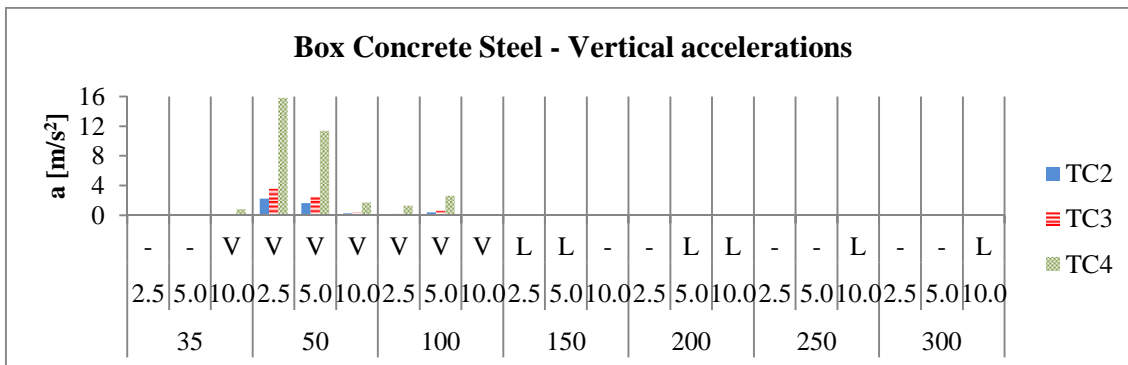


Figure 6.8. Vertical accelerations for the Box Concrete Steel bridge.

³ V and L stands for Vertical and Lateral predominant modes of vibration respectively

The problems for Graphene bridges appeared in general for larger bridges, as it was perceived in the eigenfrequency study in Section 6.1. In Figure 6.9⁴ the vertical accelerations for the Graphene bridge with Box girder are plotted.

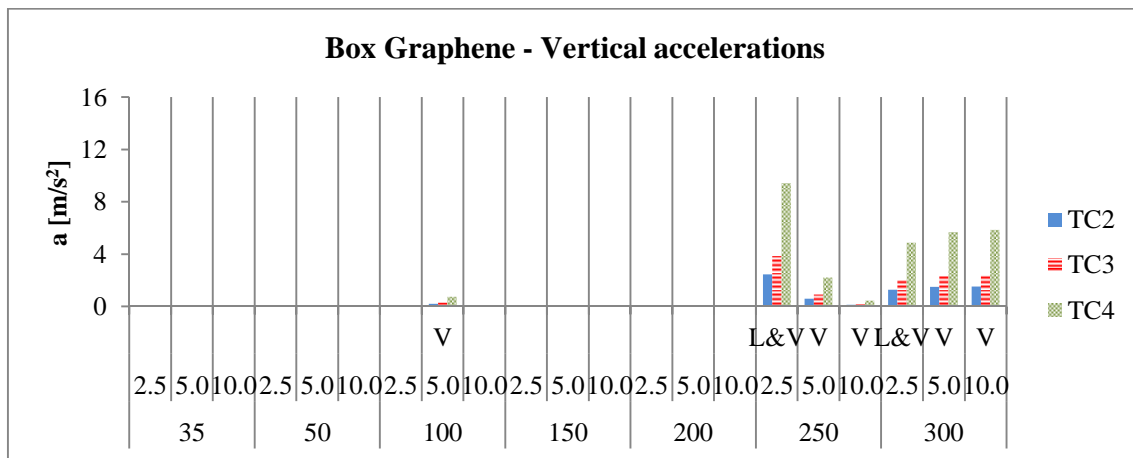


Figure 6.9. Vertical accelerations for the Box Graphene bridge.

The lateral accelerations did not show any remarkable relationship between them. Thus, their charts are just shown in APPENDIX D.

6.3 Summary charts

The figures presented in this section, Figure 6.10, Figure 6.11, Figure 6.12 and Figure 6.13, summarise the results previously presented in a more simple way. They analyse according to Eurocode 1 and the Guideline if the different bridges fulfil the requirements stated in them.

Figure 6.10 and Figure 6.11 gather the performance for vertical vibrations for the II-beams cross-section and the box girder. It can be observed how the response is more or less the same for both sections in this case.

⁴ See Footnote 3

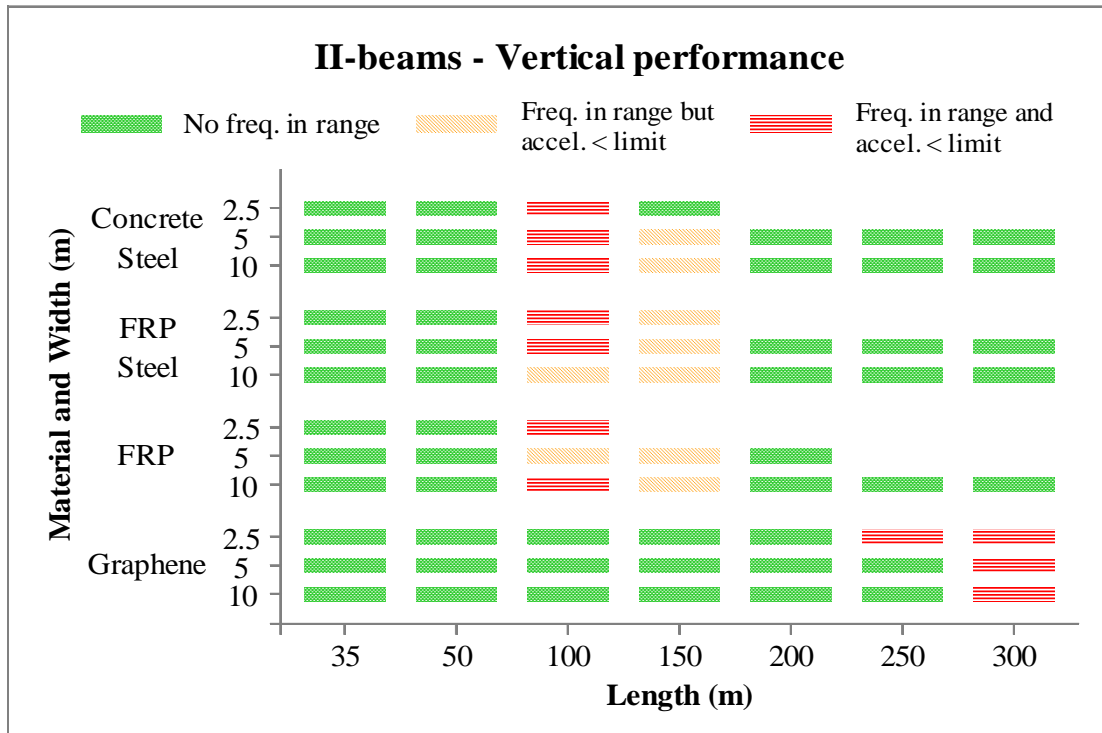


Figure 6.10. Summary table for the vertical performance of the II-beams section.

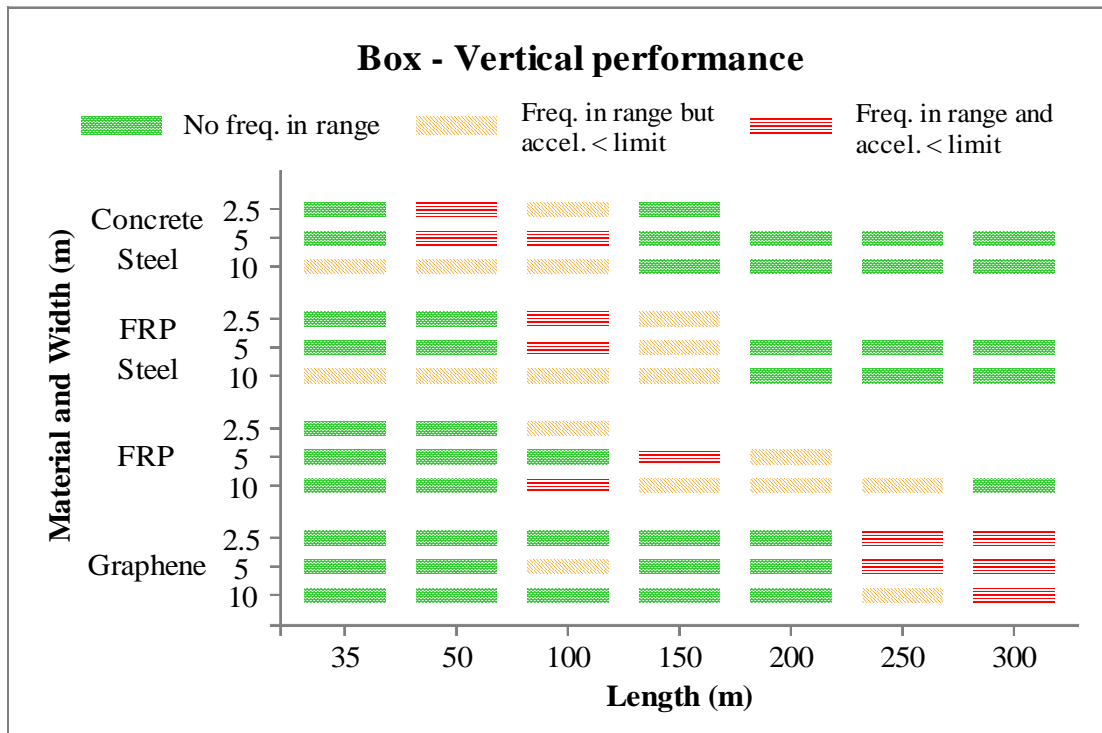


Figure 6.11. Summary table for the vertical performance of the Box section.

The performance under lateral vibrations is shown in Figure 6.12 and Figure 6.13. In this case, it can be seen how the problems disappear almost completely for bridges lower than 200 m, when the section is closed using the box girder.

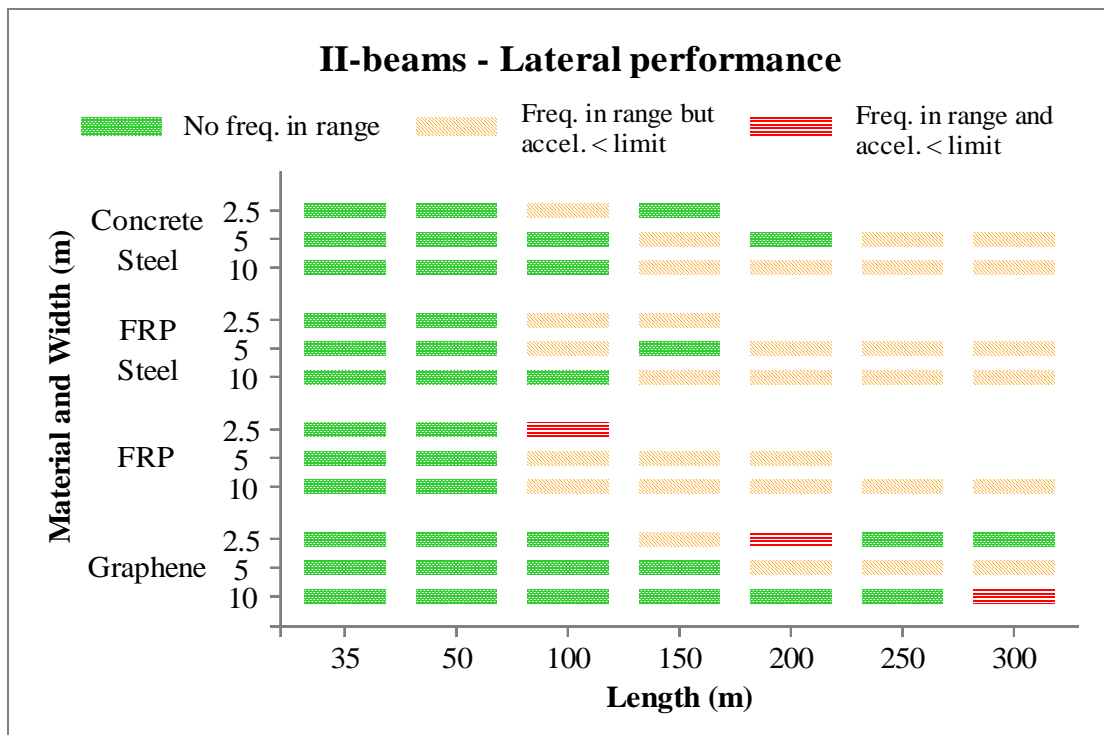


Figure 6.12. Summary table for the lateral performance of the II-beams section.

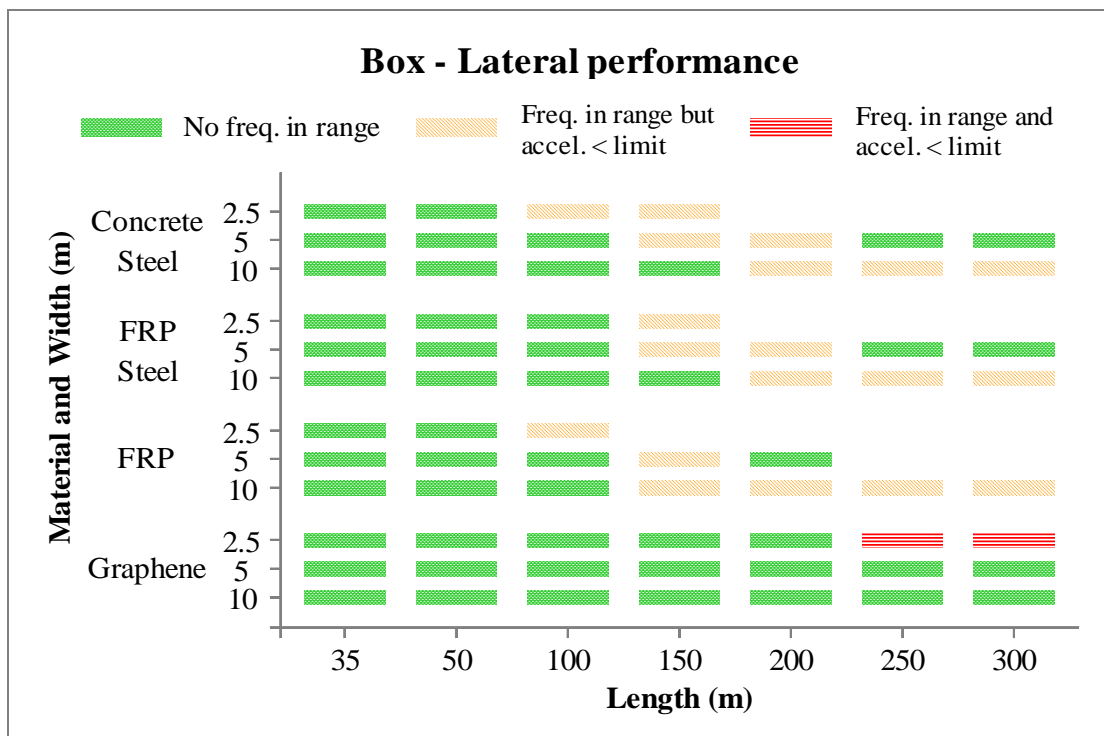


Figure 6.13. Summary table for the lateral performance of the Box section.

7 Discussion of the results

The discussion is separated in two main blocks: the eigenfrequencies and the accelerations. As it was mentioned, the eigenfrequencies can be analysed as a continuous trend. On the other hand, the accelerations depended on the ranges defined by Eurocode 1 and therefore were only possible to be calculated for the cases in range according to Section 2.4.

There are some cases in which there were important frequencies that were out of the limits stated in Eurocode 1 but really close to them. Those cases may have fallen into the limits if some small variations were introduced in the geometry. These changes could be due to other criteria introduced in the calculations, or to a more detailed design that could take into account the contribution of non-structural members such as handrails or pavement.

Nevertheless, all bridge cases were affected equally by the design criteria which aimed for the analysis of a big sample of bridges instead of a reduced range with a more detailed design. Thus, the limitations presented in Section 5.6 have to be considered for the discussion below.

7.1 Study of natural frequencies

7.1.1 Raw analysis

Natural frequencies are dependent on both mechanical and material properties of each case. As introduced in Section 2.1.1, the natural frequencies are the solution for the differential equation stated there and this solution can be explained by the expression in Equation (7.1). This means that natural frequencies are directly proportional to the stiffness of the structure, k , and inversely related to the mass, m .

$$f_n \propto \sqrt{\frac{k}{m}} \quad (7.1)$$

At the same time, the stiffness of a system is inversely related to the length of the structure, as shown in Equation (7.2). It depends on the boundary conditions and factor α , which is related to the load distribution of the structure. Therefore, the relation between frequencies and length is hyperbolic.

$$k \propto \frac{E \cdot I}{L^\alpha} \quad (7.2)$$

This shows that for short bridges, an increase of the span length produces a big decrease of the natural frequencies of the structure. Meanwhile, for long bridges, the gradient lowers down and a horizontal asymptote appears.

The results presented in Section 6.1.1, Section 6.1.2 and Section 6.1.3 present certain interesting patterns related with the previous reasoning, which are presented below.

First of all, as it can be seen in Figure 6.2 and Figure 6.3, eigenfrequencies show a decreasing trend when increasing the length, with a hyperbolic pattern, as it was explained in Equation (7.2).

For our case, α has a value of 4 in Equation (7.2), as the loads are uniformly distributed over the bridge. Thus, the bigger the length, the lower the importance of material and section parameters (E and I) on the result. Hence, the eigenfrequencies for longer bridges tend to converge for all the material and section combinations.

When comparing between sections, there did not appear big differences in results when it came to vertical frequencies. This seems logic, as the vertical stiffness should not vary when closing the section, as it was dimensioned only for vertical loads.

On the other hand, it can be observed in Figure 6.3 how the Box cross-section yields higher frequencies than the II-beams cross-section for lateral modes. Cross-section for the lateral behaviour goes from two beams connected only by the deck to a whole box with an expected better performance in that direction. The results confirmed that, as the natural frequencies showed much higher values for the Box cross-section.

When taking into account the frequencies ranges stated by Eurocode 1, we can draw the same conclusion, as depicted in Figure 6.12 and Figure 6.13. There, bridges with problems appeared for longer bridges when the section was closed, compared to the open section.

Secondly mentioned in the results, was the effect of width variation. No clear difference for vertical modes was found when varying the width, as shown in Figure 6.4. Vertical stiffness should be greater when increasing the width to bear higher loads, but so would do the mass of the structure, and therefore frequencies should not change a lot, according to the relation in Equation (7.1).

When comparing lateral frequencies, the stiffness in this direction would increase, which explains why frequencies rise when widening the bridges, as shown in Figure 6.5.

Once again the frequencies are similar for the two cross-sections for the vertical modes, see Figure 6.4, while they are higher for the Box cross-section for lateral modes, Figure 6.5.

The last effect isolated in the results was the materials change, as plotted in Figure 6.7. Here it is seen how the three actual materials combinations, Concrete-Steel, FRP-Steel and FRP had similar results for the different lengths and Graphene showed higher results. This can be explained one more time with Equation (7.1). In this case, both parameters, k and m , help Graphene yielding higher results, as the stiffness is higher meanwhile the mass is lower.

7.1.2 Dependency study

The influence of the different cross-sections and materials of the studied bridge can be compared from the results showed in Section 6. It has to be remarked that the following discussion does not expect to conclude any statement in exact relationships between these cross-sections and materials, although compare their dynamic behaviour.

Taking what presented before one step forward, Equation (7.3) rewrites Equation (4.1) to show the relationship between length, cross-section and material. Nevertheless the results of this formula are approximate; it will be used as reference to explain the influence of each of the studied elements.

$$f_n \propto \frac{K_n \cdot K_{mat} \cdot K_{cs}}{2\pi L^2} \quad (7.3)$$

Where:

- f_n : eigenfrequency of the nth harmonic
- L : length
- $K_n = \left[(2 \cdot n + 1) \cdot \frac{\pi}{2} \right]^2$ harmonic component
- $K_{mat} = \sqrt{\frac{E}{\rho}}$ material component
- $K_{cs} = \sqrt{\frac{I}{S}}$ cross-section component

Note that the above formula is related with what presented in Equation (7.1) and Equation (7.2).

The charts in Figure 7.1 contain one width case for both cross-sections studied. It shows the eigenfrequencies divided by a factor dependant on the harmonic of vibration, K_n . So that, the eigenfrequency families explained in Section 6 are gathered. It can be observed how the studied cases follow the trend showed by the formula mostly for long span bridges.

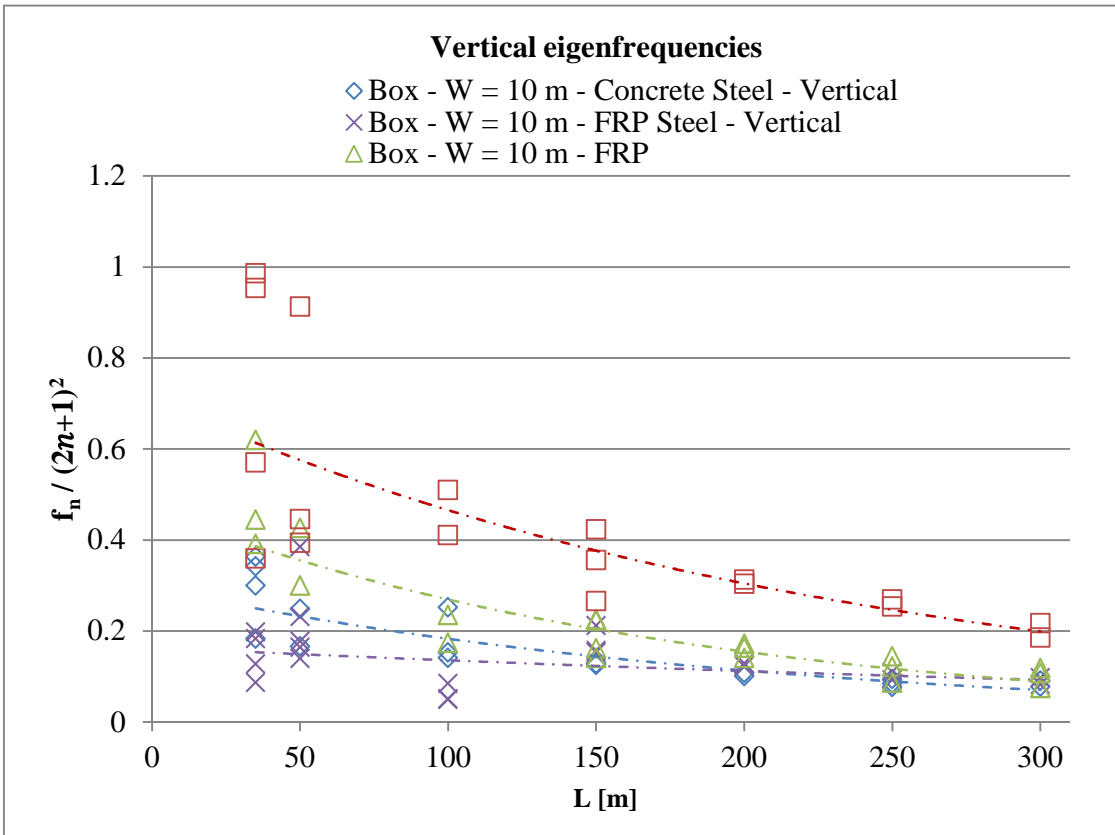
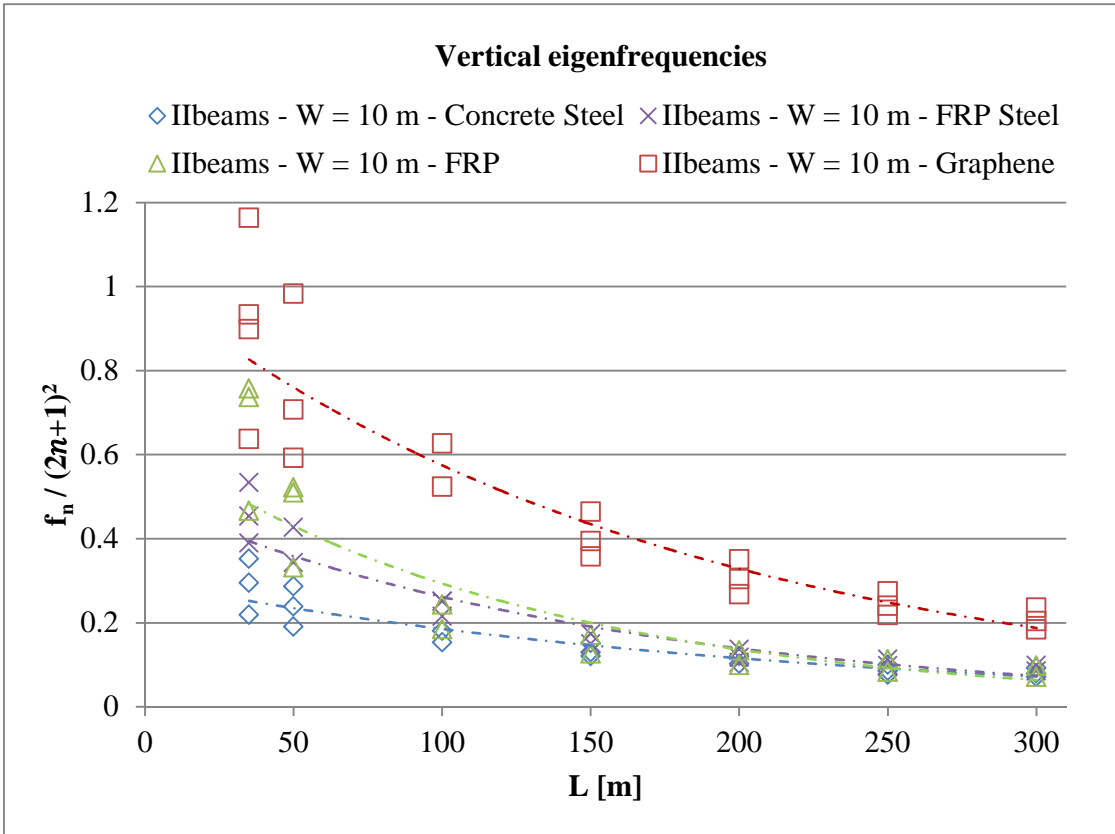


Figure 7.1. Mode shape analysis for vertical eigenfrequencies for both cross-sections.

The biggest differences appear for bridges with lower length-to-width ratio, i.e. shorter spans and larger widths. In addition, Box cross-section and FRP and Graphene cases presented larger dispersion of eigenfrequencies.

A Graphene low length-to-width ratio is depicted in Figure 7.2, where it can be observed what was previously mentioned. This eigenfrequency dispersion is due to the existence of modes of vibration that have combined oscillations in the deck and the section. Furthermore, FRP and Graphene cases have lower thickness in the deck and section, which leads to less stiffness and the existence of these combined oscillations.

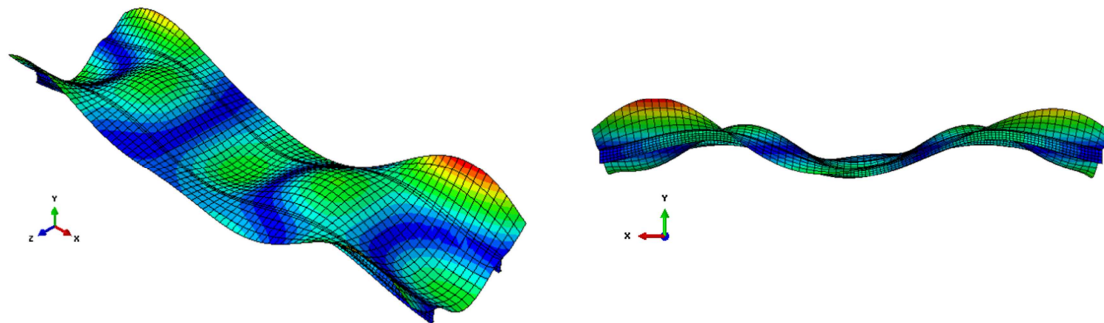


Figure 7.2. Modes of vibration for the II-beams girder for Graphene, $L = 35$ m and $W = 10$ m.

Box girder cross section, depicted in Figure 7.3, produced modes of vibration with great oscillations in the lower flange due to modelling simplifications; as a result, the lower flange had sometimes different vibration modes than the global behaviour.

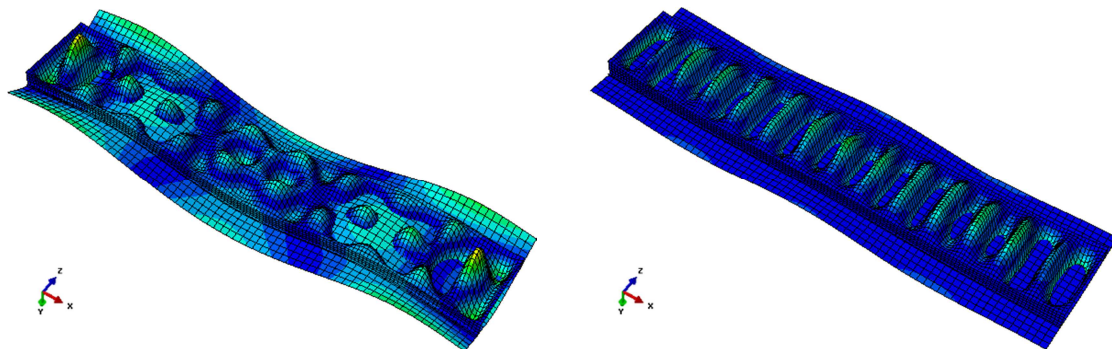


Figure 7.3. Modes of vibration for the Concrete-Steel box girder, $L = 35$ m and $W = 10$ m.

Nevertheless, the eigenfrequencies trend variation can be recognised for most of the materials and geometry combinations. In addition, the results showed in Figure 7.1 are for the case of the highest width that was observed to enhance the problem for lower bridge lengths. Therefore, this result validated the model and showed that this formula is adequate for its use as reference for the influence of each parameter.

Three main parts can be identified from Equation (7.3): the harmonic shape, material properties and cross-section properties. Therefore in order to analyse each part independently they have to be separated in some manner. The harmonic shape can be separated in the families shown in Section 6, and therefore their behaviour and discussion

can be unified; so in the following discussions the family with highest participation is analysed.

The material component in the formula is directly dependant on each combination of materials that is used. The cross-section component depends on the moment of inertia and area of the cross-section. In Equation (7.4) is shown that for the vertical eigenfrequency the most influencing parameter is the height of the section while for the lateral it is the distance of the beams.

$$K_{cs} = \sqrt{\frac{I}{S}} = \sqrt{\frac{I_{cg} + S \cdot d^2}{S}} \quad (7.4)$$

Therefore, vertical eigenfrequencies mainly depend on the height of the cross-section while lateral eigenfrequencies on the width of the cross-section. The results from dividing the frequency by the cross-section parameter are shown in Figure 7.4.

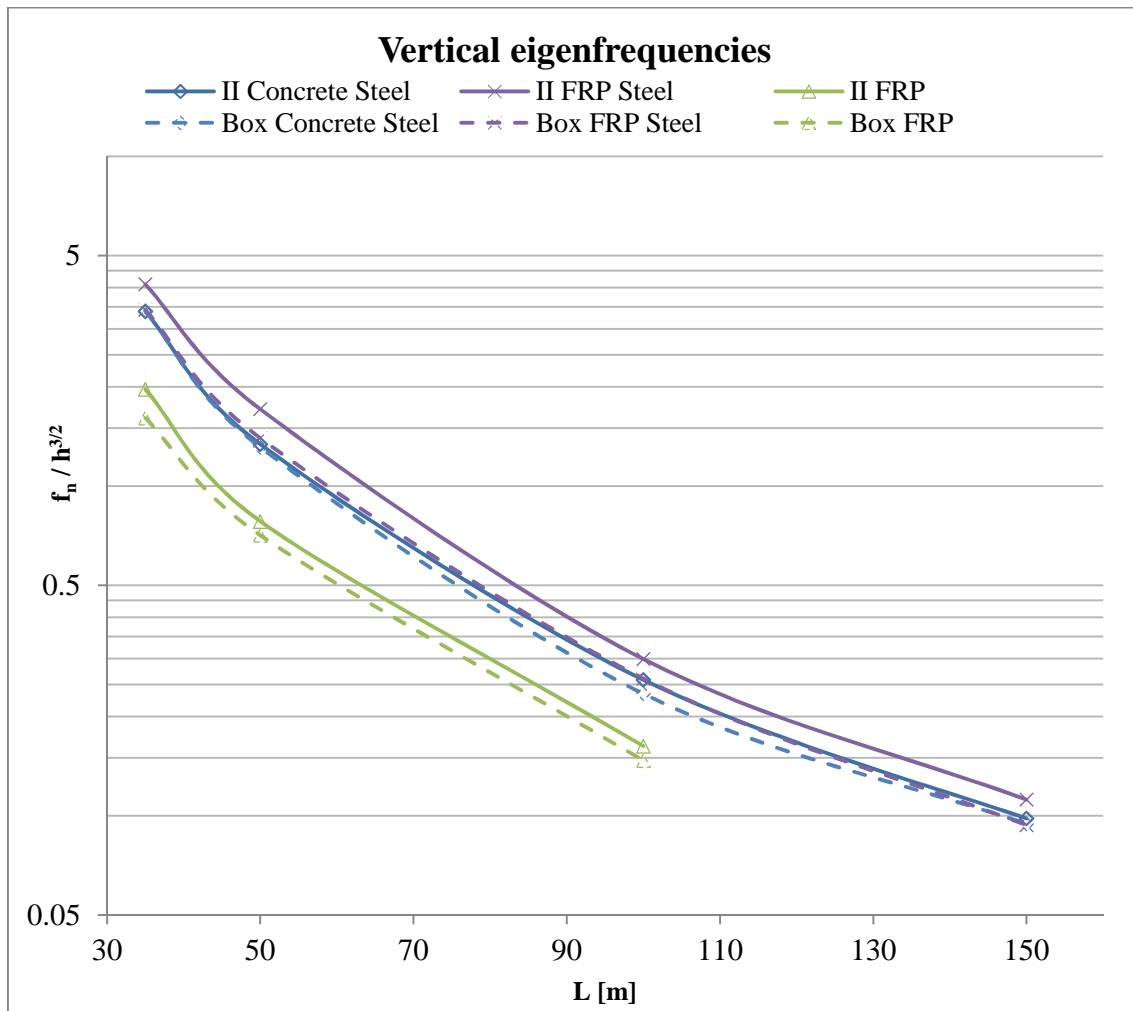


Figure 7.4. Material analysis of the vertical eigenfrequencies for W=2.5 m.

Furthermore, it can be observed how both cross-sections gather together. Therefore the cross-section influence can be considered suppressed and the material itself can be analysed independently.

Graphene has the best performance as its values have a great difference with the rest, which is why it is not showed in Figure 7.4 in order to present better the other cases. FRP-Steel and Concrete-Steel have a similar behaviour, while FRP has the lowest values.

Despite what mentioned in Section 7.1.1, it can be observed in Figure 7.4 that eigenfrequencies for the Box cross-section are slightly lower when compared to the II-beams.

The same case is presented for the other two widths in Figure 7.5. There it can be seen that the exact same observations appear. Graphene was now included so the big difference between them is reflected.

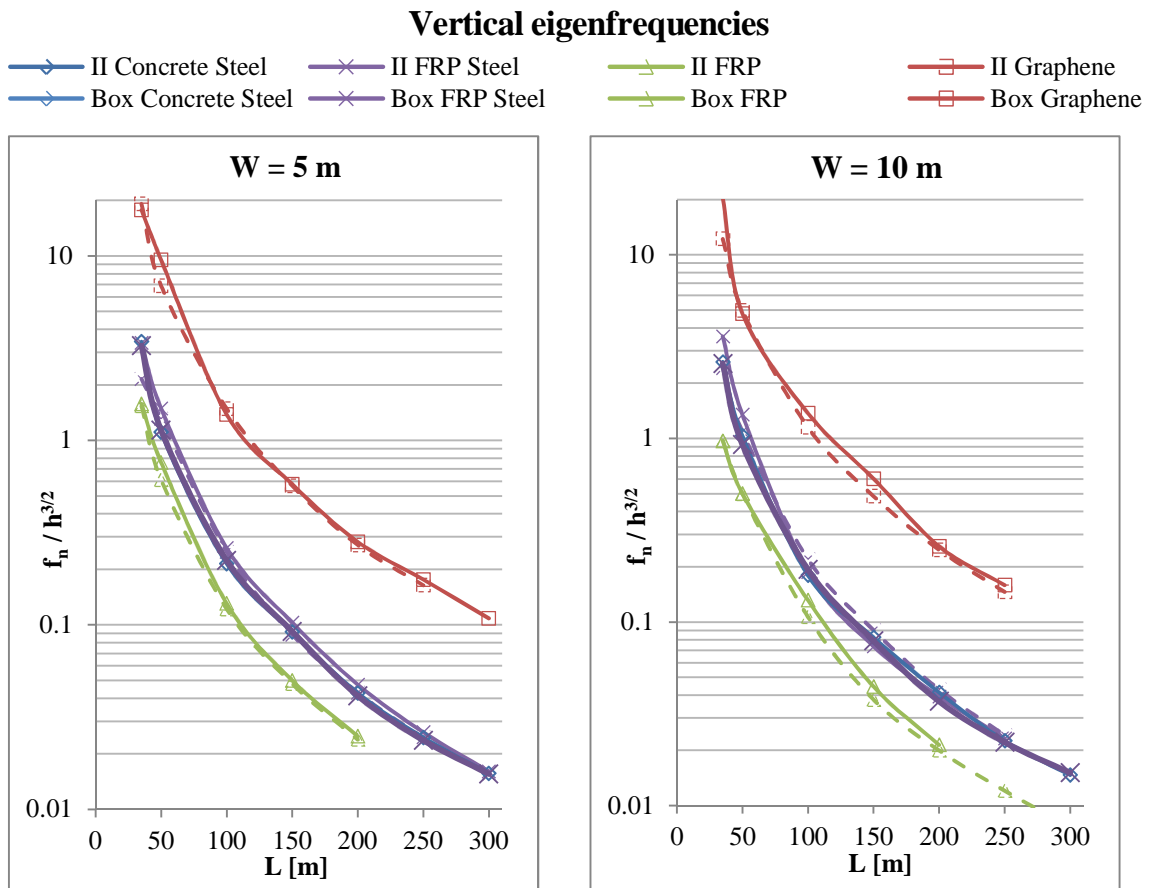


Figure 7.5. Material analysis of the vertical eigenfrequencies for the W = 5 m and W = 10 m cases.

No relation could be found for the lateral eigenfrequencies according to the material behaviour, but it could be identified that the box girder had a better performance in this direction, which matches with what was commented in Section 7.1.1. This issue can be due to the difference in the behaviour of the section and the deck and the fact that the lateral eigenfrequencies are more related to the oscillations of the deck, therefore the suitability of the formula for the lateral direction is discarded.

7.2 Accelerations

The acceleration values, as mentioned in Section 6.2, were calculated just for the studied cases and, according to that, have to be discussed. Therefore, a behaviour trend cannot be evaluated as they are directly dependant on each eigenfrequency and thus on each specific geometry.

Also, the results discussed in Section 6.2 showed that the eigenfrequencies are sometimes difficult to evaluate and categorize, see Figure 7.2 and Figure 7.3 for instance. The applied load may have a big role in the accelerations results. As it was mentioned in Section 5.3, it had to match the shape of the mode of vibration. However, this was not possible to do for all the cases with the highest accuracy, as stated in the limitations. This issue may have a big influence in the acceleration results and may have a direct influence on its final value.

It can be observed in Figure 6.8 that the acceleration results were inversely proportional to the width when all the widths had to be analysed for a certain length. This phenomenon was observed to appear for cases with Steel girder while for FRP and Graphene this effect was less important.

This can be due to the importance of the material damping which was 1.0 % for FRP and Graphene and 0.3 % for steel. Figure 7.6 depicts the accelerations for two cases, one with Concrete-Steel and another one with FRP. Here one can observe the damping phenomenon and how the time needed to damp the accelerations for the first case was much higher than for the second one. Note that the acceleration values are of completely different magnitude (but still exemplify what mentioned).

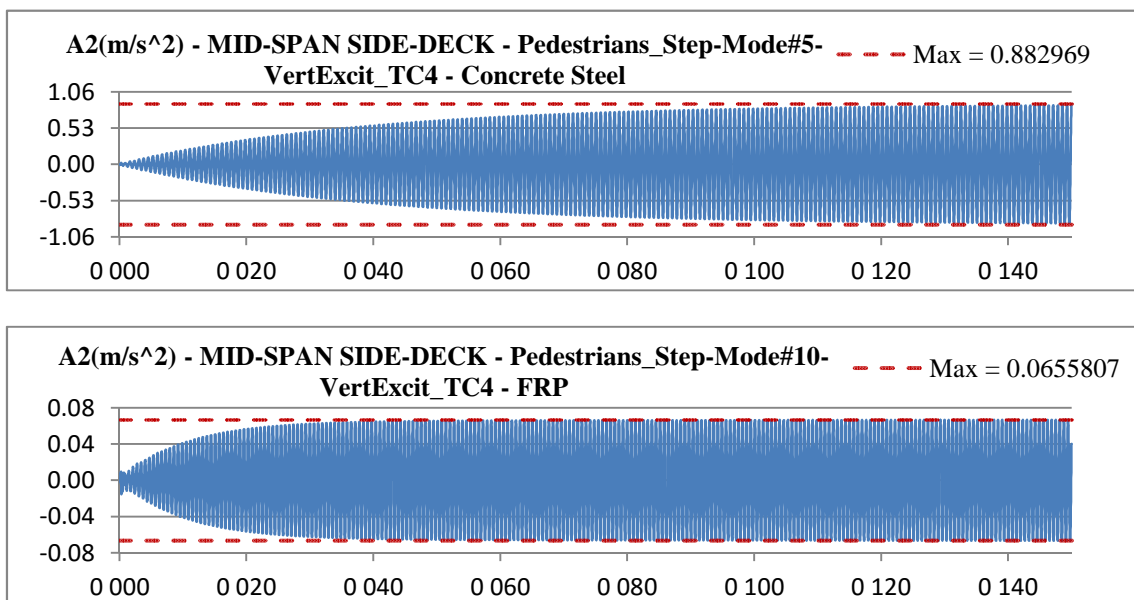


Figure 7.6. Accelerations for a Concrete Steel (above) and a FRP (below) bridge, for vertical accelerations in TC4, L=150 m and W=10 m.

The accelerations were higher when pedestrian density increased with the traffic cases. The differences between them were higher for the Steel bridges, when compared to the FRP and Graphene ones. This matches what was argued about damping effects.

It could also be observed that in most of the cases the highest accelerations were obtained for the direction for which the mode of analysis was predominant, as it was expected. However for some vertical-dominant cases, relatively high lateral accelerations appeared, as it was the case of the 100 m long and 5 m width FRP-Steel bridge with box girder.

It was expected to obtain a relationship between peak accelerations and mass participation, so that, while exciting the structure with frequencies with a high mass participation factor higher accelerations would appear. That happened in some cases, like the bridge with I-beams, FRP-Steel, 100 m long and 10 m wide. In this example, there were two vertical modes with the same frequency, 2.26 Hz, in which the one with higher participation got higher accelerations. However, for some cases such as Box, FRP, 200 m long and 10 m wide this was not observed as much smaller mass participations led to similar responses. . Here there appear two vertical modes, one with a participation of 52.4 % and another with 2.3 %. The second mode got accelerations which were double the ones of the first mode.

To sum up, there may be some patterns on the accelerations, but the reduced number of samples, together with the high dispersion due to different frequencies and participation factors, and the possible lack of accuracy in the load definition, made it impossible to get any good conclusion related to accelerations.

8 Conclusions

Research on graphene is still mainly in the nanoscale, and its presence in usable materials nowadays is almost non-existent. The properties used in the modelling have been taken from theoretical models that predict its behaviour in macroscale from the nanoscale models, taking into account the probable appearance of material imperfections. These models ended up in material properties that showed a really different and better performance compared with traditional materials.

Therefore, graphene was used in this study as a way of analysing the material properties that high-performance materials may develop for the civil construction sector in the future and how they would perform in such a case.

The problems that pedestrian bridges may suffer with the introduction of ultralight high-performance materials, such as graphene or FRP when produced in larger scale, are challenging due to the lack of knowledge in the field.

Pedestrian dynamic loads are difficult to model. The human-structure interaction is complex, mainly due to the intrinsic characteristics of human behaviour. These problems have been studied and gathered in this report in Section 2.2. After this study, it was pointed out that the codes are not yet adapted to the last findings due to the uncertainty of human behaviour. The reference Guideline (Heinemeyer, et al., 2009) defines the pedestrian load in a rather simple manner compared to all the different parameters that affect human gait.

In summary, the complexity of the human behaviour, individually and as crowds, makes it difficult to model it in an accurate way. However, the latest numerical models to define the interaction between humans and human-structure are very promising.

Gathering the previous information, together with classical ways of analysis, 72 different bridge cases were analysed. They were designed for ULS and SLS, and then, their dynamic comfort was checked. These cases combined the use of traditional materials (steel and concrete) and high-performance innovative and futuristic materials (FRP and graphene).

Different structural types were analysed in Section 4 by comparing real cases built with high-performance materials. These examples are still very far from what these materials may lead in the civil construction, especially with the discovery of very promising materials such as graphene. After considering several variables, mainly the dynamic behaviour, two different cross-sections were selected for the analysis.

It can be concluded that the results showed a better performance for graphene in short span ranges, in which the traditional materials had already dynamic problems. Graphene developed dynamic problems, but for lengths over 250 m.

Meanwhile, FRP showed a performance that was slightly lower than the one of the bridges with steel girder. This conclusion is due to the fact that the material properties for FRP are still too conservative, as the safety factors applied by the Reference Code (Fiberline Composites A/S, 2003) are relatively high, downgrading the FRP properties.

Steel girder bridges had a similar behaviour for both deck materials. This is understandable, as the girders are the main component defining the bridge performance. This was also observed in the design phase, where they showed a similar slenderness. In conclusion, when comparing the bridge with FRP and concrete deck, FRP bridges may present advantages during the construction stage and maintenance, no structural advantage was highlighted in the analysis of the present study.

The comparison of the results made with the traditional formulas from dynamic theory pointed out the influence of each parameter and how this matched relatively well the FE results. This was not completely valid for short bridges, where the formulas for 2D analysis showed not to be enough, emphasizing the need of a 3D analysis in these cases. Similarly, the different behaviour of the orthotropic deck in the transversal direction remarks this issue.

The accelerations, obtained according to the limitations of both the Guideline and this study, did not yield any remarkable results. On one hand, the ranges defined in Eurocode 1 limited the number of results to be obtained. On the other hand, some of the results within this reduced and spread group were directly influence by the way of applying the load. The complex mode shape of these cases made it difficult to apply the load in order to obtain the worst possible combinations.

Damping is another important factor in order to find the response of the structure. Both of the main components that define this factor, material and structural damping, presented uncertainties in their definition. Material damping presents different values depending on the reference used. Furthermore for FRP and graphene there are no values and damping from timber was used instead. Structural damping can only be found once the structure is built by testing it and therefore its value was impossible to simulate.

To sum up, graphene could avoid dynamic problems thanks to its higher stiffness, meanwhile traditional materials had problems for shorter lengths. It can be concluded that a stiffening of the cross section helps to avoid dynamic problems, as it raises the eigenfrequencies. However, this has to be done without increasing at the same time the mass of the structure.

Material properties appeared to be as important as cross-section properties. High-performance materials, which combine high strength and ultra-lightness allow the cross sections to be really slender. The problem then, as expected, arises with the stiffness of the cross-section. There, the box girder solution showed slightly better lateral performance and pointed out how to decrease the dynamic problems.

These high-performance materials not only allow more slender structures but also create the possibility of considering new cross-sections that could not be conceived for traditional materials. For instance, a tube closed section, with an inner deck, which is a good solution for bridges with high dynamic problems. This has been already implemented for some railway and pedestrian bridges with traditional materials, however ending up in complex solutions due to the need of holes to lighten the structure. The promising properties of graphene may simplify this solution allowing the creation of a transparent solid tube.

9 Further studies

The purpose of the present study was to analyse the dynamic problems of super-lightweight pedestrian bridges that may arise with the use of graphene. In order to evaluate this performance some limitations had to be assumed and therefore some further studies could be developed from here:

- Pedestrian load models are simplified due to their complexity. In the present study different issues that affect the pedestrian loads were mentioned but not furtherly applied due to the lack of implementation in the codes. The authors believe that it could be evaluated how these models might be applied, so that, even though all the parameters that affect human gait cannot be defined, at least different scenarios are evaluated.
- Pedestrian load definition has a high dependency on the eigenfrequency and mode of vibration that is excited. It was proved that they are dependent on many parameters and assumptions that could not be entirely evaluated. Thus, a load combination that leads to the highest acceleration cannot be directly deduced. A study that takes into account the complexity of the 3D-oscillation and worst load combination is certainly desirable.
- Mass participation factors play an important role when deciding which modes are important for the structure and which ones are just residues from the FE calculations. It could not be proved what is the role of the mass participation factor in the response of the structure. It is suggested to study above at which limit of mass participation resonance problems can be encountered, meaning a danger to the structure or its users.
- The methodology used in this study is a consequence of applying the Guideline load model. It did not allow finding good conclusions for the accelerations. It could be interesting to analyse all the bridges for their natural frequencies with no consideration to the limits. This may allow evaluating the accelerations as a trend, similar to the analyses developed for the eigenfrequencies, so that the material and cross-section influence could be extensively analysed.

The limited time for this study together with the methodology used in the whole design and evaluation process required simplifications. Below are mentioned some assumptions that could be evaluated to verify the validity of some results in this study:

- The design process was done based on some (but not all) checks for ULS and SLS. It could be evaluated how neglecting other checks affected the dynamic analysis and how the results would differ.
- The simplifications in the design stage implied simplifications in the modelling. Basic bridge structures were used in the FE analysis without details like the

stiffening of the plates. It could be evaluated if the dynamic behaviour with proper modelling would affect the results and conclusions.

- There are more sections that can be analysed and compared apart from I-beams and box section. A design using a tube section could be interesting, as it was commented in the conclusion.

Finally, the material properties used in this study for graphene and FRP were in line with the state of the art for these materials. In this study their properties were justified according to a wide literature review and extrapolating from numerical models. Further studies could be developed including new developments of the research on graphene properties as it is still in a primary stage. It therefore needs to get to a more mature point in order to yield more realistic conclusions about it.

Properties such as material damping are not well defined for FRP materials, it was observed to play an important role in the acceleration response. Thus, the influence of these properties in a more extensive research should be developed, evaluating different values and their real influence.

10 References

- Acciona infraestructuras, 2013. *Composites Conference & Trade show*. Melbourne, s.n.
- Anon., 2005. *Footbridge vibrations due to pedestrian load. Danish Guidelines and examples..* s.l.:s.n.
- Ávila, A. F. & Lacerda, G. S. R., 2008. Molecular Mechanics Applied to Single-Walled Carbon Nanotubes. *Materials Research*, 11(3), pp. 325-333.
- Bachmann, H. & Ammann, W., 1986. Vibration in structures induced by man and machines. En: *Structural engineering documents*. Zurich: IABSE.
- Bank, L. C., 2006. *Composites for construction: structural design with FRP materials*. New Jersey: s.n.
- BD, 9., 2005. HIGHWAY STRUCTURES: APPROVAL PROCEDURES AND GENERAL DESIGN.. En: *DESIGN MANUAL FOR ROADS AND BRIDGES AND HIGHWAY STRUCTURES*. s.l.:s.n., p. 25.
- Bellomo, N. & Dogbé, C., 2008. On the modelling crowd dynamics from scaling to hyperbolic macroscopic models. En: *Mathematical Models and Methods in Applied Sciences*. s.l.:s.n., pp. 1317-46.
- Bethune, D. S. y otros, 1993. Cobalt-catalysed growth of carbon nanotubes with single-atomic-layer walls. *Nature*, 363(6430), pp. 605-607.
- Bødker, R. & Christensen, H., 2010. *Dynamisk personlast og stokastiske lastmodeller til estimering af gangbroers dynamiske respons*. s.l.:Civilingeniør i Bygge- og Anlægskonstruktion, Aalborg Universitet.
- Boehm, H. P., Setton, R. & Stumpp, E., 1985. Nomenclature and terminology of graphite intercalation compounds.. *Synthetic Metals*, Volumen 11, pp. 363-371.
- Brodie, B. C., 1859. On the Atomic Weight of Graphite. *Philosophical Transactions of the Royal Society of London*, Volumen 149, pp. 249-259.
- Brownjohn, J., Živanović, S. & Pavic, A., 2008. *Crowd dynamic loading on footbridges*. Porto, s.n.
- Buchmueller, S. & Weidmann, U., 2006. Parameters of pedestrians, pedestrian traffic and walking facilities. *Tech. Rep*, October. Volumen 132.
- Butz, C., 2006. *Beitrag zur Berechnung fußgängerinduzierter Brückenschwingungen (On the calculation of pedestrian-induced vibration of bridges)*. Ph.D. thesis ed. Aachen, Germany: s.n.
- Butz, C., 2008. *A probabilistic engineering load model for pedestrian stream*. s.l., s.n.
- Butz, C. y otros, 2008. *Advanced load models for synchronous pedestrian excitation and optimised design guidelines for steel footbridges*, s.l.: s.n.

Canning, L., 2014. Examples and Case Studies. En: M. Zoghi, ed. *The International Handbook of FRP Composites in Civil Engineering*. s.l.:s.n., p. 28.

Carpinteri, A., 1994. Scaling laws and renormalization groups for strength and toughness of disordered materials. *International Journal of Solids and Structures*, Volumen 31, pp. 291-302.

Carpinteri, A. & Pugno, N. M., 2008. Super-bridges suspended over carbon nanotube cables. *Condensed Matter*.

CECM, 1989. *Recommendations for the calculation of the effects of wind on constructions*. s.l.:s.n.

CEN, 2002. *EN1990-0, Eurocode 0 – Basis of structural design*. s.l.:European Committee for Standardization.

CEN, 2003. *EN1991-2, Eurocode 1: Actions on structures - Part 2: Traffic loads on bridges*. s.l.:s.n.

CEN, 2003. *EN1991-2, UK National Annex to Eurocode 1-Actions on structures, Part 2: Traffic load on bridges*. s.l.:s.n.

CEN, 2003. *EN1995-2, Eurocode 5-Design of timber structures, Part 2: Traffic load on bridges*. s.l.:s.n.

CEN, 2006. *EN 1993-2: Steel structures - Steel bridges*. s.l.:s.n.

Chopra, A. K., 1995. *Dynamics of structures. Theory and applications to earthquake engineering*. s.l.:Prentice Hall.

Colombo, R. & Rosini, M., 2005. Pedestrian flows and non-classical shocks. Volumen 28, p. 1553–67.

Craig Jr, R. R. & Kurdila, A. J., 2006. *Fundamentals of Structural Dynamics*. s.l.:John Wiley & Sons, Inc..

Cusen, A. & Pama, R., 1975. *Bridge Deck Analysis*. s.l.:John Wiley & Sons.

da Silva, J. y otros, 2007. Vibration analysis of footbridges due to vertical human loads. En: *Computers and Structures*. s.l.:s.n., pp. 85(21-22):1693–1703.

Daamen, W., 2004. *Modelling passenger flows in public transport facilities*. s.l.:Delft University of Technology.

Dallard, P. y otros, 2001. The London Millenium Footbridge. *Structural Engineer*, Volumen 22, pp. 17-33.

Davalos, J., Qiao, P. & Shan, L., 2006. Advanced Fiber Reinforced Polymer (FRP) Structural Composites for Use In Civil Engineering.. En: H. C. Wu, ed. *Advanced Civil Infrastructure Materials – Science, Mechanics and Applications*.. s.l.:CRC Press, pp. 118-202.

- Estrada, H. & Lee, L. S., 2014. FRP Composite Constituent Material. En: M. Zoghi, ed. *The International Handbook of FRP Composites in Civil Engineering*. s.l.:s.n., p. 20.
- Estrada, H. & Lee, L. S., 2014. FRP Composite Constituent Material. En: M. Zoghi, ed. *The International Handbook of FRP Composites in Civil Engineering*. s.l.:s.n., p. 20.
- Estrada, H. & Lee, L. S., 2014. Mechanics of Composite Materials. En: M. Zoghi, ed. *The International Handbook of FRP Composites in Civil Engineering*. s.l.:s.n., p. 28.
- EUROCODE, s.f. s.l.:s.n.
- F., R., 2005. *Lateral loading of footbridges by walkers*. Venezia, s.n.
- Federation internationale du beton, 2006. *Guidelines for the design of*. Lausanne: FIB Bulletin.
- Fiberline Composites A/S, 2003. *Fiberline Design Manual*. Kolding, Denmark, s.n.
- Fiberline Composites A/S, 2015. *Characteristic Properties FBD 600 Profile*, Middelfart, Denmark: s.n.
- Fu, C., AlAyed, H., Amde, A. & Robert, J., 2007. Field Performance of the Fiber-Reinforced Polymer Deck of a Truss Bridge. *Journal of Performance of Constructed Facilities*, 21(1), p. 53–60.
- Geim, A. K. & Novoselov, K. S., 2007. The rise of graphene. *Nature materials*, pp. 183-191.
- Gibson, R. F., 2010. A review of recent research on mechanics of multifunctional composite materials and structures. *Composite Structures*, Volumen 92, pp. 2793-2810.
- Griffin, M., 1996. *Handbook of Human Vibration*. London: s.n.
- Harper, F., 1962. The mechanics of walking, *Research Applied in Industry* 15.
- Harper, F., Warlow, W. & Clarke, B., 1961. The forces applied to the floor by the foot in walking. Volumen *Research Paper* 32.
- Heinemeyer, C. y otros, 2009. *Design of Lightweight Footbridges for Human Induced Vibrations*. First Edition ed. s.l.:JRC Scientific and Technical Reports.
- Helbing, D., Johansson, A. & Al-Abideen, H., 2007. Dynamics of crowd disasters: An empirical study. *Physical Review*. Issue 75:0406109.
- HIVOSS, 2008. *Design of Footbridges Guideline, Human Induced Vibrations of Steel Structures*. s.l.:s.n.
- Hu, Z. & Lu, X., 2014. Mechanical Properties of Carbon Nanotubes and Graphene. En: *Carbon Nanotubes and Graphene*. s.l.:s.n., pp. 165-200.

- Hyo, S. J., Wenchao, S. & Zhongguo, J. M., 2010. Design, test and field application of a GFRP corrugated-core sandwich bridge. *Engineering Structures*, Volumen 32, pp. 2814-2824.
- Iijima, S., 1991. Helical Microtubules of Graphitic Carbon. *Nature*, 354(6348), pp. 56-58.
- Iijima, S. & Ichihashi, T., 1993. Single-shell carbon nanotubes of 1-nm diameter. *Nature*, 363(6430), pp. 603-605.
- Ingólfsson, E. T., Georgakis, C. T., Ricciardelli, F. & Jönsson, J., 2011. Experimental identification of pedestrian-induced lateral forces on footbridges.. *J. Sound Vib.*, Volumen 330(6), p. 1265–1284.
- Ingólfsson, E. T., Georgakis, C. T. & Svendsen, M. N., 2008. *Vertical footbridge vibrations: details regarding and experimental validation of the response spectrum methodology*. s.l., s.n.
- ISO, 2005. *ISO 10137:2004, Bases for design*. Geneva: s.n.
- Keller, T. & Schollmayer, M., 2004. Plate bending behavior of a pultruded GFRP bridge deck system. *Composite Structures*, Volumen 64, pp. 284-295.
- Lee, C., Wei, X., Kysar, J. W. & Hone, J., 2008. Measurement of the Elastic Properties and Intrinsic Strength of Monolayer Graphene. *Science*, 321(5887), pp. 385-388.
- López, O. A. & Cruz, M., 1996. Number of modes for the seismic design of buildings. *Earthquake engineering and structural dynamics*, Volumen 25, pp. 837-855.
- Lu, X. & Hu, Z., 2012. Mechanical property evaluation of single-walled carbon nanotubes by finite element modeling. *Composites Part B*, 43(4), pp. 1902-1913.
- Macdonald, J. H. G., 2009. *Lateral excitation of bridges by balancing*. s.l., Proc. R. Soc. London, Ser. A, p. 1055–1073.
- Masani, K., Kouzaki, M. & Fukunaga, T., 2002. Variability of ground reaction forces during treadmill walking. *Journal of Applied Physiology*, Volumen 92 (5), pp. 1885-1890.
- McClure, J. W., 1956. Diamagnetism of Graphite. *Physical Review*, 104(3), pp. 666-671.
- McRobie, A., Morghental, G., Lasenby, J. & Ringer, M., 2003. Parallels between wind and crowd loading of bridges. Volumen 156(BE2), p. 71–79.
- Monthieux, M. & Kuznetsov, V. L., 2006. Who should be given the credit for the discovery of carbon nanotubes?. *Carbon*, 44(9), pp. 1621-1623.
- Nakamura, S.-i. & Kawasakib, T., 2006. Lateral vibration of footbridges by synchronous walking. *Journal of Constructional Steel Research*, Volumen 62, p. 1148–1160.
- Nakamura, S.-i., Katsuura, H. & Yokoyama, K., 2008. *Experimental study on lateral forces induced by pedestrians*. Zurich, Switzerland, IABSE Symp. Rep, p. 182–187.

- Novoselov, K. S. y otros, 2004. Electric Field Effect in Atomically Thin Carbon Films. *Science, New Series*, 306(5696), pp. 666-669.
- Oeding, D., s.f. Verkehrsbelastung und Dimensionierung von Gehwegen und anderen Anlagen des Fußgängerverkehrs. *Straßenbau und Straßenverkehrstechnik*, Volumen 22.
- P. Moses, J., Harries, K. A., Earls, C. J. & Yulisma, W., 2006. Evaluation of Effective Width and Distribution Factors for GFRP Bridge Decks Supported on Steel Girders. *Journal of Bridge Engineering*, Volumen 11, pp. 401-409.
- Palaci, I. y otros, 2005. Radial Elasticity of Multiwalled Carbon Nanotubes. *Physical Review Letters*, 94(175502), pp. 1-4.
- Pedersen, L. e. a., 2009. *Predicting Statistical Distributions of Footbridge Vibrations*. s.l., s.n.
- Pizzimenti, A., 2005. *Analisi sperimentale dei meccanismi di eccitazione laterale delle passerelle ad opera dei pedoni*. Ph.D. thesis ed. s.l.:Università degli Studi di Catania.
- Potts, J. R., Dreyer, D. R., Bielawski, C. W. & Ruoff, R. S., 2011. Graphene-based polymer nanocomposites. *Polymer*, Volumen 52, pp. 5-25.
- Priestley, M., Seible, F. & Calvi, G., 1996. *Seismic design and retrofit of bridges*. New York: John Wiley & Sons, Inc..
- Pugno, N. M., 2006. A general shape/size-effect law for nanoindentation. *Acta Materialia*, Volumen 55, pp. 1947-1953.
- Pugno, N. M., 2006. On the strenght of the carbon nanotube-based space elevator cable: from nanomechanics to megamechanics. *Condensed Matter*, Issue 18, pp. 1971-1990.
- Pugno, N. M., 2013. Towards the Artsutanov's dream of the space elevator: The ultimate design of a 35 GPa strong tether thanks to graphene. *Acta Astronautica*, Issue 82, pp. 221-224.
- Pugno, N. M., Bosio, F. & Carpinteri, A., 2008. Multiscale Stochastic Simulations for Tensile Testing of Nanotube-Based Macroscopic Cables. *Small (Weinheim an der Bergstrasse, Germany)*, 4(8), pp. 1044-1052.
- Pugno, N. M. & Ruoff, R., 2006. Nanoscale Weibull statistics. *Journal of Applied Physics*, Volumen 99.
- Rainer, J., Pernica, G. & Allen, D., 1988. Dynamic loading and response of footbridges. *Canadian Journal of Civil Engineering*, Volumen 15, p. 66-71.
- Ricciardelli, F., Mafri, M. & Ingólfsson, E. T., 2014. Lateral Pedestrian-Induced Vibrations of Footbridges: Characteristics of Walking Forces.
- S. Yao, J. W. A. P. P. R., 2002,. *Forces generated when bouncing or jumping on a flexible Structure*. Leuven, Belgium, s.n., p. 563-572.

- S. Yao, J. W. A. P. P. R. R. S., 2003. *The effect of people jumping on a flexible structure*. Kissimmee, FL, s.n.
- S. Zivanovic, A. P. a. E. I., 2010. Modelling spatially. *ASCE Journal of Structural Engineering*, Volumen 136, 10.
- Saafi, M. y otros, 2015. Enhanced properties of graphene/fly ash geopolymeric composite cement. *Cement and Concrete Research*, Volumen 67, pp. 292-299.
- Sétra, 2006. *Technical guide. Footbridges: Assessment of vibrational behavior*. Paris: s.n.
- Seyfried, A., Steffen, B., Klingsch, W. & Boltes, M., 2005. The fundamental diagram of pedestrian movement revisited. *Journal of Statistical Mechanics: Theory and Experiment 2005*, Issue 10:P10002.
- Sihn, S., Varshney, V., Roy, A. K. & Farmer, B. L., 2012. Prediction of 3D elastic moduli and Poisson's ratios of pillared graphene nanostructures. *Carbon*, Volumen 50, pp. 603-611.
- Slonczewski, J. C. & Weiss, P. R., 1958. Band Structure of Graphite. *Physical Review*, 109(2), pp. 272-279.
- Sobek, W. & Trumpf, H., 2008. *The new lightweight bridge deck FBD300 made from pultruded*. Zurich, s.n.
- Spyrou, K. & Rudolf, P., 2010. *An Introduction to Graphene*. Göteborg: Chalmers.
- Strogatz, S. y otros, 2005. Crowd synchrony on the Millennium Bridge. *Nature*, Volumen 438, p. 43-4.
- Sun, L. & Yuan, X., 2008. *Study on pedestrian-induced vibration of footbridge*. Porto, Portugal, s.n.
- The Royal Swedish Academy of Sciences, 2010. The Nobel Prize in Physics 2010. 5 October.
- Venuti, F. & Bruno, L., 2009. Crowd-structure interaction in lively footbridges under synchronous lateral excitation: A literature review. *Physics of Life Reviews*, Volumen 6.
- Venuti, F., Bruno, L. & Bellomo, N., 2005. *Crowd-structure interaction: dynamics modelling and computational simulation*. Venezia, s.n.
- Venuti, F., Bruno, L. & Bellomo, N., 2007. Crowd dynamics on a moving platform: Mathematical modelling and application to lively footbridges. *Mathematical and Computer Modelling*, Volumen 45, pp. 252-269.
- W. Davey, S., M. Van Erp, G. & Marsh, R., 2001. Fibre composite bridge decks - an alternative approach. *Composites Part A: Applied Science and Manufacturing*, pp. 1339-1343.
- Wallace, P. R., 1947. The Band Theory of Graphite. *Physical Review*, 71(9), pp. 622-634.

- Wheeler, J., 1980. Pedestrian—Induced vibrations in footbridges, in: Proceedings of the 10th. 27-29 August .pp. 21-35.
- Wheeler, J., 1982. Prediction and control of pedestrian induced vibration in footbridges. pp. 2045-2065.
- Willford, M., 2002. *Dynamic actions and reactions of pedestrians*. Paris, s.n.
- Xiao, J. R., Gama, B. A. & Gillespie-Jr., J. W., 2005. An analytical molecular structural mechanics model for the mechanical properties of carbon nanotubes. *International Journal of Solids and Structures*, 42(24), pp. 3075-3092.
- Yoneda, M., 2002. *A simplified method to evaluate pedestrian-induced maximum response of cable-supported pedestrian bridges*. Paris, France, s.n.
- Young, P., 2001. *Improved floor vibration prediction methodologies*. s.l., s.n.
- Živanović, S., Pavić, A. & Reynolds, P., 2005. Vibration serviceability of footbridges under human-induced excitation. A literature review. Volumen 279, No. 1-2, pp. 1-74.
- Zivanovi, M. & Pavic, A., 2011. *Dynamic response of footbridges due to vertical load models of pedestrians*, *EURODYN*. Leuven, Belgium, G. De Roeck, G. Degrande, G. Lombaert, G. Müller.

APPENDIX A Bridge design

The studied bridges were based on an actual case from NCC which was used as a reference and validation of the method and model. The cross-section consisted of a concrete deck resting over two stainless steel I-beams distributed symmetrically. This case was further developed for the box girder cross-section and different material combinations, with FRP and Graphene.

As the purpose of this thesis was to evaluate different geometry and material combinations, some assumptions and relations were made in order to be able to achieve a series of rational geometries.

The dimensioning of the cross-section was divided in *fixed parameters* (Section A.2), obtained from the mentioned real case, and *variable parameters* (Section A.3). The latter were obtained based on a set-based approach, i.e. all the solutions that did not fulfill certain requirements from checks were rejected and from the ones that did so, the final solution was obtained based on an optimization criterion.

The longitudinal profile and boundary conditions were obtained from the NCC reference bridge. To reduce the number of unknown parameters, the flange width in the transversal direction was also assumed.

A.1 Analysed bridges

The analysed bridges are a combination of two cross-sections, II-beams and Box girder, and different materials, as concrete, steel, FRP and graphene. Combinations were defined for different lengths and widths as shown in Figure A.1. It has to be noted that some bridge combinations were impossible, according to the design process used in the present study.

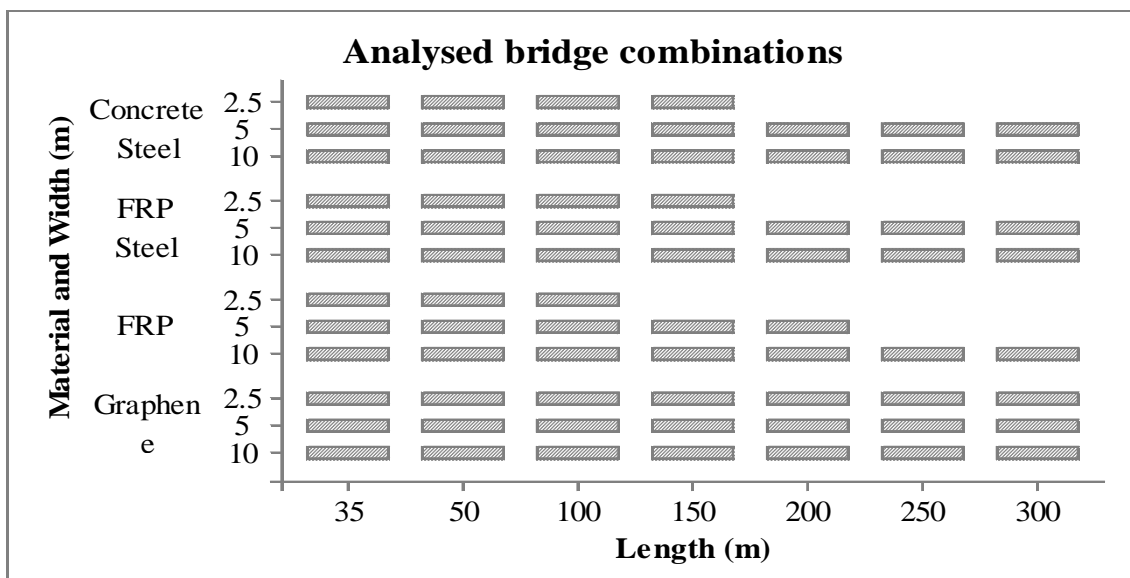


Figure A.1. Analysed bridge combinations.

A.2 Fixed parameters

The assumed geometry relationship for the longitudinal profile, showed in Figure A.2 **Error! Reference source not found.**, is reflected on Table A.1.

Table A.1. Assumed geometry dependant on unknown parameters.

$h_{\text{beam support}}$	L_{bridge} and B_{bridge}
$h_{\text{beam middle}} = 0.62 \cdot h_{\text{beam support}}$	$L_{\text{sides}} = 0.16 \cdot L_{\text{bridge}}$
$h_{\text{beam transition}} = 0.7 \cdot h_{\text{beam support}}$	$B_{\text{distance}} = 0.6 \cdot B_{\text{bridge}}$

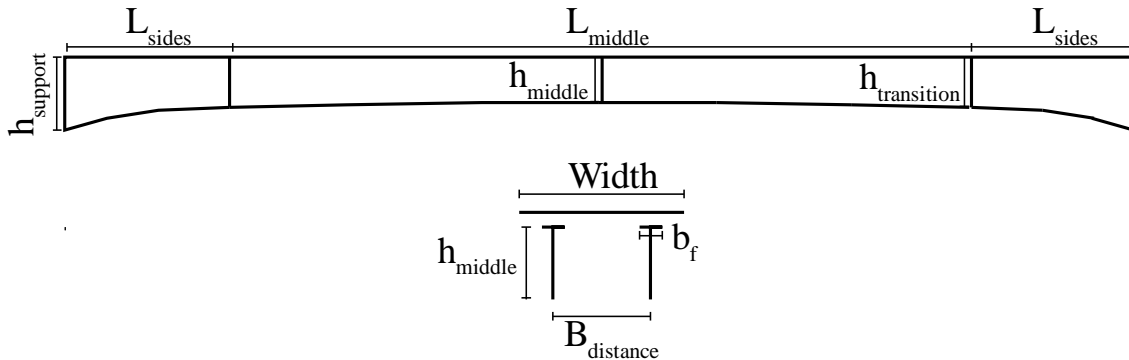


Figure A.2. General longitudinal profile sketch of the studied bridges.

A.2.1 Flange width

To avoid a large calculation time, the flange width was assumed as a relation between the unknown geometry. A reasonable relationship was achieved by studying the existing relations in commercial IPE profiles that were believed to have the same characteristics as the ones studied in this project.

The relationship between the height and flange width of the beams is represented in Figure A.3. One can observe that the initial values have a logarithmic trend that linearizes for larger heights. In this study high beams were used and therefore the linear trend relationship was used.

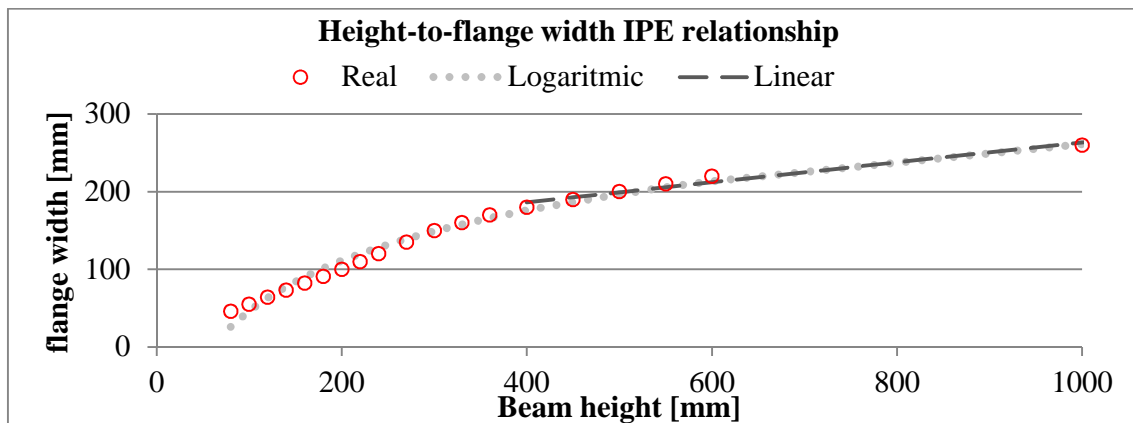


Figure A.3. Height-to-flange width IPE relationship.

To validate this premise, the relationship between flange width and bending resistance of IPE beams was studied. It can be observed in Figure A.5 that this relationship follows a logarithmic trend.

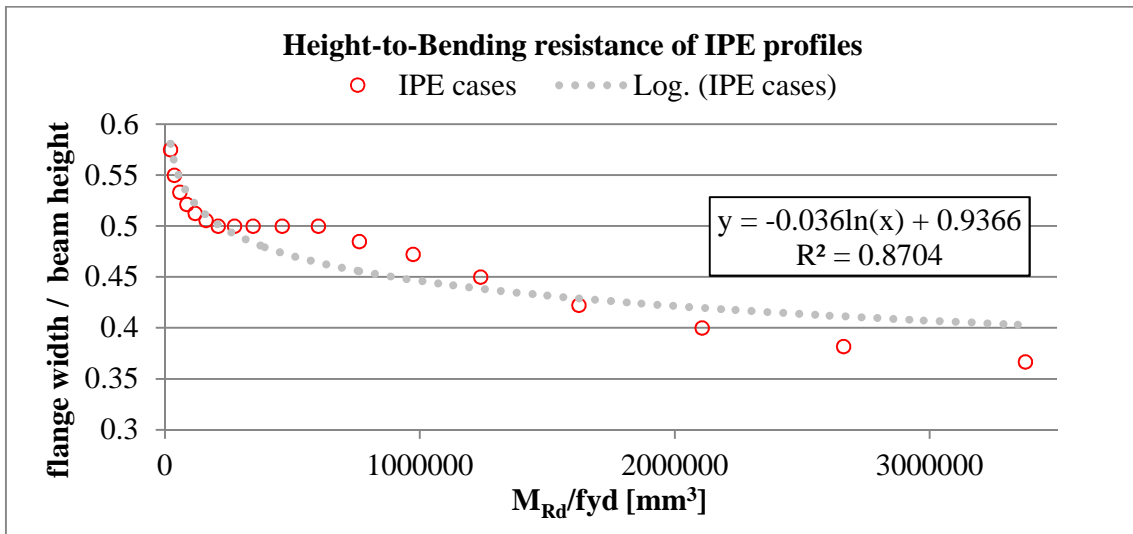


Figure A.4. Height-to-bending resistance of IPE profiles.

This relationship was then compared with both the defined relationship and as an unknown variable, see Figure A.5. The latter calculation was done just for a few cases due to the increase in computation time that each unknown variable produced.

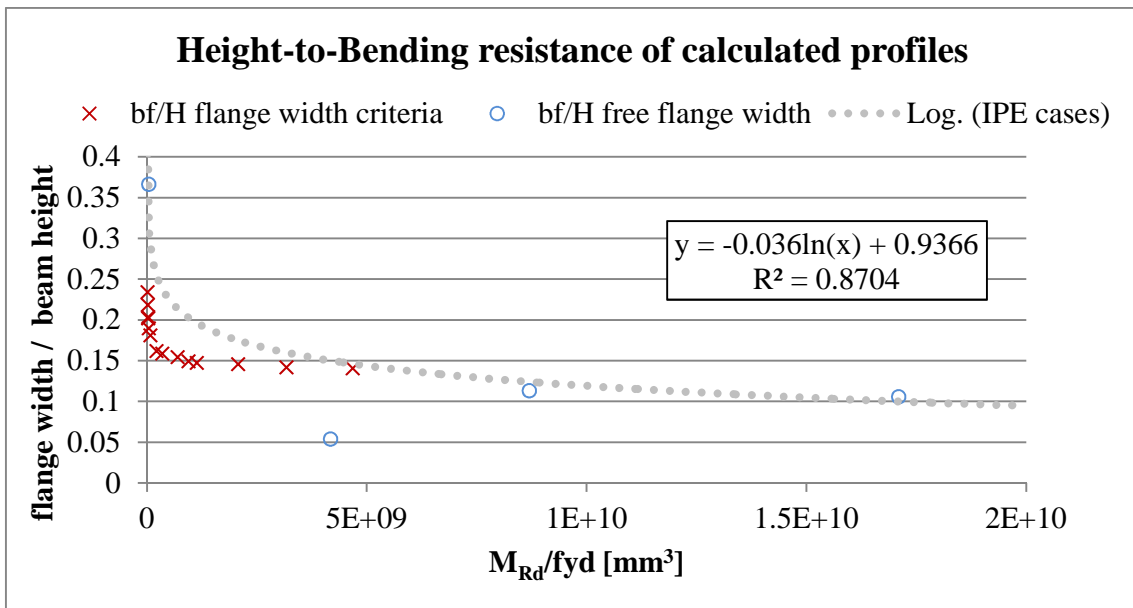


Figure A.5. Height-to-bending resistance of the calculated profiles.

The results showed that the imposed relationship followed the logarithmic trend for both cases, which validated the model.

A.3 Variable parameters

The following geometry was used in the design MATLAB tool as variable data in order to obtain the final geometry with the optimization criterion mentioned in Section A.6

- Beam height at the support.
- Web thickness at the middle and the sides.
- Flange thickness:
 - Same at the sides and the middle.
 - Same at top and bottom for the beams bridge and different for the box girder.
- Deck thickness
 - Checked for transversal actions.
 - For the concrete deck the minimum thickness was set to 0.2 m to let enough room for rebars, and it was allowed to grow to help the steel in the composite action.
 - For the orthotropic deck the variation was proportional with the deck flanges that were considered the resistant parts as presented in Section A.4.3.2.

These variable parameters were defined between ranges and with certain increments. It was then checked that the final solution was within the defined limits. Therefore avoiding the influence of the authors in the final geometry.

The results obtained have a resolution that can be unrealistic from a production point of view. However, the code was very sensitive to the increments of each range of values and therefore had to be settled to small ranges and finally used for the dynamic analysis.

To avoid unreasonable solutions given by the optimization criterion set in Section A.6 some geometry limitations were imposed according to relationships analysed from the IPE profiles. The web-thickness-to-beam-height and web-thickness-to-flange-thickness relationship are reflected in Equation (A.1). They almost follow a perfect linear relationship, as they have a R-square value of 0.999. and 0.9977 respectively.

$$\begin{aligned}t_w &= 0.0155 \cdot h_{beam} + 2.4921 \\t_w &= 1.6522 \cdot t_f - 0.8304\end{aligned}\tag{A.1}$$

To avoid settling on the geometry it was imposed upper and lower limits of 1.5 and 0.5 times the relation from Equation (A.1) so some freedom was given to the MATLAB design tool.

The achieved results are showed for this criterion in Figure A.6 and Figure A.7. It can be observed that the web-thickness-to-beam-height relationship had some influence from the optimization criterion of high slenderness. However, the geometries fulfil the ULS and SLS limitations so the geometries were considered to be valid for further analysis.

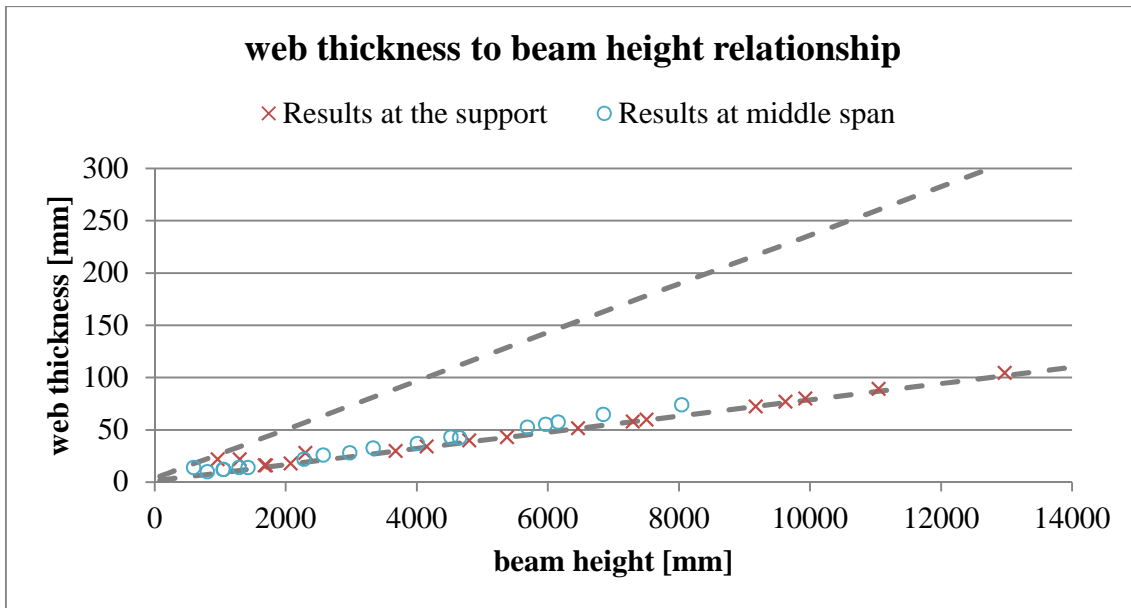


Figure A.6. web thickness-to-beam height relationship.

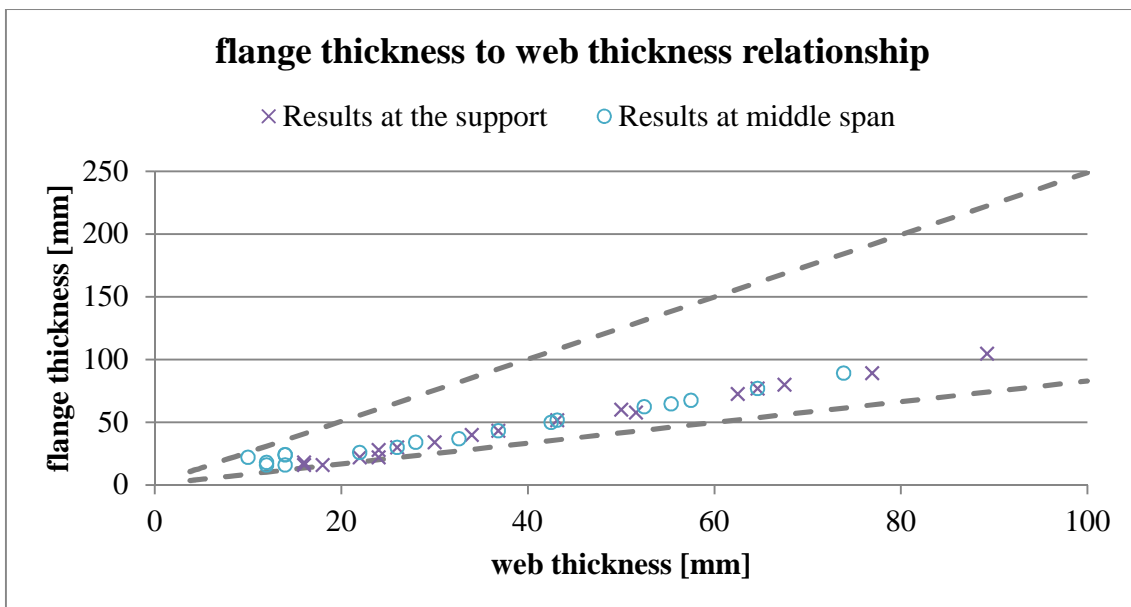


Figure A.7. Flange thickness-to-web thickness relationship.

A.4 ULS checks

A.4.1 General verification

Following EC3 and EC4 together with the Guideline, the verifications needed for the studied double-fixed structure are identified and depicted in Figure A.8.

- I. Bending and Shear.
- II. Bending, shear and bending-shear interaction.
- III. Shear longitudinal connection.

- IV. Local introduction of longitudinal forces in the slab.
- V. Longitudinal shear.
- VI. Lateral torsional buckling.

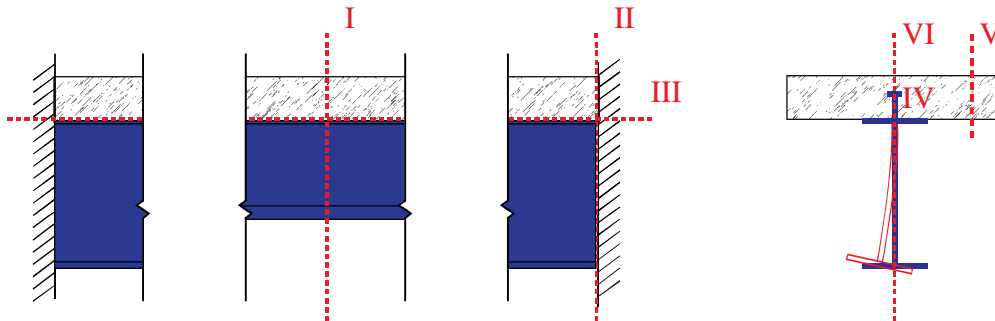


Figure A.8. Identification of the checks to be evaluated for the studied longitudinal girder profile.

According to these verifications, the following elements were checked according to the assumptions and simplifications mentioned. All the rules enumerated in the next list are presented according to what it is defined in EC3 and EC4 for Stainless Steel and the Guideline for FRP and Graphene.

- I. At middle span, sagging bending, and in the transition, shear, were verified for according to:
 - a. Stainless Steel: EC4 with plastic analysis as it is stated for CS1 and CS2.
 - b. FRP and Graphene: Elastic analysis according to the Guideline.
- II. At the supports bending and shear resistance were checked for hogging bending according to:
 - a. Stainless Steel: EC4 with plastic analysis as it is stated for CS1 and CS2. The bending and shear interaction is taken into account according to EC3
 - b. FRP and Graphene: Elastic analysis according to the Guideline.
- III. The longitudinal connection was assumed to be fulfilled as it mainly concerns the characteristic of the connection, which is out of the scope of the present study. Moreover, the longitudinal load for pedestrian bridges is very small as it is 10% of the vertical case.
- IV. Local verifications in the connection were assumed to be fulfilled as it was out of the scope of this study.
- V. Longitudinal shear of the deck was checked according to:
 - a. Concrete: was checked assuming the condition to avoid shear reinforcement in the deck.
 - b. FRP and Graphene: assumed to be fulfilled as it was deduced from a scaled commercial case and the truss-shape should be able to handle the relatively small pedestrian and dead loads.
- VI. Lateral torsional buckling check was out of the scope of the present work and according to:

- a. Stainless Steel: EC4 lateral torsional buckling does not need to be checked if the connections satisfy the stability condition. The present case is assumed to fulfil it.
- b. FRP and Graphene: There is a lack of information about this issue and, even though the authors are concerned about the importance of this matter for the height profiles obtained, the local behaviour of the girder was not an objective of this work. Furthermore, this problem was not believed to affect the global dynamic behaviour of the analysed bridges.

A.4.2 Girder

Depending on the material case being analysed different assumptions and checks were evaluated.

A.4.2.1 Stainless steel girders

The stainless steel beams and box girder were assumed to be of CS1 and CS2 to avoid local buckling. This takes into account that high slenderness will reduce the height-to-thickness ratio and therefore reduce the buckling problem itself.

These conditions limit the width-to-thickness ratio for web and flanges separately. According to EC4, the restrained buckling in the connection between concrete and steel is assumed as CS1 due to the restrained buckling by the connectors. Therefore web and low flange have geometry limitations.

Cross-section classes 1 or 2 conditions and assumptions:

- Full interaction between steel, reinforcement and concrete.
- The effective area of structural steel sections are stressed to its yield strength f_{yd} in tension and compression.
- The bending and shear interaction is accounted for the Steel girders as reflected in EC3.

The Steel girder was used for both concrete and orthotropic FRP decks. Concrete deck design was performed with plastic theory and therefore no further discussion had to be done. For the case of orthotropic deck, where elastic theory had to be used, a comparison between the solutions with or without full interaction between girder and deck was performed in order to compare these two different analyses:

- No interaction between the girder and deck, and therefore use of plastic calculation applied to the girder.
- Full interaction between the girder and deck, and therefore use of combination of plastic and elastic theory had to be applied.

In the case of full interaction, it is important to analyse the possible deformation domains that can occur and which case would be the most effective for the considered cross-section.

These deformation domains are depicted and explained in Figure A.9. In the present study all the analysed cross-sections had their limit in the Domain 4, as the materials used in the

deck had their deformation limit considerably higher than the steel and a relatively small thickness, therefore the steel deck always reached yielding point.

All the described domains assume that the limitation part is the steel girder, but it can occur that the upper part of the orthotropic deck reaches its yielding point in a domain, and therefore its limit as elastic analysis applies here. If this situation is reached the maximum capacity of the cross-section would have been reached and no further deformation scenarios have to be analysed.

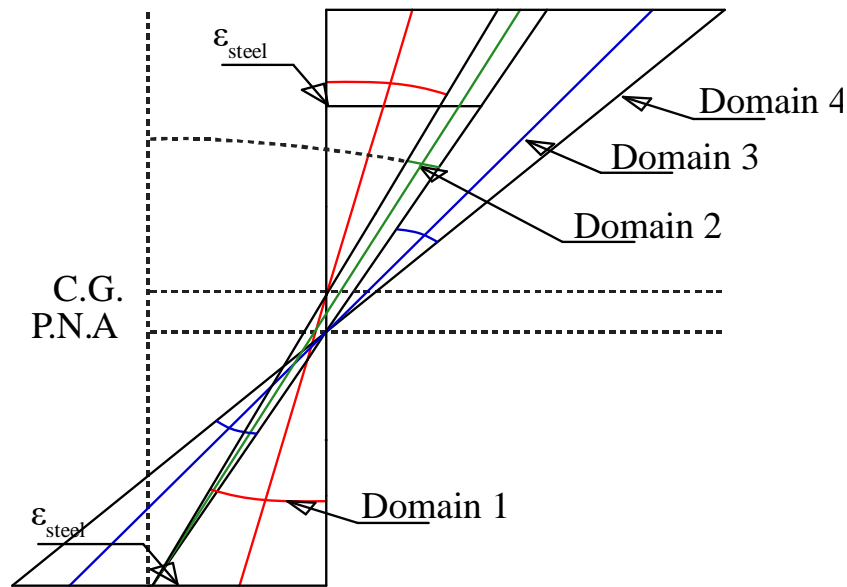


Figure A.9. Deformation domains for the steel girder and FRP deck.

Domain 1:

- No fibre has reached plasticity.
- Deformation plane rotates with its centre in the centre of gravity.

Domain 2:

- Lower flange of the steel girder reached plasticity.
- The rotation plane rotates with its centre in the lower flange and the deformation corresponding with the yield point of the steel.
- Neutral fibre moves from the centre of gravity downwards.

Domain 3:

- Upper flange has reached plasticity.
- The neutral fibre has reached its lower value and the deformation plane starts rotation with centre at this point.
- Inner parts of the web start to yield.

Domain 4:

- The steel girder fully yields before the upper flange of the orthotropic deck reaches its yielding point.

A.4.2.2 FRP and Graphene girders

The design approach for the high-performance materials studied in the present project was dimensioned according to the latest guidelines published by manufactures. It has to be remarked that there is yet a lack of official codes and standards.

The reference guide used for this study was the *Fiberline Design Manual* (Fiberline Composites A/S, 2003). FRP material properties are presented in this document, together with design recommendations.

The design reduction factors included in this guided were used for *long-term situations*, $\gamma_M = 3.2$. It is important to remark that these reduction factors reduce significantly the mechanical properties of the profiles.

Graphene was studied in this project as a futuristic material for which any experiments or reference data does not exist; therefore it made no sense to apply a reduction factor to its properties, $\gamma_M = 1.0$.

A.4.3 Bridge deck

Bridge deck and girder were considered to have full interaction in their connection. This was because it was found to be the optimal solution according to the design process explained in Section A.4.2.1.

A.4.3.1 Concrete deck

An initial check in the transversal direction was calculated according to EC 1 to avoid shear reinforcement in the deck. Nevertheless, this condition was never a limitation for the dimensioning of the deck.

The effective width was considered according to EC 4 and the deck thickness obtained as a variable parameter with a minimum thickness obtained from the transversal design of the bridge and the minimum concrete cover required for protection of the rebars.

Conditions and assumptions:

- Full interaction between steel, reinforcement and concrete.
- The effective area of longitudinal reinforcement in tension and compression are stressed to the yield strength f_{sd} .
- The effective area of concrete in compression is stressed over the whole depth between the plastic neutral axis (PNA) and the most compressed fibre of the concrete under f_{cd} . The design cylinder compressive strength of concrete.
- The area of the reinforcement was assumed to be a 6.3 % percent of the total area of the concrete deck. This relation is obtained from the NCC reference bridge. The minimum area of the reinforcement stated in the EC is less restricted than this condition, therefore this percentage is used.

- Creep and shrinkage for Cross-Sections 1 and 2 do not need to be taken into account. Therefore the homogenization factor is reduced to a relationship between the Poisson's modulus.

A.4.3.2 Orthotropic deck

The orthotropic deck selected for the FRP and Graphene deck cases corresponds to the ASSET Fiberline concept (Fiberline Composites A/S, 2015) that is presented in Figure A.10. This concept was scaled to different levels, in order to find the optimal solution for the studied bridge widths, according to static ULS requirements.

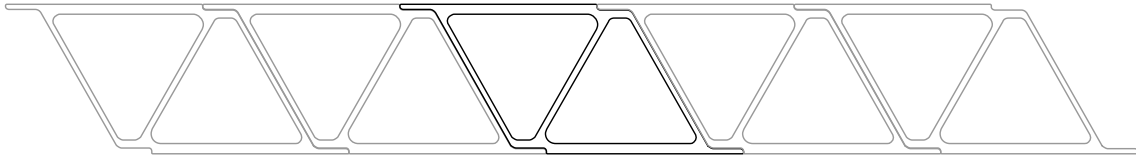


Figure A.10. ASSET concept sketch (Fiberline Composites A/S, 2015)

The dimension requirements were checked in the transversal direction of the cross-section. The orthotropic deck width for the ASSET deck was calculated as 70% of the effective concrete deck according to (Fu, et al., (2007), P. Moses, et al., (2006) and Keller & Schollmayer, (2004).

The thicknesses were used considering the flanges as the elements contributing to the bending capacity and therefore they were the limiting design parameter. Once the thickness was fixed for the three studied thicknesses the longitudinal analysis was carried out.

A.5 SLS checks

The SLS was only checked for the deflection limitation in both longitudinal and transversal directions. The transversal criterion did only limit the orthotropic deck.

A.5.1 Girder

The deflection was obtained from the Bernoulli-Euler law. The present case with height variation of the section was simplified to reduce the computation time, reducing the problem to two constant cross-sections in L_{sides} and L_{middle} lengths mentioned in Section 5.1 with the mean height between $h_{support}$ and h_{trans} , and the mean between h_{trans} and h_{middle} respectively.

$$v(x) = \int \int \frac{M(x)}{E_s I_{composite 1}} + \int \int \frac{M(x)}{E_s I_{composite 2}} \quad (A.2)$$

The equations for slope and deflection were derived from the integral, including the boundary and compatibility conditions for the cross-section height change along the bridge.

A.5.2 Deck

The transversal deflection was checked as a simply supported beam with overhang on both sides, as easily seen with the cross-section sketch from Figure 5.1.

A.6 Optimization criterion

All the geometries that fulfilled the ULS and SLS checks were collected. The geometries within the 10% higher utilization ratios were gathered then to find the optimal solution, and from them, the solution with minimum distance to the origin of the 2D-plot of weight vs. height of the beam at the support was selected as as the best solution.

$$\text{Solution} \begin{cases} \max \left(\frac{M_{Ed}}{M_{Rd}}, \frac{N_{Ed}}{N_{Rd}}, \frac{V_{Rd,section}}{V_{Ed}}, \frac{N_{Rd,section}}{N_{Ed}} \right) > 0.9 \cdot \max(\text{Utilization}) \\ \min \left(\sqrt{\text{weight}^2 + h_{beam\ support}^2} \right) \end{cases}$$

This methodology provides a solution that fulfils the geometry requirements of the codes, together with the conditions needed to maximize the dynamics problems aimed to identify in this study.

The results for the case of L=250 m and B=5 m for the sections with more than 90% of utilization ratio are presented in Figure A.11.

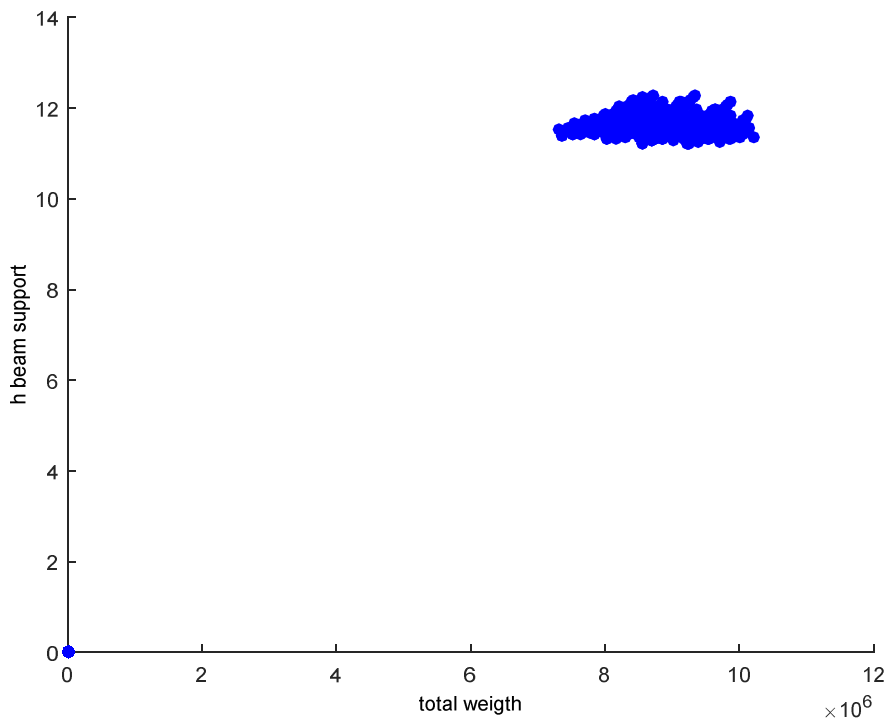


Figure A.11. Result of the geometry optimization criterion for the II-beams bridge with concrete deck, steel girder a width of 5 m and a length of 250 m.

This procedure, used for all the different bridge cases, made it possible to obtain objective geometries, in an automatic manner. So that, always the most optimal bridge according to the explained criterion could be chosen in order to be analysed later regarding dynamic problems.

A.7 Calculation Flow-Chart

Summarizing the presented design process, Figure A.12 presents the process followed for each of the geometry and material combination considered.

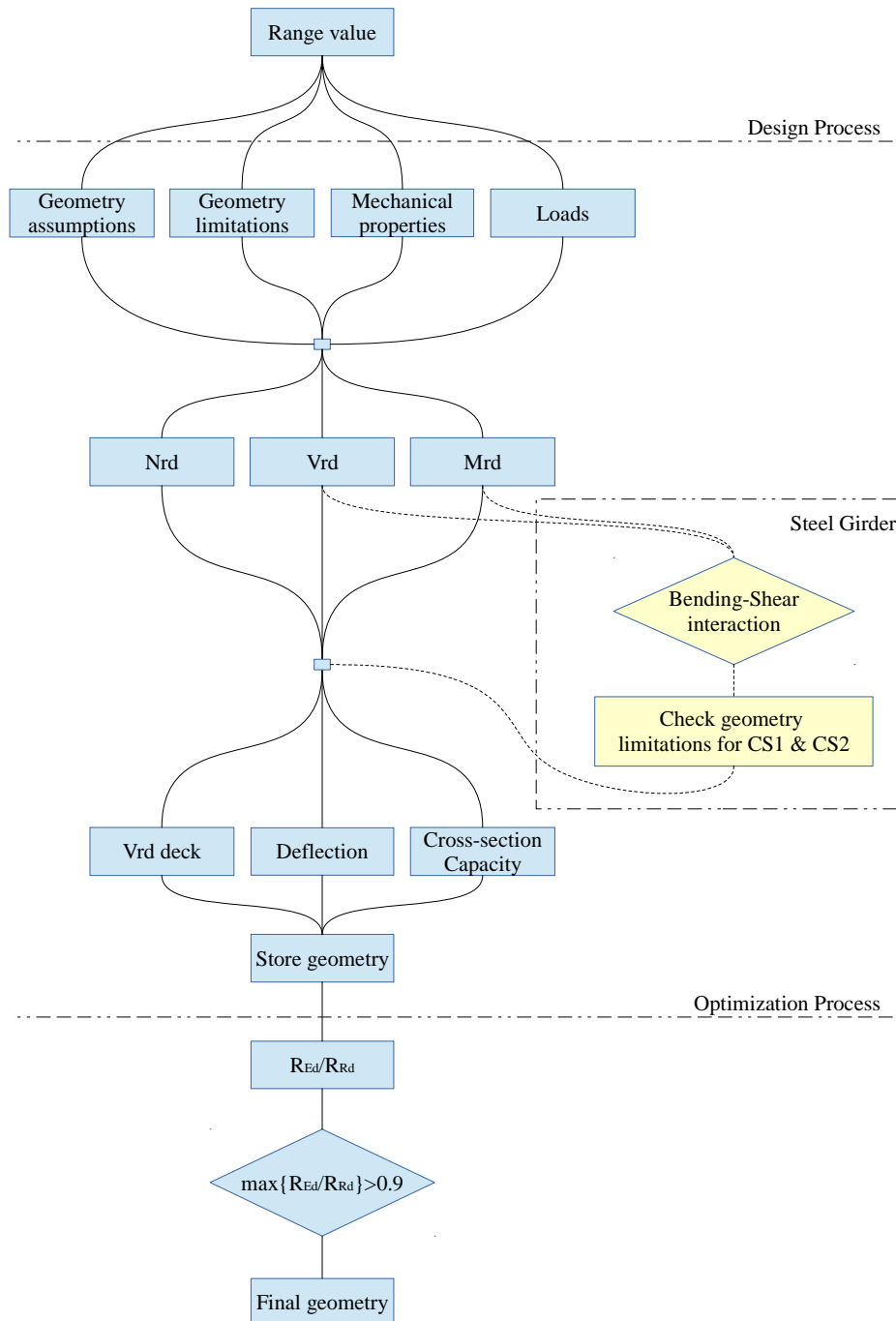


Figure A.12. Calculation flow chart to obtain the bridge geometries.

APPENDIX B FE modelling in BRIGADE

The modelling of bridges in BRIGADE was carried out with python scripts that allowed creating the models for the analysis in a fast and secure way, avoiding possible mistakes due to the need of repeating the same process several times.

All the elements of the bridge were modelled as *shell* elements, taking lamina properties for the deck. It is important to remark that the FRP and graphene girders had their material orientation with their strong axis in the longitudinal direction while the deck had the orientation according to the equivalent properties calculated from Section A.4.3.2

The connection between deck and girder was designed as *tie* connection, as it was assumed a full interaction between them in the design stage, as explained in Section A.4.2.1.

The fixed boundary conditions were implemented by restraining all the movements along the edges of the beams.

The mesh seed was obtained from a convergence study done for each material and geometry configuration. After this study, there were concluded a group of *mesh families* that allowed achieving accurate results without needing to analyse each bridge independently.

B.1 Orthotropic deck

The orthotropic sandwich deck was modelled in BRIGADE as a shell with equivalent properties. This was done due to the high number of elements that modelling the real deck would have created. For the kind of analysis performed, this would have ended up in a great computation time. Furthermore, the evaluation of local effects was not the aim of this project.

The equivalent deck used in BRIGADE was a shell with *lamina* properties. A *shell* with *orthotropic* properties was studied as well, but it gave similar results as the *lamina* properties. Therefore the equivalent properties needed where:

- E_1 : principal direction of the fibre.
- E_2 : perpendicular to the direction of the fibre.
- ν_{12} : in-plane poisson moduli.
- G_{12} : in-plane shear moduli.
- G_{13} : transversal shear moduli.
- G_{23} : longitudinal shear moduli.

The equivalent properties were calculated from mathematical derivations and then checked with a small model of the orthotropic sandwich deck in detail..

Local axis and material properties used in the mathematical calculations are shown in Figure B.1. These numerical calculations were based on Cusen & Pama (1975) and Davalos, et al, (2006).

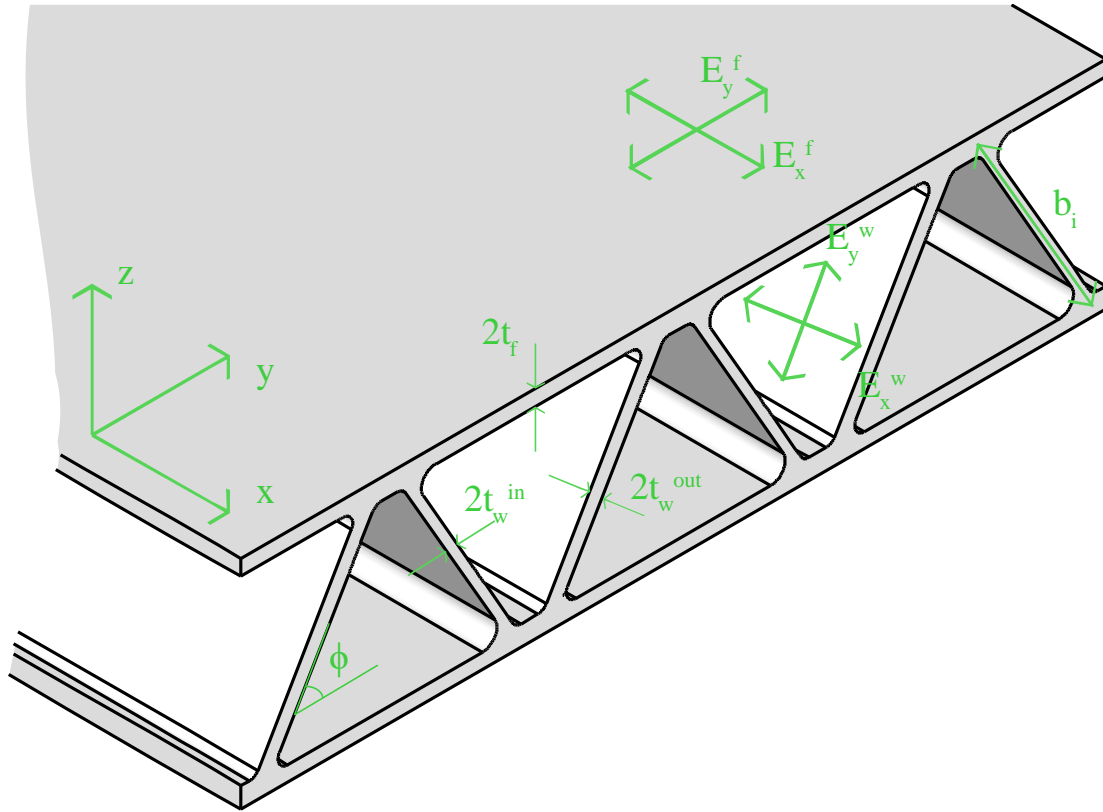


Figure B.1. Local deck axis and material orientation of flanges and web

where:

- $E_{x,i}$: Elastic moduli in the x-direction. It corresponds to the strong axis of the flanges and weak axis of the webs due to the material orientation.
- $E_{y,i}$: Elastic moduli in the y-direction. It corresponds to the weak axis of the flanges and strong axis of the webs due to the material orientation.

The transversal stiffness of the orthotropic deck corresponds to the longitudinal stiffness of a beam with the cross-section of each trapezoidal element from the deck. Thus, the total stiffness can be obtained multiplying the total number of elements, n_c , by the longitudinal stiffness of each element, D_b .

$$(EI)_x = n_c \cdot D_b = n_c \cdot \sum_{flanges, inner\ web, outer\ web} E_{x,i} \cdot I_{x,i} \quad (B.1)$$

The shear stiffness in the bridge width in-plane corresponds to the shear stiffness of a beam approximated in terms of the shear modulus component and cross-sectional area of the beams.

$$(GJ)_{xz} = n_c \cdot G_{xy} \cdot \sum_{inner\ web, outer\ web} b_i \cdot t_i \quad (B.2)$$

The longitudinal stiffness of the deck corresponds to the transversal stiffness of a beam with the defined cross-section. Neglecting the effect of the webs, the stiffness is obtained as:

$$(EI)_y = n_c \cdot \sum_{flanges} E_{y,i} \cdot I_{y,i} \quad (B.3)$$

If the multi-cell structure is treated as a Vierendeel frame and it is assumed that the inflections points are present at the midway of the long flanges and web, and that the influence of the short flange is neglected as it is considerably stiff. The torsional stiffness can be calculated as:

$$(GJ)_{yz} = \frac{V}{\theta} = \frac{12}{b^* \cdot \sum_{mean\ webs, flanges} \frac{b_i}{E_{y,i}} \cdot I_{y,i}}$$

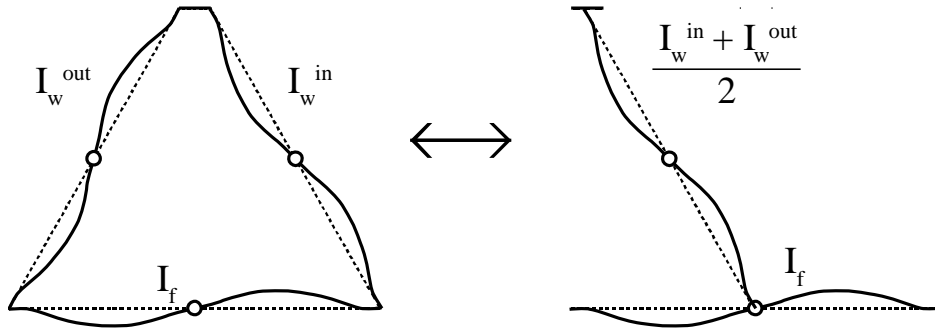


Figure B.2. Vierendeel frame for the analysed deck element according to Cusens and Pama (1975).

Considering the shear flow around the cross-section of the multi-cell deck as depicted in Figure B.3, Cusens and Pama (1975) showed that the influence of the web and flanges compared with the overall dimensions of the section is negligible and therefore the torsional rigidity can be calculated as follows:

$$(GJ)_{xy} = \frac{4A^2 G_{xy}}{\sum \frac{ds}{t}} + \sum G_{xy} \cdot ds \cdot \frac{t^3}{3} = \quad (B.4)$$

$$= \frac{4 \cdot (n_c \cdot b^* \cdot h)^2 \cdot G_{xy}}{2 \cdot n_c \cdot b^* \cdot t_f + \frac{2 \cdot h \cdot \sin\phi}{t_{w,out}}} + G_{xy} \cdot \left(2 \cdot n_c \cdot b^* \cdot \frac{t_f^3}{3} + 2 \cdot h \cdot \frac{\left(\frac{t_w^{out}}{\sin\phi}\right)^3}{3} \right)$$

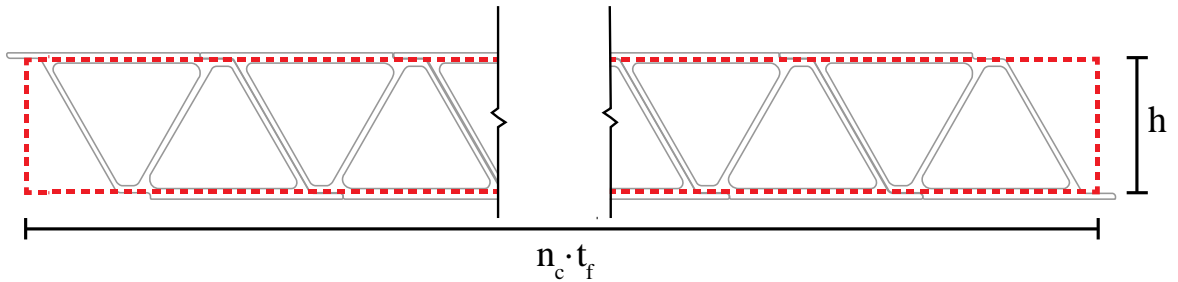


Figure B.3. Shear flow around the cross-section according to Cusens and Pama (1975)

Finally, the equivalent deck properties are calculated by imposing that stiffness of both decks have to match.

APPENDIX C Results tables from dynamic analysis

C.1 II-beams – Concrete-Steel

Length	Width	Mode no.	Direction	Shape	Mass part. (%)	Eigenfreq. (Hz)	Traffic Class	Confort Level	Vertical Accel. Max (m/s ²)	Lateral Accel. Max (m/s ²)
35	2.5	1	Vertical		66.0%	3.09				
		2	Lateral		28.2%	5.97				
		4	Lateral		43.2%	8.69				
		6	Vertical		14.5%	15.22				
		27	Vertical		6.2%	34.92				
		30	Lateral		11.2%	40.44				
		39	Longitudinal		68.6%	57.04				
		40	Longitudinal		10.8%	58.10				
No mode in range -> Bridge OK										
35	5.0	1	Vertical		67.1%	3.12				
		5	Lateral		69.1%	12.65				
		6	Vertical		14.5%	15.09				
		24	Vertical		5.8%	32.86				
		42	Longitudinal		75.5%	54.22				
45	Vertical		10.5%	57.70						
No mode in range -> Bridge OK										
35	10.0	1	Vertical		67.0%	3.17				
		9	Lateral		13.6%	14.16				
		10	Vertical		8.6%	14.48				
		11	Lateral		20.5%	15.60				
		20	Lateral		39.2%	19.54				
		31	Vertical		5.7%	26.54				
		56	Longitudinal		8.6%	44.21				
		59	Longitudinal		13.8%	47.28				
		60	Longitudinal		35.1%	48.19				
61	Longitudinal		23.0%	48.55						
No mode in range -> Bridge OK										
50	2.5	1	Vertical		64.7%	2.56				
		2	Lateral		49.1%	3.28				
		3	Lateral		20.1%	5.59				
		18	Vertical		14.7%	12.40				
		30	Lateral		7.4%	23.85				
		34	Vertical		6.6%	28.10				
48	Longitudinal		70.3%	42.00						
No mode in range -> Bridge OK										
50	5.0	1	Vertical		66.1%	2.54				
		2	Lateral		8.2%	3.16				
		6	Lateral		14.1%	5.52				
		12	Lateral		50.4%	7.85				
		18	Vertical		14.7%	12.11				
		31	Vertical		6.4%	26.30				
		42	Lateral		6.3%	33.99				
51	Longitudinal		74.8%	39.35						
No mode in range -> Bridge OK										
50	10.0	1	Vertical		65.8%	2.58				
		8	Lateral		48.9%	9.73				
		12	Vertical		9.9%	11.69				
		18	Lateral		14.5%	13.68				
		38	Vertical		6.6%	23.05				
		64	Longitudinal		23.6%	36.93				
		67	Longitudinal		48.5%	37.51				
79	Lateral		8.6%	44.33						
No mode in range -> Bridge OK										
100	2.5	1	Lateral	1 all	62.2%	0.74	TC2	CL1	0.044	0.061
							TC3	CL2	0.069	0.096
							TC4	CL3	0.305	0.423
		3	Vertical	1 all	63.9%	1.62	TC2	CL1	0.861	0.005
							TC3	CL2	1.361	0.008

Length	Width	Mode no.	Direction	Shape	Mass part. (%)	Eigenfreq. (Hz)	Traffic Class	Confort Level	Vertical Accel. Max (m/s ²)	Lateral Accel. Max (m/s ²)
							TC4	CL3	6.018	0.035
		4	Lateral		14.9%	2.28				
		18	Lateral		5.0%	5.27				
		25	Vertical		15.5%	7.73				
		56	Vertical		6.7%	17.65				
		98	Longitudinal		52.0%	22.35				
		116	Longitudinal		25.6%	24.74				
100	5.0	1	Lateral		41.4%	1.44				
		2	Vertical	1 all	64.0%	1.59	TC2 TC3 TC4	CL1 CL2 CL3	0.461 0.728 3.221	0.001 0.001 0.005
		8	Lateral		25.3%	2.74				
		23	Vertical		14.9%	7.56				
		35	Lateral		8.1%	12.70				
		93	Longitudinal		71.9%	21.44				
100	10.0	1	Lateral		15.0%	1.55				
		2	Vertical	1 all	64.8%	1.63	TC2 TC3 TC4	CL1 CL2 CL3	0.457 0.722 3.193	0.001 0.001 0.004
		13	Lateral		54.4%	4.11				
		22	Vertical		14.9%	7.54				
		101	Longitudinal		73.9%	20.44				
150	2.5	1	Lateral		60.1%	0.37				
		3	Vertical		61.4%	1.24				
		4	Lateral		6.0%	1.33				
		5	Lateral		9.3%	1.40				
		28	Vertical		15.0%	6.00				
		80	Vertical		7.1%	13.68				
		101	Longitudinal		73.9%	20.44				
		No mode in range -> Bridge OK								
150	5.0	1	Lateral	1 all	49.5%	0.59	TC2 TC3 TC4	CL1 CL2 CL3	0.006 0.010 0.044	0.007 0.011 0.049
		3	Vertical	1 all	61.5%	1.31	TC2 TC3 TC4	CL1 CL2 CL3	0.056 0.088 0.390	0.001 0.002 0.007
		6	Lateral		5.5%	1.52				
		8	Lateral		15.6%	1.79				
		28	Vertical		15.2%	6.22				
		95	Vertical		6.9%	13.93				
		118	Longitudinal		74.9%	16.15				
150	10.0	1	Lateral	1 all	34.6%	0.85	TC2 TC3 TC4	CL1 CL2 CL3	0.024 0.038 0.168	0.008 0.013 0.056
		5	Vertical	1 all	62.1%	1.37	TC2 TC3 TC4	CL1 CL2 CL3	0.127 0.201 0.888	0.001 0.001 0.004
		13	Lateral		32.5%	2.68				
		28	Vertical		14.5%	6.37				
		117	Vertical		5.6%	14.59				
		127	Longitudinal		76.0%	15.69				
200	2.5	No possible bridge due to geometry								
200	5.0	1	Lateral		58.4%	0.33				
		3	Vertical		62.5%	1.02				
		4	Lateral		10.2%	1.03	TC2 TC3 TC4	CL1 CL2 CL3	0.002 0.003 0.013	0.001 0.002 0.009
		7	Lateral		7.9%	1.19	TC2 TC3 TC4	CL1 CL2 CL3	0.000 0.000 0.001	0.000 0.001 0.003
		16	Lateral		5.3%	2.56				
		29	Vertical		15.8%	4.80				
		108	Vertical		7.0%	10.79				
		125	Longitudinal		72.7%	12.16				

Length	Width	Mode no.	Direction	Shape	Mass part. (%)	Eigenfreq. (Hz)	Traffic Class	Confort Level	Vertical Accel. Max (m/s ²)	Lateral Accel. Max (m/s ²)
200	10.0	1	Lateral		46.6%	0.49				
		5	Lateral	3 beams	6.1%	1.07	TC2	CL1	0.027	0.001
							TC3	CL2	0.004	0.001
							TC4	CL3	0.019	0.004
		7	Vertical		62.0%	1.09				
		8	Lateral		10.9%	1.35				
		12	Lateral		5.5%	1.77				
		13	Lateral		12.6%	1.88				
		29	Vertical		11.8%	5.02				
120	Longitudinal		10.4%	11.62						
128	Longitudinal		57.3%	12.14						
250	2.5	No possible bridge due to geometry								
250	5.0	1	Lateral		60.6%	0.23				
		3	Lateral	3 all	9.4%	0.77	TC2	CL1	0.001	0.000
							TC3	CL2	0.001	0.001
							TC4	CL3	0.006	0.003
		6	Lateral	1 all	6.4%	0.85	TC2	CL1	0.007	0.017
							TC3	CL2	0.010	0.027
							TC4	CL3	0.046	0.121
		7	Vertical		62.5%	0.88				
		16	Lateral		6.4%	1.94				
32	Vertical		15.7%	4.12						
120	Vertical		7.1%	9.20						
129	Longitudinal		74.0%	9.88						
250	10.0	1	Lateral		52.5%	0.35				
		5	Lateral	3 all	6.5%	0.89	TC2	CL1	0.001	0.000
							TC3	CL2	0.002	0.000
							TC4	CL3	0.009	0.001
		6	Vertical		63.2%	0.90				
		10	Lateral	1 all	15.3%	1.16	TC2	CL1	0.000	0.002
							TC3	CL2	0.000	0.003
							TC4	CL3	0.001	0.015
		32	Vertical		15.6%	4.21				
114	Vertical		6.9%	9.31						
119	Longitudinal		74.8%	9.60						
300	2.5	No possible bridge due to geometry								
300	5.0	1	Lateral		57.1%	0.16				
		3	Lateral	3 all	9.9%	0.59	TC2	CL1	0.000	0.000
							TC3	CL2	0.000	0.000
							TC4	CL3	0.001	0.000
		6	Lateral	1 all	7.1%	0.68	TC2	CL1	0.004	0.012
							TC3	CL2	0.006	0.019
							TC4	CL3	0.020	0.083
		8	Vertical		53.4%	0.82				
		9	Vertical		6.7%	0.82				
11	Lateral	5 all	3.6%	1.09	TC2	CL1	0.001	0.000		
					TC3	CL2	0.001	0.000		
					TC4	CL3	0.004	0.001		
300	10.0	41	Vertical		14.7%	3.85				
		136	Vertical		7.6%	8.54				
		139	Longitudinal		72.5%	8.73				
		1	Lateral		51.3%	0.26				
		5	Lateral	3 all	6.6%	0.69	TC2	CL1	0.000	0.000
							TC3	CL2	0.001	0.000
							TC4	CL3	0.003	0.002
		7	Vertical		60.9%	0.83				
		10	Lateral	1 all	12.7%	0.94	TC2	CL1	0.002	0.013
					TC3	CL2	0.003	0.021		
					TC4	CL3	0.012	0.094		
12	Lateral	5 beams	2.3%	1.15	TC2	CL1	0.000	0.000		
					TC3	CL2	0.000	0.000		
					TC4	CL3	0.001	0.001		
40	Vertical		13.3%	3.89						
128	Longitudinal		6.7%	8.45						
129	Longitudinal		60.8%	8.46						

Length	Width	Mode no.	Direction	Shape	Mass part. (%)	Eigenfreq. (Hz)	Traffic Class	Confort Level	Vertical Accel. Max (m/s ²)	Lateral Accel. Max (m/s ²)
		131	Vertical		7.0%	8.58				
			Longitudinal		2.9%					

C.2 II-beams – FRP-Steel

Length	Width	Mode no.	Direction	Shape	Mass part. (%)	Eigenfreq. (Hz)	Traffic Class	Confort Level	Vertical Accel. Max (m/s ²)	Lateral Accel. Max (m/s ²)
35	2.5	1	Lateral		40.6%	3.27				
		2	Vertical		62.6%	5.39				
		6	Lateral		8.6%	7.65				
		11	Lateral		27.1%	11.3				
		22	Vertical		15.0%	25.95				
		79	Longitudinal		71.5%	70.2				
		No mode in range -> Bridge OK								
35	5.0	1	Lateral		27.2%	4.16				
		3	Vertical		38.9%	5.6				
		4	Vertical		24.8%	5.61				
		11	Lateral		46.0%	13.63				
		20	Vertical		5.8%	25.79				
		21	Vertical		8.8%	26.15				
		96	Longitudinal		10.0%	62.31				
97	Longitudinal		63.5%	62.47						
No mode in range -> Bridge OK										
35	10.0	1	Lateral		11.1%	4.43				
		3	Vertical		65.9%	4.8				
		13	Lateral		13.3%	15.03				
		15	Lateral		53.5%	15.36				
		16	Vertical		6.1%	19.11				
		24	Vertical		8.0%	22.22				
		78	Longitudinal		46.3%	47.42				
79	Longitudinal		15.6%	47.49						
No mode in range -> Bridge OK										
50	2.5	1	Lateral		47.0%	1.84				
		3	Vertical		61.2%	3.75				
		6	Lateral		9.5%	5.04				
		10	Lateral		11.9%	6.91				
		11	Lateral		8.0%	7.18				
		24	Vertical		15.1%	18.12				
		77	Longitudinal		29.5%	51.19				
78	Longitudinal		41.0%	51.22						
No mode in range -> Bridge OK										
50	5.0	1	Lateral		35.6%	2.59				
		5	Vertical		62.6%	4.06				
		11	Lateral		37.6%	8.73				
		24	Vertical		15.0%	19.27				
		99	Longitudinal		27.1%	47.36				
100	Longitudinal		44.4%	47.37						
No mode in range -> Bridge OK										
50	10.0	1	Lateral		18.3%	3.07				
		5	Vertical		64.5%	3.84				
		15	Lateral		54.6%	10.18				
		20	Vertical		12.7%	16.83				
		111	Longitudinal		7.4%	38.02				
		113	Longitudinal		38.0%	38.04				
114	Longitudinal		27.3%	38.19						
No mode in range -> Bridge OK										
100	2.5	1	Lateral	1 all	54.1%	0.55	TC2	CL1	0.009	0.012
							TC3	CL2	0.014	0.019
							TC4	CL3	0.059	0.084
		3	Vertical	1 all	59.3%	1.94	TC2	CL1	1.674	0.008
							TC3	CL2	2.647	0.012
							TC4	CL3	11.061	0.051

Length	Width	Mode no.	Direction	Shape	Mass part. (%)	Eigenfreq. (Hz)	Traffic Class	Confort Level	Vertical Accel. Max (m/s ²)	Lateral Accel. Max (m/s ²)
100	5.0	5	Lateral		13.6%	2.00				
		8	Lateral		8.5%	2.71				
		28	Vertical		15.5%	9.30				
		90	Vertical		7.2%	21.10				
		129	Longitudinal		61.8%	27.10				
		1	Lateral	1 all	48.8%	0.89	TC2	CL1	0.078	0.049
							TC3	CL2	0.123	0.077
							TC4	CL3	0.514	0.324
		5	Vertical	1 all	58.6%	2.18	TC2	CL1	0.984	0.008
							TC3	CL2	1.556	0.012
					TC4	CL3	5.971	0.047		
100	10.0	6	Lateral		8.6%	2.20				
		10	Lateral		7.6%	3.37				
		13	Lateral		10.2%	3.89				
		29	Vertical		11.6%	10.33				
		116	Vertical		7.5%	23.17				
		133	Longitudinal		71.7%	26.43				
		1	Lateral	1 deck	38.5%	2.26	TC2	CL1	0.289	0.004
		3 beam			TC3	CL2	0.457	0.006		
					TC4	CL3	1.618	0.020		
7	Vertical	1 deck	23.0%	2.26	TC2	CL1	0.262	0.003		
		3 beam			TC3	CL2	0.415	0.005		
					TC4	CL3	1.588	0.019		
150	2.5	1	Lateral		56.8%	0.27				
		3	Lateral	3 all	14.8%	1.12	TC2	CL1	0.003	0.003
							TC3	CL2	0.005	0.005
							TC4	CL3	0.021	0.020
		6	Vertical	1 all	60.2%	1.32	TC2	CL1	0.085	0.001
					TC3	CL2	0.134	0.002		
					TC4	CL3	0.576	0.008		
150	5.0	7	Lateral		5.1%	1.39				
		30	Vertical		15.3%	6.32				
		97	Vertical		7.2%	14.30				
		137	Longitudinal		67.6%	18.08				
		1	Lateral	1 all	60.0%	1.44	TC2	CL1	0.274	0.001
					TC3	CL2	0.434	0.002		
					TC4	CL3	1.784	0.010		
150	10.0	10	Lateral		11.3%	1.92				
		31	Vertical		15.4%	6.87				
		113	Vertical		7.4%	15.41				
		137	Longitudinal		70.4%	17.93				
		1	Lateral	1 all	45.1%	0.70	TC2	CL1	0.023	0.012
					TC3	CL2	0.036	0.022		
					TC4	CL3	0.149	0.079		
5	Lateral	1 all	6.2%	1.41	TC2	CL1	0.393	0.004		
					TC3	CL2	0.621	0.007		
					TC4	CL3	2.242	0.025		
150	10.0	13	Lateral		20.2%	2.76				
		32	Vertical		15.2%	7.35				
		130	Longitudinal		33.2%	16.99				
		131	Longitudinal		35.8%	16.99				
		No possible bridge due to geometry								
200	5.0	1	Lateral		55.5%	0.26				
		5	Lateral	3 all	12.5%	0.91	TC2	CL1	0.002	0.003
							TC3	CL2	0.004	0.005
							TC4	CL3	0.016	0.002
7	Vertical		59.3%	1.14						

Length	Width	Mode no.	Direction	Shape	Mass part. (%)	Eigenfreq. (Hz)	Traffic Class	Confort Level	Vertical Accel. Max (m/s ²)	Lateral Accel. Max (m/s ²)
200	10.0	10	Lateral		8.4%	1.29				
		36	Vertical		15.4%	5.40				
		147	Longitudinal		71.4%	13.68				
		1	Lateral		50.1%	0.44				
		5	Lateral	3 all	8.1%	1.03	TC2	CL1	0.003	0.000
							TC3	CL2	0.005	0.000
							TC4	CL3	0.022	0.002
		7	Vertical		59.2%	1.23				
		10	Lateral		8.4%	1.57				
		13	Lateral		10.1%	2.10				
41	Vertical		13.1%	5.78						
134	Vertical		7.6%	12.77						
140	Longitudinal		71.9%	13.30						
250	2.5	No possible bridge due to geometry								
250	5.0	1	Lateral		56.1%	0.18				
		5	Lateral	3 all	13.9%	0.67	TC2	CL1	0.001	0.001
							TC3	CL2	0.002	0.001
							TC4	CL3	0.009	0.005
		7	Lateral	1 all	6.3%	0.92	TC2	CL1	0.015	0.040
							TC3	CL2	0.024	0.063
							TC4	CL3	0.099	0.263
		9	Vertical		8.3%	0.96				
		10	Vertical		50.1%	0.96				
		45	Vertical		15.7%	4.52				
151	Longitudinal		71.3%	11.08						
250	10.0	1	Lateral		52.6%	0.30				
		5	Lateral	3 all	9.2%	0.78	TC2	CL1	0.002	0.000
							TC3	CL2	0.003	0.001
							TC4	CL3	0.013	0.003
		7	Vertical		58.1%	1.02				
		10	Lateral	1 all	10.2%	1.18	TC2	CL1	0.000	0.001
							TC3	CL2	0.000	0.002
							TC4	CL3	0.000	0.007
		51	Vertical		15.4%	4.78				
		143	Longitudinal		58.1%	10.85				
145	Longitudinal		8.4%	10.87						
300	2.5	No possible bridge due to geometry								
300	5.0	1	Lateral		56.5%	0.13				
		5	Lateral	3 all	14.6%	0.53	TC2	CL1	0.000	0.000
							TC3	CL2	0.000	0.000
							TC4	CL3	0.001	0.001
		7	Lateral	1 all	5.1%	0.71	TC2	CL1	0.007	0.023
							TC3	CL2	0.010	0.036
							TC4	CL3	0.044	0.156
		10	Vertical		58.4%	0.85				
		12	Lateral	5 all	4.8%	1.05	TC2	CL1	0.001	0.000
							TC3	CL2	0.001	0.000
					TC4	CL3	0.006	0.001		
55	Vertical		15.8%	3.96						
154	Longitudinal		19.4%	9.27						
156	Longitudinal		51.5%	9.28						
300	10.0	1	Lateral		54.1%	0.21				
		5	Lateral	3 all	10.4%	0.62	TC2	CL1	0.000	0.000
							TC3	CL2	0.000	0.000
							TC4	CL3	0.001	0.001
		9	Vertical		58.2%	0.89				
		10	Lateral	1 all	9.6%	0.94	TC2	CL1	0.002	0.018
							TC3	CL2	0.003	0.028
							TC4	CL3	0.014	0.113
		12	Lateral	5 all	3.2%	1.11	TC2	CL1	0.001	0.000
							TC3	CL2	0.002	0.000
					TC4	CL3	0.008	0.001		
16	Lateral		4.7%	1.59						
62	Vertical		15.8%	4.15						

Length	Width	Mode no.	Direction	Shape	Mass part. (%)	Eigenfreq. (Hz)	Traffic Class	Confort Level	Vertical Accel. Max (m/s ²)	Lateral Accel. Max (m/s ²)
		151	Longitudinal		26.9%	9.14				
			Vertical		4.6%					
		152	Longitudinal		43.3%	9.19				
			Vertical		3.0%					

C.3 II-beams – FRP

Length	Width	Mode no.	Direction	Shape	Mass part. (%)	Eigenfreq. (Hz)	Traffic Class	Confort Level	Vertical Accel. Max (m/s ²)	Lateral Accel. Max (m/s ²)		
35	2.5	1	Lateral		39.6%	2.29						
		7	Vertical		21.7%	5.75						
			Lateral		6.7%							
		8	Vertical		42.9%	5.86						
			Lateral		3.3%							
		11	Lateral		8.4%	9.62						
		13	Lateral		17.6%	9.93						
		58	Vertical		4.1%	24.07						
		59	Vertical		6.3%	24.13						
		128	Longitudinal		44.8%	52.72						
129	Longitudinal		27.7%	52.75								
No mode in range -> Bridge OK												
35	5.0	1	Lateral		28.6%	3.14						
		7	Vertical		62.5%	6.21						
			Lateral		0.3%							
		8	Vertical		4.2%	6.47						
			Lateral		3.6%							
		12	Lateral		5.3%	10.84						
		13	Lateral		39.6%	11.86						
		39	Vertical		13.3%	23.91						
10	Longitudinal		78.5%	48.84								
No mode in range -> Bridge OK												
35	10.0	1	Lateral		14.2%	2.67						
		7	Vertical		60.6%	6.63						
			Lateral		0.4%							
		8	Vertical		9.1%	6.82						
			Lateral		2.2%							
		15	Lateral		48.0%	13.38						
		32	Lateral		6.6%	18.17						
		50	Vertical		10.9%	22.86						
		103	Longitudinal		35.5%	41.28						
		106	Longitudinal		26.3%	41.42						
107	Longitudinal		16.5%	41.51								
108	Longitudinal		6.2%	41.68								
No mode in range -> Bridge OK												
50	2.5	1	Lateral	1 all	40.7%	1.12	TC2	CL1	0.054	0.021		
							TC3	CL2	0.086	0.033		
							TC4	CL3	0.208	0.079		
		5	Lateral		4.1%	2.81						
		7	Lateral		19.0%	3.19						
		10	Vertical		63.8%	4.33						
		11	Lateral		6.3%	5.11						
		20	Lateral		11.3%	6.87						
		88	Vertical		12.3%	17.89						
		214	Longitudinal		21.2%	37.87						
		215	Longitudinal		33.4%	37.91						
		216	Longitudinal		20.6%	38.12						
		50	5.0	1	Lateral		39.1%	2.14				
				5	Lateral		3.6%	3.72				
				7	Vertical		35.4%	4.00				
13	Lateral				32.0%	7.53						
32	Vertical				15.1%	16.45						
99	Longitudinal				7.4%	35.31						
101	Longitudinal				52.0%	35.76						
102	Longitudinal				15.6%	36.10						

Length	Width	Mode no.	Direction	Shape	Mass part. (%)	Eigenfreq. (Hz)	Traffic Class	Confort Level	Vertical Accel. Max (m/s ²)	Lateral Accel. Max (m/s ²)
		No mode in range -> Bridge OK								
50	10.0	1	Lateral		19.9%	2.06				
		7	Vertical		52.7%	4.59				
			Lateral		1.1%					
		8	Vertical		15.7%	4.70				
			Lateral		3.2%					
		15	Lateral		49.7%	8.90				
		44	Vertical		14.3%	16.27				
		105	Longitudinal		79.8%	31.73				
		No mode in range -> Bridge OK								
100	2.5	1	Lateral		45.8%	0.37				
		5	Lateral	1 all	14.5%	1.09	TC2	CL1	0.856	0.172
							TC3	CL2	1.353	0.272
							TC4	CL3	3.279	0.660
		6	Lateral		8.3%	1.26				
		11	Vertical	1 all	59.6%	2.21	TC2	CL1	0.894	0.134
							TC3	CL2	1.414	0.211
							TC4	CL3	3.424	0.512
		12	Lateral		6.3%	2.43				
		18	Lateral		8.2%	2.96				
		105	Vertical		4.7%	9.05				
		106	Vertical		8.9%	9.10				
		107	Vertical		3.3%	9.11				
		289	Longitudinal		68.0%	20.44				
100	5.0	1	Lateral	1 all	40.9%	0.52	TC2	CL1	0.001	0.001
							TC3	CL2	0.133	0.001
							TC4	CL3	0.003	0.004
		5	Lateral		5.0%	1.26				
		7	Lateral		19.7%	1.55				
		11	Lateral		6.2%	2.24				
		12	Vertical	1 all	63.9%	2.29	TC2	CL1	0.128	0.005
							TC3	CL2	0.202	0.008
							TC4	CL3	0.490	0.019
		26	Lateral		4.7%	3.52				
		94	Vertical		13.8%	9.34				
		227	Longitudinal		73.0%	19.04				
100	10.0	1	Lateral	1 all	45.3%	0.98	TC2	CL1	0.018	0.015
							TC3	CL2	0.283	0.024
							TC4	CL3	0.686	0.057
		6	Lateral		4.8%	1.67				
		8	Vertical	1 all	64.4%	2.19	TC2	CL1	0.624	0.021
							TC3	CL2	0.986	0.033
							TC4	CL3	2.389	0.080
		15	Lateral		26.1%	3.82				
		50	Vertical		15.5%	9.05				
		126	Longitudinal		47.4%	18.91				
		127	Longitudinal		22.5%	18.93				
150	2.5	No possible bridge due to geometry								
150	5.0	1	Lateral		42.7%	0.27				
(No x-part considered)		5	Lateral	3 beams	3.8%	0.79	TC2	CL1	0.018	0.004
							TC3	CL2	0.028	0.007
							TC4	CL3	0.068	0.016
		7	Lateral	1 all	21.3%	0.81	TC2	CL1	0.246	0.066
							TC3	CL2	0.389	0.104
							TC4	CL3	0.941	0.252
		10	Lateral		6.3%	1.39				
		17	Vertical	1 all	59.7%	1.63	TC2	CL1	0.263	0.066
							TC3	CL2	0.415	0.104
							TC4	CL3	1.006	0.251
		138	Vertical		15.8%	6.59				
		313	Longitudinal		58.6%	13.59				
		314	Longitudinal		13.2%	13.60				
150	10.0	1	Lateral		39.5%	0.45				
(No x-part considered)		5	Lateral	3 beams	4.3%	0.95	TC2	CL1	0.014	0.001

Length	Width	Mode no.	Direction	Shape	Mass part. (%)	Eigenfreq. (Hz)	Traffic Class	Confort Level	Vertical Accel. Max (m/s ²)	Lateral Accel. Max (m/s ²)
considered)							TC3	CL2	0.002	0.002
							TC4	CL3	0.055	0.004
		7	Lateral		17.0%	1.25				
		10	Vertical	1 all	64.9%	1.54	TC2	CL1	0.100	0.003
							TC3	CL2	0.157	0.005
							TC4	CL3	0.382	0.011
		20	Lateral		11.5%	2.46				
76	Vertical		16.2%	6.22						
174	Longitudinal		21.5%	12.33						
176	Longitudinal		18.4%	12.38						
177	Longitudinal		36.2%	12.39						
200	2.5	No possible bridge due to geometry								
200	5.0	1	Lateral		46.8%	0.18				
		5	Lateral	1 all	12.7%	0.53	TC2	CL1	0.002	0.008
							TC3	CL2	0.003	0.013
							TC4	CL3	0.008	0.031
		6	Lateral	3 beams	9.9%	0.58	TC2	CL1	0.001	0.001
							TC3	CL2	0.001	0.001
							TC4	CL3	0.003	0.003
		11	Lateral	5 beams	6.5%	1.03	TC2	CL1	0.013	0.001
							TC3	CL2	0.020	0.002
							TC4	CL3	0.049	0.005
		16	Lateral	7 beams	1.2%	1.19	TC2	CL1	0.001	0.000
							TC3	CL2	0.000	0.000
							TC4	CL3	0.000	0.000
17	Vertical		58.7%	1.24						
20	Lateral		5.2%	1.29						
143	Vertical		13.5%	5.01						
313	Longitudinal		10.6%	10.34						
315	Longitudinal		59.5%	10.39						
200	10.0	1	Lateral		42.8%	0.26				
		5	Lateral	3 beams	5.1%	0.61	TC2	CL1	0.000	0.001
							TC3	CL2	0.000	0.001
							TC4	CL3	0.001	0.002
		7	Lateral	1 all	19.8%	0.78	TC2	CL1	0.021	0.045
							TC3	CL2	0.034	0.071
							TC4	CL3	0.082	0.171
		11	Lateral	5 beams	5.8%	1.07	TC2	CL1	0.005	0.000
							TC3	CL2	0.008	0.001
							TC4	CL3	0.019	0.002
		14	Vertical		62.5%	1.21				
		97	Vertical		15.9%	4.88				
		210	Longitudinal		10.5%	9.40				
214	Vertical		5.7%							
	Longitudinal		61.8%	9.49						
250	2.5	No possible bridge due to geometry								
250	5.0	No possible bridge due to geometry								
250 (No x-part considered)	10.0	1	Lateral		43.3%	0.18				
		5	Lateral	3 beams	4.2%	0.52	TC2	CL1	0.000	0.000
							TC3	CL2	0.000	0.000
							TC4	CL3	0.000	0.000
		7	Lateral	1 all	21.9%	0.54	TC2	CL1	0.002	0.004
							TC3	CL2	0.003	0.007
							TC4	CL3	0.006	0.017
		10	Lateral	5 beams	6.8%	0.83	TC2	CL1	0.003	0.001
							TC3	CL2	0.005	0.001
							TC4	CL3	0.011	0.003
		16	Lateral	7 beams	1.1%	0.99	TC2	CL1	0.002	0.000
							TC3	CL2	0.003	0.000
							TC4	CL3	0.004	0.001
17	Vertical		62.2%	1.02						
40	Lateral		4.8%	1.53						
129	Vertical		16.4%	4.08						
279	Longitudinal		73.8%	7.88						
300	2.5	No possible bridge due to geometry								

Length	Width	Mode no.	Direction	Shape	Mass part. (%)	Eigenfreq. (Hz)	Traffic Class	Confort Level	Vertical Accel. Max (m/s ²)	Lateral Accel. Max (m/s ²)	
300	5.0	No possible bridge due to geometry									
300 (No x-part considered)	10.0	1	Lateral		45.2%	0.14					
		5	Lateral		12.9%	0.41					
		6	Lateral		12.4%	0.43					
		10	Lateral	5 beams	7.0%	0.68	TC2	CL1	0.000	0.000	
							TC3	CL2	0.001	0.001	
							TC4	CL3	0.002	0.001	
		16	Lateral	7 beams	1.1%	0.79	TC2	CL1	0.001	0.000	
							TC3	CL2	0.002	0.000	
							TC4	CL3	0.006	0.001	
		20	Lateral	9 beams	1.2%	0.87	TC2	CL1	0.001	0.000	
							TC3	CL2	0.001	0.000	
							TC4	CL3	0.003	0.001	
		21	Vertical			61.7%	0.88				
		24	Lateral	3 deck 11 beams	1.3%	0.93	TC2	CL1	0.001	0.000	
					TC3	CL2	0.002	0.001			
					TC4	CL3	0.004	0.001			
40	Lateral	1 all	2.5%	1.19	TC2	CL1	0.000	0.001			
					TC3	CL2	0.000	0.002			
					TC4	CL3	0.000	0.004			
139	Vertical			17.1%	3.49						
287	Vertical			7.8%	6.60						
292	Longitudinal			73.8%	6.70						

C.4 II-beams – Graphene

Length	Width	Mode no.	Direction	Shape	Mass part. (%)	Eigenfreq. (Hz)	Traffic Class	Confort Level	Vertical Accel. Max (m/s ²)	Lateral Accel. Max (m/s ²)
35	2.5	1	Lateral		17.6%	12.65				
		2	Vertical		65.3%	14.49				
		6	Lateral		15.4%	24.16				
		13	Lateral		40.6%	51.41				
		16	Vertical		13.9%	67.43				
		114	Longitudinal		10.4%	322.11				
		115	Longitudinal		43.9%	324.51				
		116	Longitudinal		21.6%	325.24				
		No mode in range -> Bridge OK								
35	5.0	1	Vertical		29.6%	13.20				
			Lateral		2.6%					
		2	Vertical		37.1%	13.36				
			Lateral		2.0%					
		4	Lateral		8.6%	17.57				
		15	Vertical		12.9%	57.71				
			Lateral		1.1%					
		16	Lateral		5.2%	59.07				
			Vertical		1.4%					
		17	Lateral		54.5%	69.63				
149	Longitudinal		23.4%	280.60						
150	Longitudinal		54.7%	280.98						
No mode in range -> Bridge OK										
35	10.0	1	Vertical		67.1%	10.47				
		4	Lateral		4.6%	16.57				
		18	Vertical		6.5%	44.04				
		19	Vertical		4.8%	45.76				
		31	Vertical		6.1%	77.09				
		37	Lateral		68.3%	86.95				
		146	Longitudinal		75.6%	225.57				
		250	Lateral		6.0%	328.68				
No mode in range -> Bridge OK										
50	2.5	1	Lateral		32.7%	8.21				
		2	Vertical		62.5%	12.20				
		6	Lateral		7.6%	17.94				

Length	Width	Mode no.	Direction	Shape	Mass part. (%)	Eigenfreq. (Hz)	Traffic Class	Confort Level	Vertical Accel. Max (m/s ²)	Lateral Accel. Max (m/s ²)
		12	Lateral		13.2%	30.35				
		13	Lateral		6.5%	30.91				
		14	Lateral		12.9%	31.30				
		21	Vertical		15.1%	57.57				
		93	Vertical		6.9%	126.18				
		207	Longitudinal		22.5%	237.47				
		208	Longitudinal		18.6%	237.70				
		209	Longitudinal		33.7%	238.93				
		No mode in range -> Bridge OK								
50	5.0	1	Lateral		9.3%	10.32				
		2	Vertical		64.5%	10.99				
		6	Lateral		14.2%	18.40				
		17	Lateral		49.2%	40.58				
		20	Vertical		14.7%	50.41				
		63	Vertical		5.9%	107.94				
		211	Longitudinal		73.9%	208.72				
		No mode in range -> Bridge OK								
50	10.0	1	Vertical		64.6%	8.85				
		4	Lateral		5.1%	11.82				
		15	Vertical		4.7%	34.67				
		28	Lateral		6.5%	53.11				
		29	Lateral		50.3%	53.98				
		30	Lateral		7.5%	54.43				
		43	Vertical		4.5%	71.66				
		206	Longitudinal		47.0%	173.03				
		213	Longitudinal		14.9%	177.93				
		216	Longitudinal		5.6%	178.88				
		250	Lateral		9.3%	211.69				
		No mode in range -> Bridge OK								
100	2.5	1	Lateral		47.5%	2.46				
		3	Vertical		59.9%	5.89				
		6	Lateral		10.5%	7.75				
		10	Lateral		18.6%	11.76				
		25	Vertical		14.8%	27.95				
		106	Vertical		7.2%	62.83				
		224	Longitudinal		58.6%	128.44				
		No mode in range -> Bridge OK								
100	5.0	1	Lateral		33.2%	4.10				
		2	Vertical		61.2%	6.33				
		6	Lateral		5.8%	7.83				
		15	Lateral		30.1%	15.49				
		25	Vertical		15.5%	29.56				
		119	Vertical		6.1%	63.76				
		242	Longitudinal		72.7%	120.07				
		No mode in range -> Bridge OK								
100	10.0	1	Lateral		10.6%	5.24				
		2	Vertical		64.8%	5.64				
		6	Lateral		10.2%	8.26				
		19	Lateral		49.5%	20.14				
		22	Vertical		14.7%	25.66				
		184	Lateral		7.7%	84.88				
		235	Longitudinal		59.5%	104.11				
		239	Longitudinal		15.7%	105.19				
		No mode in range -> Bridge OK								
150	2.5	1	Lateral	1 all	51.5%	1.15	TC2	CL1	0.058	0.069
	(No x-part considered)						TC3	CL2	0.092	0.109
							TC4	CL3	0.222	0.265
		3	Vertical		58.8%	3.78				
		4	Lateral		12.8%	4.34				
		10	Lateral		11.3%	6.53				
		28	Vertical		15.6%	17.91				
		109	Vertical		7.7%	40.44				
		245	Longitudinal		11.6%	86.58				
		254	Longitudinal		55.1%	88.55				
150	5.0	1	Lateral		43.0%	2.06				

Length	Width	Mode no.	Direction	Shape	Mass part. (%)	Eigenfreq. (Hz)	Traffic Class	Confort Level	Vertical Accel. Max (m/s ²)	Lateral Accel. Max (m/s ²)		
		3	Vertical		59.9%	4.24						
		6	Lateral		7.5%	4.92						
		14	Lateral		20.7%	8.98						
		28	Vertical		15.6%	19.88						
		133	Vertical		7.5%	44.00						
		264	Longitudinal		56.9%	84.30						
		265	Longitudinal		15.7%	84.35						
No mode in range -> Bridge OK												
150	10.0	1	Lateral		25.2%	3.18						
		2	Vertical		62.9%	4.18						
		6	Lateral		5.5%	5.24						
		17	Lateral		33.5%	11.53						
		19	Lateral		8.0%	11.66						
		27	Vertical		14.4%	19.32						
		137	Vertical		4.7%	43.31						
		164	Lateral		7.0%	50.90						
		245	Longitudinal		69.8%	76.10						
		No mode in range -> Bridge OK										
200 (No x-part considered)	2.5	1	Lateral	1 all	54.9%	0.64	TC2	CL1	0.074	0.111		
							TC3	CL2	0.117	0.175		
							TC4	CL3	0.282	0.424		
		3	Vertical		59.6%	2.58						
		4	Lateral		14.6%	2.77						
		8	Lateral		7.2%	4.18						
		27	Vertical		14.5%	12.39						
		68	Vertical		7.2%	28.43						
		225	Longitudinal		70.2%	65.78						
200 (No x-part considered)	5.0	1	Lateral	1 all	50.2%	1.15	TC2	CL1	0.036	0.030		
							TC3	CL2	0.056	0.048		
							TC4	CL3	0.136	0.115		
		3	Vertical		61.0%	2.86						
		4	Lateral		12.4%	3.90						
		12	Lateral		12.5%	5.96						
		27	Vertical		14.4%	13.73						
		84	Vertical		6.5%	31.37						
		202	Longitudinal		70.5%	62.77						
200	10.0	1	Lateral		35.0%	2.03						
		2	Vertical		62.3%	3.16						
		6	Lateral		6.6%	3.95						
		15	Lateral		26.0%	7.76						
		16	Lateral		5.1%	8.14						
		28	Vertical		15.0%	14.87						
		116	Vertical		6.3%	32.43						
		229	Longitudinal		73.8%	59.41						
		No mode in range -> Bridge OK										
		250 (No x-part considered)	2.5	1	Lateral		56.6%	0.42				
3	Vertical			3 all	2.7%	1.91	TC2	CL1	0.292	0.023		
	Lateral				14.4%		TC3	CL2	0.461	0.037		
							TC4	CL3	1.117	0.088		
4	Vertical			1 all	58.3%	1.96	TC2	CL1	2.531	0.124		
							TC3	CL2	4.002	0.195		
							TC4	CL3	9.694	0.474		
6	Lateral				4.1%	2.89						
11	Lateral				4.1%	3.84						
26	Vertical				15.0%	9.49						
65	Vertical		6.6%	21.92								
229	Longitudinal		9.1%	52.08								
230	Longitudinal		58.3%	52.27								
231	Longitudinal		5.5%	52.31								
250 (No x-part considered)	5.0	1	Lateral	1 all	50.6%	0.79	TC2	CL1	0.116	0.094		
							TC3	CL2	0.183	0.149		
							TC4	CL3	0.444	0.360		
		3	Vertical		59.0%	2.37						
		4	Lateral		11.4%	2.67						
		11	Lateral		8.5%	4.09						

Length	Width	Mode no.	Direction	Shape	Mass part. (%)	Eigenfreq. (Hz)	Traffic Class	Confort Level	Vertical Accel. Max (m/s ²)	Lateral Accel. Max (m/s ²)
		12	Lateral		6.6%	4.34				
		29	Vertical		14.9%	11.23				
		118	Vertical		7.7%	25.25				
		231	Longitudinal		8.6%	52.24				
		232	Longitudinal		57.4%	52.32				
250	10.0	1	Lateral		41.5%	1.38				
		2	Vertical		62.6%	2.47				
		6	Lateral		8.9%	3.30				
		12	Lateral		7.4%	5.09				
		15	Lateral		18.2%	5.89				
		29	Vertical		15.0%	11.79				
		111	Vertical		6.7%	26.37				
		228	Longitudinal		74.7%	48.47				
		No mode in range -> Bridge OK								
300	2.5	1	Lateral		55.9%	0.30				
(No x-part considered)		3	Lateral		15.2%	1.39				
		4	Vertical	1 all	59.2%	1.65	TC2	CL1	1.613	0.030
							TC3	CL2	2.550	0.048
							TC4	CL3	6.177	0.116
		6	Lateral		5.3%	2.16				
		10	Lateral		4.5%	2.90				
		27	Vertical		14.6%	7.90				
		71	Vertical		7.3%	18.13				
		249	Longitudinal		65.6%	44.46				
300	5.0	1	Lateral	1 all	52.6%	0.55	TC2	CL1	0.015	0.019
(No x-part considered)							TC3	CL2	0.024	0.030
							TC4	CL3	0.058	0.073
		3	Vertical	1 all	59.2%	1.91	TC2	CL1	1.919	0.009
							TC3	CL2	3.034	0.014
							TC4	CL3	7.349	0.033
		4	Lateral		12.9%	2.09				
		10	Lateral		13.0%	3.28				
		30	Vertical		15.2%	9.09				
		114	Vertical		7.6%	20.59				
		238	Longitudinal		52.9%	43.57				
		245	Longitudinal		12.9%	44.61				
300	10.0	1	Lateral	1 all	44.7%	1.01	TC2	CL1	0.573	0.044
(No x-part considered)							TC3	CL2	0.906	0.069
							TC4	CL3	2.196	0.167
		3	Vertical	1 all	60.5%	2.12	TC2	CL1	1.538	0.012
							TC3	CL2	2.431	0.019
							TC4	CL3	5.889	0.047
		6	Lateral		8.4%	2.50				
		15	Lateral		20.8%	4.53				
		30	Vertical		15.1%	9.99				
		129	Vertical		6.6%	22.26				
		73.3	Longitudinal		73.3%	41.84				

C.5 Box – Concrete-Steel

Length	Width	Mode no.	Direction	Shape	Mass part. (%)	Eigenfreq. (Hz)	Traffic Class	Confort Level	Vertical Accel. Max (m/s ²)	Lateral Accel. Max (m/s ²)
35	2.5	1	Vertical		65.9%	2.34				
		3	Lateral		71.1%	7.49				
		19	Vertical		7.2%	12.32				
		142	Longitudinal		68.9%	55.96				
		No mode in range -> Bridge OK								
35	5.0	1	Vertical		64.9%	2.42				
		26	Lateral		62.1%	11.94				
		29	Lateral		10.6%	13.22				
		30	Vertical		7.9%	13.58				
		35	Vertical		4.9%	14.52				
		164	Longitudinal		59.1%	52.07				
		No mode in range -> Bridge OK								

Length	Width	Mode no.	Direction	Shape	Mass part. (%)	Eigenfreq. (Hz)	Traffic Class	Confort Level	Vertical Accel. Max (m/s ²)	Lateral Accel. Max (m/s ²)		
35	10.0	1	Vertical	1 all	15.5%	1.65	TC2	CL1	0.120	0.001		
									TC3	CL2	0.189	0.001
									TC4	CL3	0.836	0.005
				9	Vertical		49.8%	3.27				
				71	Vertical		4.9%	14.69				
				82	Lateral		7.4%	16.14				
				86	Vertical		5.2%	16.78				
				87	Lateral		55.2%	17.03				
				97	Lateral		6.2%	18.62				
		278	Longitudinal		8.2%	45.46						
		299	Longitudinal		46.8%	48.46						
50 (No x-part considered)	2.5	1	Vertical	1 all	64.5%	1.99	TC2	CL1	2.261	0.020		
									TC3	CL2	3.578	0.032
									TC4	CL3	15.825	0.142
				2	Lateral		69.4%	4.06				
				29	Vertical		9.7%	10.04				
				79	Lateral		10.6%	21.18				
				86	Vertical		5.4%	23.80				
				195	Longitudinal		12.2%	41.50				
				196	Longitudinal		65.6%	41.90				
50	5.0	1	Vertical	1 all	64.6%	1.92	TC2	CL1	1.630	0.001		
									TC3	CL2	2.578	0.002
									TC4	CL3	11.401	0.009
				23	Lateral		71.7%	6.77				
				49	Vertical		4.4%	11.04				
				185	Lateral		13.9%	31.92				
		217	Longitudinal		76.6%	38.76						
50	10.0	1	Vertical	1 all	35.5%	1.50	TC2	CL1	0.228	0.001		
									TC3	CL2	0.361	0.001
									TC4	CL3	1.597	0.005
				7	Vertical	1 all	29.5%	2.24	TC2	CL1	0.243	0.000
									TC3	CL2	0.385	0.001
									TC4	CL3	1.702	0.003
				61	Vertical		5.5%	9.94				
				63	Lateral		22.4%	10.02				
				66	Lateral		21.2%	10.41				
				71	Lateral		14.5%	10.96				
		291	Longitudinal		79.4%	36.11						
100	2.5	1	Lateral	1 all	71.0%	1.06	TC2	CL1	0.015	0.092		
									TC3	CL2	0.024	0.146
									TC4	CL3	0.103	0.646
				2	Vertical	1 all	65.5%	1.32	TC2	CL1	0.182	0.002
									TC3	CL2	0.288	0.003
									TC4	CL3	1.273	0.012
				5	Lateral		14.4%	5.06				
				6	Vertical		15.1%	6.45				
				19	Vertical		6.4%	15.04				
		31	Longitudinal		19.4%	19.80						
		48	Longitudinal		13.3%	22.73						
		50	Longitudinal		42.9%	22.89						
100	5.0	1	Vertical	1 all	64.6%	1.43	TC2	CL1	0.378	0.011		
									TC3	CL2	0.597	0.017
									TC4	CL3	2.641	0.075
				2	Lateral		69.0%	2.07				
				7	Vertical		6.8%	6.94				
				8	Vertical		7.8%	7.04				
				9	Lateral		7.8%	10.24				
				18	Vertical		6.0%	15.82				
				40	Longitudinal		7.2%	20.98				
				45	Longitudinal		11.6%	21.57				
				47	Longitudinal		30.9%	21.75				
		53	Longitudinal		20.5%	22.50						
100	10.0	1	Vertical	1 all	62.0%	1.27	TC2	CL1	0.033	0.000		
							TC3	CL2	0.053	0.001		

Length	Width	Mode no.	Direction	Shape	Mass part. (%)	Eigenfreq. (Hz)	Traffic Class	Confort Level	Vertical Accel. Max (m/s ²)	Lateral Accel. Max (m/s ²)
							TC4	CL3	0.232	0.003
		9	Vertical	1 all	2.0%	2.27	TC2	CL1	0.020	0.000
				Low Flange Probl.			TC3	CL2	0.031	0.000
							TC4	CL3	0.137	0.002
		21	Lateral		71.4%	3.48				
		59	Vertical		9.8%	7.49				
		131	Lateral		14.5%	15.68				
		186	Longitudinal		13.0%	19.65				
		191	Longitudinal		7.2%	19.88				
		199	Longitudinal		17.6%	20.66				
		203	Longitudinal		34.1%	21.00				
150	2.5	1	Lateral	1 all	63.1%	0.59	TC2	CL1	0.000	0.025
							TC3	CL2	0.000	0.040
							TC4	CL3	0.001	0.178
		2	Vertical		60.0%	1.17				
		4	Lateral		15.1%	2.86				
		8	Vertical		15.3%	5.60				
		10	Lateral		6.8%	6.29				
		18	Lateral		6.1%	9.21				
		53	Vertical		6.0%	12.85				
		98	Longitudinal		28.1%	16.84				
		100	Longitudinal		26.7%	17.04				
		105	Longitudinal		17.5%	17.49				
150	5.0	1	Lateral	1 all	64.7%	1.07	TC2	CL1	0.007	0.043
							TC3	CL2	0.011	0.069
							TC4	CL3	0.049	0.303
		2	Vertical		61.0%	1.22				
		7	Lateral		8.7%	4.63				
		8	Lateral		6.8%	5.51				
		9	Vertical		15.1%	5.79				
		16	Lateral		7.2%	8.71				
		75	Vertical		4.6%	13.15				
		103	Longitudinal		68.0%	16.22				
150	10.0	1	Vertical		62.0%	1.13				
		2	Lateral		35.5%	1.71				
		3	Lateral		33.6%	2.01				
		54	Vertical		7.1%	6.31				
		64	Lateral		8.5%	7.48				
		238	Longitudinal		58.8%	15.15				
		241	Longitudinal		15.2%	15.40				
		No mode in range -> Bridge OK								
200	2.5	No possible bridge due to geometry								
200	5.0	1	Lateral	1 all	66.1%	0.63	TC2	CL1	0.000	0.022
							TC3	CL2	0.000	0.035
							TC4	CL3	0.002	0.155
		2	Vertical		60.7%	0.98				
		5	Lateral		12.8%	2.57				
		10	Vertical		16.0%	4.57				
		11	Lateral		7.6%	4.70				
		91	Vertical		7.4%	10.35				
		111	Longitudinal		67.4%	12.59				
200	10.0	1	Vertical		61.2%	0.97				
		2	Lateral	1 all	69.6%	1.03	TC2	CL1	0.009	0.035
				Low Flange Probl.			TC3	CL2	0.014	0.055
							TC4	CL3	0.063	0.241
		38	Lateral		7.8%	3.24				
		61	Lateral		10.8%	4.33				
		75	Vertical		4.8%	4.96				
		301	Longitudinal		35.6%	12.01				
		305	Longitudinal		35.1%	12.13				
250	2.5	No possible bridge due to geometry								
250	5.0	1	Lateral		64.0%	0.42				
		2	Vertical		60.1%	0.86				
		4	Lateral		16.8%	1.91				

Length	Width	Mode no.	Direction	Shape	Mass part. (%)	Eigenfreq. (Hz)	Traffic Class	Confort Level	Vertical Accel. Max (m/s ²)	Lateral Accel. Max (m/s ²)	
250	10.0	10	Lateral		9.4%	3.69					
		12	Vertical		15.7%	4.03					
		100	Vertical		7.6%	9.06					
		116	Longitudinal		71.1%	10.41					
		No mode in range -> Bridge OK									
		1	Lateral	1 all	68.3%	0.74	TC2	CL1	0.002	0.022	
							TC3	CL2	0.003	0.035	
							TC4	CL3	0.014	0.155	
		2	Vertical		61.3%	0.85					
		7	Lateral		10.5%	2.56					
8	Lateral		9.0%	3.43							
28	Vertical		5.9%	4.14							
178	Vertical		4.2%	9.32							
188	Longitudinal		52.7%	9.95							
190	Longitudinal		17.5%	10.02							
300	2.5	No possible bridge due to geometry									
300	5.0	1	Lateral		61.2%	0.31					
		3	Vertical		54.9%	0.81					
		4	Lateral		16.0%	1.47					
		10	Lateral		8.1%	3.07					
		15	Vertical		11.9%	3.79					
		17	Lateral		6.1%	3.98					
		118	Longitudinal		70.6%	9.08					
		No mode in range -> Bridge OK									
		1	Lateral	1 all	62.9%	0.59	TC2	CL1	0.000	0.006	
							TC3	CL2	0.000	0.009	
					TC4	CL3	0.001	0.041			
2	Vertical		59.0%	0.82							
7	Lateral		13.4%	2.33							
16	Lateral		7.9%	3.22							
32	Vertical		13.7%	3.82							
143	Longitudinal		7.1%	8.69							
148	Longitudinal		21.3%	8.84							
149	Longitudinal		30.4%	8.89							

C.6 Box – FRP-Steel

Length	Width	Mode no.	Direction	Shape	Mass part. (%)	Eigenfreq. (Hz)	Traffic Class	Confort Level	Vertical Accel. Max (m/s ²)	Lateral Accel. Max (m/s ²)		
35	2.5	1	Vertical		61.6%	4.28						
		2	Lateral		12.2%	7.74						
		3	Lateral		56.4%	7.81						
		59	Vertical		11.2%	23.86						
		157	Vertical		4.4%	52.74						
		219	Longitudinal		21.3%	70.95						
		224	Longitudinal		18.4%	71.40						
		No mode in range -> Bridge OK										
		35	5.0	1	Vertical		29.6%	3.19				
				13	Vertical		29.1%	5.78				
38	Lateral				65.4%	11.95						
298	Longitudinal				7.9%	61.19						
299	Longitudinal				4.0%	61.29						
311	Longitudinal				55.8%	63.19						
No mode in range -> Bridge OK												
35	10.0	1	Vertical	1 all	17.2%	1.65	TC2	CL1	0.136	0.002		
							TC3	CL2	0.216	0.003		
							TC4	CL3	0.930	0.014		
		3	Vertical	1 all	1.7%	1.78	TC2	CL1	0.063	0.002		
							TC3	CL2	0.100	0.003		
							TC4	CL3	0.444	0.014		
		11	Vertical		43.0%	4.26						

Length	Width	Mode no.	Direction	Shape	Mass part. (%)	Eigenfreq. (Hz)	Traffic Class	Confort Level	Vertical Accel. Max (m/s ²)	Lateral Accel. Max (m/s ²)
		61	Lateral		14.8%	14.04				
		72	Lateral		41.9%	15.29				
		73	Vertical		4.5%	15.43				
		78	Lateral		6.7%	16.21				
		345	Longitudinal		34.2%	54.04				
		355	Longitudinal		41.5%	55.34				
50	2.5	1	Vertical		61.6%	3.32				
		2	Lateral		69.2%	4.33				
		54	Lateral		4.6%	14.39				
		36	Lateral		5.0%	17.75				
			Vertical		2.8%					
		37	Vertical		8.8%	17.88				
			Lateral		2.3%					
		259	Longitudinal		18.6%	50.31				
		263	Longitudinal		38.5%	50.92				
		266	Longitudinal		6.7%	51.56				
		274	Longitudinal		9.8%	53.19				
		No mode in range -> Bridge OK								
50	5.0	1	Vertical		55.7%	3.27				
		14	Lateral		68.9%	6.97				
		35	Vertical		4.9%	13.73				
		69	Vertical		8.6%	20.52				
		87	Lateral		8.5%	25.19				
		88	Lateral		5.8%	25.44				
		249	Longitudinal		56.9%	47.67				
		No mode in range -> Bridge OK								
50	10.0	1	Vertical	1 all	19.8%	1.48	TC2	CL1	0.096	0.003
							TC3	CL2	0.152	0.005
							TC4	CL3	0.647	0.022
		3	Vertical	1 all	2.0%	1.60	TC2	CL1	0.027	0.003
							TC3	CL2	0.042	0.005
							TC4	CL3	0.185	0.022
		14	Vertical		40.4%	3.47				
		56	Lateral		68.9%	9.16				
		75	Vertical		4.1%	11.35				
		124	Vertical		5.1%	16.89				
		360	Longitudinal		30.3%	38.95				
		371	Longitudinal		26.2%	39.63				
		379	Longitudinal		9.2%	40.37				
100	2.5	1	Lateral		65.8%	1.28				
		2	Vertical	1 all	60.4%	1.86	TC2	CL1	1.477	0.029
							TC3	CL2	2.335	0.045
							TC4	CL3	9.815	0.190
		5	Lateral		12.9%	4.95				
		11	Vertical		15.0%	8.93				
		17	Lateral		5.0%	11.81				
		75	Vertical		7.0%	20.45				
		112	Longitudinal		61.4%	26.68				
		117	Longitudinal		12.2%	27.81				
100	5.0	1	Vertical	1 all	57.5%	2.09	TC2	CL1	1.234	0.249
			Lateral		2.6%		TC3	CL2	1.951	0.394
							TC4	CL3	7.638	1.553
		2	Vertical	1 all	2.3%	2.17	TC2	CL1	0.150	0.160
			Lateral		64.1%		TC3	CL2	0.237	0.253
							TC4	CL3	0.916	0.978
		7	Lateral		4.8%	6.70				
		27	Lateral		10.0%	8.60				
		49	Lateral		4.8%	10.97				
		51	Vertical		4.4%	11.09				
		212	Longitudinal		64.4%	26.31				
100	10.0 (No x-part considered)	1	Vertical	1 all	43.5%	1.62	TC2	CL1	0.413	0.002
							TC3	CL2	0.652	0.003
							TC4	CL3	2.492	0.011
		11	Vertical		5.6%	2.45				
		12	Vertical		11.6%	2.49				
		21	Lateral		68.3%	3.50				

Length	Width	Mode no.	Direction	Shape	Mass part. (%)	Eigenfreq. (Hz)	Traffic Class	Confort Level	Vertical Accel. Max (m/s ²)	Lateral Accel. Max (m/s ²)
		98	Vertical		8.4%	10.30				
		107	Lateral		6.1%	11.20				
		108	Lateral		5.1%	11.28				
		319	Longitudinal		9.8%	22.99				
		331	Longitudinal		48.9%	23.48				
		335	Longitudinal		14.4%	23.63				
150	2.5	1	Lateral	1 all	62.9%	0.62	TC2	CL1	0.001	0.038
							TC3	CL2	0.001	0.060
							TC4	CL3	0.005	0.257
		2	Vertical	1 all	58.1%	1.36	TC2	CL1	0.136	0.005
							TC3	CL2	0.215	0.008
							TC4	CL3	0.926	0.033
		4	Lateral		15.7%	2.53				
		9	Lateral		6.7%	4.78				
		12	Vertical		13.7%	6.36				
		100	Vertical		7.5%	14.40				
		128	Longitudinal		64.4%	18.42				
150	5.0	1	Lateral	1 all	65.5%	1.07	TC2	CL1	0.009	0.053
							TC3	CL2	0.015	0.084
							TC4	CL3	0.059	0.345
		2	Vertical	1 all	58.8%	1.43	TC2	CL1	0.247	0.005
							TC3	CL2	0.390	0.008
							TC4	CL3	1.612	0.034
		5	Lateral		10.5%	3.56				
		9	Lateral		4.0%	5.07				
		10	Lateral		5.3%	5.75				
		11	Vertical		5.6%	6.11				
		29	Vertical		4.6%	7.12				
		219	Longitudinal		31.8%	18.02				
		221	Longitudinal		37.7%	18.15				
150	10.0 (No x-part considered)	1	Vertical	1 all	47.4%	1.38	TC2	CL1	0.088	0.002
							TC3	CL2	0.140	0.003
							TC4	CL3	0.539	0.013
		4	Lateral		50.5%	1.72				
		13	Vertical	2 all	10.9%	1.91	TC2	CL1	0.007	0.001
							TC3	CL2	0.011	0.002
							TC4	CL3	0.046	0.006
		20	Lateral		16.4%	2.20				
		90	Lateral		9.0%	5.90				
		149	Vertical		6.9%	7.70				
		399	Longitudinal		42.3%	17.10				
		402	Longitudinal		23.1%	17.23				
200	2.5	No possible bridge due to geometry								
200	5.0	1	Lateral	1 all	64.4%	0.64	TC2	CL1	0.002	0.024
							TC3	CL2	0.002	0.039
							TC4	CL3	0.010	0.164
		2	Vertical		58.4%	1.14				
		4	Lateral		12.3%	2.25				
		10	Lateral		8.0%	3.90				
		24	Vertical		7.4%	5.29				
		27	Vertical		6.3%	5.39				
		167	Longitudinal		9.1%	13.72				
		171	Longitudinal		46.1%	13.82				
200	10.0 (No x-part considered)	1	Lateral	1 all	64.9%	1.09	TC2	CL1	0.005	0.023
							TC3	CL2	0.007	0.036
							TC4	CL3	0.028	0.136
		2	Vertical		58.1%	1.16				
		41	Lateral		6.2%	4.14				
		54	Lateral		7.8%	4.53				
		101	Vertical		12.1%	6.03				
		301	Longitudinal		63.7%	13.29				
250	2.5	No possible bridge due to geometry								
250	5.0	1	Lateral		63.5%	0.42				

Length	Width	Mode no.	Direction	Shape	Mass part. (%)	Eigenfreq. (Hz)	Traffic Class	Confort Level	Vertical Accel. Max (m/s ²)	Lateral Accel. Max (m/s ²)
		2	Vertical		56.9%	0.97				
		4	Lateral		14.9%	1.62				
		9	Lateral		6.2%	2.96				
		31	Vertical		15.5%	4.51				
		115	Vertical		7.4%	10.02				
		128	Longitudinal		70.6%	11.07				
		No mode in range -> Bridge OK								
250	10.0	1	Lateral	1 all	65.7%	0.74	TC2	CL1	0.002	0.024
							TC3	CL2	0.003	0.037
							TC4	CL3	0.014	0.150
		2	Vertical		59.0%	0.99				
		5	Lateral		10.4%	2.33				
		9	Lateral		5.1%	3.25				
		13	Lateral		7.1%	3.53				
		37	Vertical		8.5%	4.52				
		191	Longitudinal		32.9%	10.78				
		193	Longitudinal		20.7%	10.83				
300	2.5	No possible bridge due to geometry								
300	5.0	1	Lateral		63.0%	0.30				
		3	Vertical		58.8%	0.85				
		4	Lateral		15.6%	1.24				
		9	Lateral		6.8%	2.41				
		29	Vertical		11.3%	3.96				
		119	Vertical		4.8%	8.75				
		125	Longitudinal		50.1%	9.22				
		126	Longitudinal		13.2%	9.24				
		127	Longitudinal		7.6%	9.26				
		No mode in range -> Bridge OK								
300	10.0	1	Lateral	1 all	64.9%	0.54	TC2	CL1	0.000	0.002
							TC3	CL2	0.000	0.004
							TC4	CL3	0.001	0.016
		2	Vertical		58.8%	0.88				
		5	Lateral		13.1%	1.81				
		12	Lateral		7.2%	2.83				
		43	Vertical		12.7%	4.06				
		161	Longitudinal		43.5%	9.05				
		169	Longitudinal		13.3%	9.37				

C.7 Box – FRP

Length	Width	Mode no.	Direction	Shape	Mass part. (%)	Eigenfreq. (Hz)	Traffic Class	Confort Level	Vertical Accel. Max (m/s ²)	Lateral Accel. Max (m/s ²)
35	2.5	20	Vertical	1 all	1.1%	1.99	TC2	CL1	0.251	0.042
							TC3	CL2	0.398	0.066
							TC4	CL3	0.963	0.160
		61	Lateral		44.3%	4.69				
		62	Lateral		15.4%	4.70				
		79	Vertical		24.4%	5.84				
		80	Vertical		35.9%	5.91				
		158	Lateral		13.5%	10.68				
		326	Vertical		4.8%	24.06				
		604	Longitudinal		71.2%	52.72				
35	5.0	173	Vertical		17.3%	5.08				
		174	Vertical		43.3%	5.08				
		176	Lateral		22.3%	5.22				
		274	Lateral		14.1%	8.12				
		275	Lateral		11.1%	8.13				
		399	Lateral		26.6%	12.09				
		475	Lateral		7.5%	15.40				
		633	Vertical		7.0%	20.78				
		1076	Longitudinal		7.7%	47.99				
		1077	Longitudinal		68.1%	48.09				
		No mode in range -> Bridge OK								

Length	Width	Mode no.	Direction	Shape	Mass part. (%)	Eigenfreq. (Hz)	Traffic Class	Confort Level	Vertical Accel. Max (m/s ²)	Lateral Accel. Max (m/s ²)	
35	10.0	405	Vertical		66.8%	5.58					
		413	Lateral		8.2%	5.69					
		500	Lateral		13.5%	6.92					
		895	Lateral		57.7%	13.55					
		1164	Vertical		4.2%	19.18					
		1313	Vertical		3.8%	21.81					
		2086	Longitudinal		49.3%	39.99					
		2087	Longitudinal		15.7%	40.02					
No mode in range -> Bridge OK											
50	2.5	1	Lateral		57.3%	3.12					
		2	Lateral		10.2%	4.20					
		3	Vertical		59.8%	4.33					
		7	Lateral		9.7%	6.59					
		120	Vertical		4.8%	19.42					
		124	Lateral		5.0%	19.97					
		295	Vertical		6.8%	36.60					
		312	Longitudinal		39.2%	39.08					
		318	Longitudinal		24.9%	39.68					
No mode in range -> Bridge OK											
50	5.0	166	Lateral		48.8%	3.41					
		193	Vertical		60.9%	4.11					
		387	Lateral		19.4%	7.65					
		388	Lateral		13.0%	7.65					
		790	Vertical		10.3%	16.57					
		1448	Longitudinal		19.7%	35.61					
		1452	Longitudinal		18.8%	35.72					
		1453	Longitudinal		21.7%	35.73					
No mode in range -> Bridge OK											
50	10.0	406	Lateral		18.9%	3.75					
		415	Vertical		59.3%	3.84					
		531	Lateral		10.8%	4.94					
		928	Lateral		13.1%	8.74					
		945	Lateral		11.4%	8.94					
		948	Lateral		27.6%	8.97					
		1458	Vertical		6.6%	14.70					
		2627	Longitudinal		11.1%	30.81					
		2639	Longitudinal		30.3%	30.99					
		2644	Longitudinal		26.7%	31.05					
No mode in range -> Bridge OK											
100	2.5	1	Lateral	1 all	63.1%	0.99	TC2	CL1	0.126	0.161	
							TC3	CL2	0.199	0.255	
							TC4	CL3	0.483	0.617	
		3	Vertical	2 all	1.2%	2.29	TC2	CL1	0.001	0.001	
							TC3	CL2	0.002	0.001	
							TC4	CL3	0.004	0.003	
		4	Vertical		58.3%	2.39					
		6	Lateral		14.4%	3.42					
		12	Lateral		7.8%	4.23					
		75	Vertical		11.8%	9.70					
180	Vertical		6.9%	18.38							
203	Longitudinal		58.6%	20.69							
No mode in range -> Bridge OK											
100	5.0	1	Lateral		60.1%	1.61					
		2	Lateral		6.5%	2.04					
		3	Vertical		57.7%	2.37					
		8	Lateral		6.6%	3.05					
		13	Lateral		6.3%	3.21					
		255	Vertical		5.9%	19.56					
		262	Longitudinal		11.1%	19.94					
		265	Longitudinal		9.1%	19.98					
266	Longitudinal		46.5%	19.99							
No mode in range -> Bridge OK											
100 (No x-part considered)	10.0	114	Lateral		49.1%	1.90					
		103	Vertical	1 all	61.8%	2.12	TC2	CL1	0.832	0.049	
							TC3	CL2	1.316	0.077	
							TC4	CL3	3.188	0.187	

Length	Width	Mode no.	Direction	Shape	Mass part. (%)	Eigenfreq. (Hz)	Traffic Class	Confort Level	Vertical Accel. Max (m/s ²)	Lateral Accel. Max (m/s ²)
		112	Lateral		5.1%	2.31				
		206	Lateral		25.6%	3.99				
		514	Vertical		5.4%	8.55				
		945	Longitudinal		65.2%	17.71				
150	2.5	No possible bridge due to geometry								
150	5.0	1	Lateral	1 all	64.8%	0.83	TC2	CL1	0.313	0.076
							TC3	CL2	0.495	0.120
							TC4	CL3	1.198	0.291
		3	Vertical	1 all	59.3%	1.68	TC2	CL1	0.531	0.063
							TC3	CL2	0.839	0.100
							TC4	CL3	2.033	0.243
		6	Lateral		15.0%	2.31				
		74	Vertical		6.4%	6.35				
		80	Vertical		5.3%	6.74				
		213	Longitudinal		36.1%	13.45				
		220	Longitudinal		8.3%	13.77				
		222	Longitudinal		10.5%	13.95				
150	10.0 (No x-part considered)	1	Lateral	1 all	47.8%	1.18	TC2	CL1	0.004	0.006
							TC3	CL2	0.007	0.009
							TC4	CL3	0.017	0.022
		2	Vertical	1 all	53.8%	1.46	TC2	CL1	0.163	0.010
							TC3	CL2	0.257	0.015
							TC4	CL3	0.623	0.037
		3	Lateral		23.1%	1.48				
		13	Lateral		7.0%	1.97				
		15	Vertical	1 all	4.5%	2.01	TC2	CL1	0.125	0.007
							TC3	CL2	0.197	0.011
							TC4	CL3	0.478	0.026
		16	Vertical	1 all	5.0%	2.03	TC2	CL1	0.140	0.007
							TC3	CL2	0.221	0.012
							TC4	CL3	0.536	0.028
		147	Vertical		7.0%	6.93				
		312	Longitudinal		15.8%	12.46				
		315	Longitudinal		43.2%	12.52				
200	2.5	No possible bridge due to geometry								
200	5.0	1	Lateral		63.6%	0.48				
		4	Vertical	2 all	59.7%	1.32	TC2	CL1	0.001	0.000
							TC3	CL2	0.002	0.000
							TC4	CL3	0.004	0.001
		6	Lateral		14.0%	1.61				
		12	Lateral		7.7%	1.96				
		80	Vertical		15.1%	5.20				
		198	Longitudinal		71.3%	10.29				
200	10.0 (No x-part considered)	1	Lateral	1 all	63.8%	0.81	TC2	CL1	0.025	0.038
							TC3	CL2	0.040	0.060
							TC4	CL3	0.097	0.146
		2	Lateral	1 all	3.1%	1.01	TC2	CL1	0.024	0.011
							TC3	CL2	0.038	0.018
							TC4	CL3	0.091	0.043
		3	Vertical	1 all	52.4%	1.27	TC2	CL1	0.008	0.002
							TC3	CL2	0.013	0.003
							TC4	CL3	0.031	0.007
		8	Lateral		8.5%	1.47				
		9	Vertical	1 all	2.3%	1.47	TC2	CL1	0.017	0.007
							TC3	CL2	0.026	0.012
							TC4	CL3	0.064	0.028
		15	Vertical	1 all	4.6%	1.55	TC2	CL1	0.025	0.014
							TC3	CL2	0.040	0.023
							TC4	CL3	0.096	0.055
		97	Lateral		5.6%	4.77				
		249	Longitudinal		46.8%	9.97				
		258	Longitudinal		14.8%	10.23				
250	2.5	No possible bridge due to geometry								
250	5.0	No possible bridge due to geometry								

Length	Width	Mode no.	Direction	Shape	Mass part. (%)	Eigenfreq. (Hz)	Traffic Class	Confort Level	Vertical Accel. Max (m/s ²)	Lateral Accel. Max (m/s ²)	
250	10.0	1	Lateral	1 all	65.0%	0.57	TC2	CL1	0.000	0.006	
							TC3	CL2	0.000	0.010	
							TC4	CL3	0.001	0.024	
		4	Vertical		52.2%	1.10					
		7	Lateral		9.1%	1.27					
		9	Vertical	1 all	3.5%	1.30	TC2	CL1	0.003	0.002	
							TC3	CL2	0.004	0.003	
							TC4	CL3	0.010	0.007	
		14	Lateral		6.7%	1.36					
		68	Lateral		5.4%	3.35					
101	Vertical		11.0%	4.25							
223	Longitudinal		31.7%	7.96							
225	Longitudinal		12.1%	8.05							
243	Longitudinal		14.3%	8.48							
300	2.5	No possible bridge due to geometry									
300	5.0	No possible bridge due to geometry									
300	10.0	1	Lateral		63.6%	0.41					
											4
		5	Lateral	3 all	8.6%	0.99	TC2	CL1	0.002	0.001	
							TC3	CL2	0.009	0.002	
							TC4	CL3	0.023	0.005	
		10	Vertical		4.2%	1.07					
		14	Lateral	5 all	7.8%	1.11	TC2	CL1	0.000	0.001	
							TC3	CL2	0.001	0.001	
							TC4	CL3	0.002	0.002	
		16	Lateral	7 all	1.4%	1.14	TC2	CL1	0.000	0.000	
TC3	CL2						0.000	0.000			
TC4	CL3						0.001	0.000			
112	Vertical		15.6%	3.68							
234	Longitudinal		61.2%	6.85							

C.8 Box – Graphene

Length	Width	Mode no.	Direction	Shape	Mass part. (%)	Eigenfreq. (Hz)	Traffic Class	Confort Level	Vertical Accel. Max (m/s ²)	Lateral Accel. Max (m/s ²)
35	2.5	1	Vertical		61.5%	12.65				
		7	Lateral		66.9%	37.93				
		32	Vertical		7.1%	81.96				
		91	Lateral		12.9%	172.77				
		166	Longitudinal		16.7%	330.04				
		167	Longitudinal		46.5%	332.20				
		No mode in range -> Bridge OK								
35	5.0	1	Vertical		46.1%	8.07				
		9	Vertical		13.2%	15.44				
		25	Vertical		7.5%	34.49				
		41	Lateral		5.2%	49.55				
		42	Lateral		14.2%	51.84				
		46	Vertical		9.2%	54.20				
		49	Lateral		5.9%	56.49				
		52	Lateral		12.6%	60.38				
		53	Lateral		29.9%	63.37				
		288	Lateral		11.6%	245.90				
337	Longitudinal		76.4%	296.85						
No mode in range -> Bridge OK										
35	10.0	1	Vertical		20.5%	3.24				
		8	Vertical		5.1%	8.59				
		9	Vertical		35.8%	8.88				
		42	Vertical		9.8%	27.97				
		161	Lateral		23.9%	79.76				
		162	Lateral		21.7%	80.28				
		164	Lateral		16.0%	81.00				

Length	Width	Mode no.	Direction	Shape	Mass part. (%)	Eigenfreq. (Hz)	Traffic Class	Confort Level	Vertical Accel. Max (m/s ²)	Lateral Accel. Max (m/s ²)
		175	Lateral		6.3%	85.47				
		505	Longitudinal		71.8%	238.71				
		625	Lateral		6.8%	302.30				
		No mode in range -> Bridge OK								
50	2.5	1	Vertical		63.7%	9.23				
		2	Lateral		66.5%	18.89				
		6	Vertical		12.3%	38.42				
		33	Lateral		12.7%	92.11				
		81	Lateral		5.6%	195.99				
		99	Longitudinal		19.5%	238.81				
		102	Longitudinal		46.0%	241.91				
		No mode in range -> Bridge OK								
50	5.0	1	Vertical		58.3%	7.57				
		19	Vertical		8.9%	31.57				
		20	Lateral		63.8%	32.27				
		30	Vertical		8.6%	49.53				
		139	Lateral		12.5%	142.97				
		233	Longitudinal		76.2%	225.48				
		No mode in range -> Bridge OK								
50	10.0	1	Vertical		30.2%	3.55				
		9	Vertical		28.4%	8.22				
		29	Vertical		10.6%	21.88				
		79	Lateral		12.5%	46.52				
		89	Lateral		31.9%	49.58				
		92	Lateral		10.1%	50.16				
		402	Longitudinal		31.5%	191.71				
		407	Lateral		11.2%	193.61				
		413	Longitudinal		40.4%	196.24				
		No mode in range -> Bridge OK								
100	2.5	1	Vertical		60.9%	4.89				
		2	Lateral		66.1%	6.18				
		89	Lateral		4.8%	24.54				
			Vertical		0.9%					
		90	Lateral		4.7%	24.63				
			Vertical		0.6%					
		95	Vertical		9.4%	25.76				
		650	Longitudinal		10.7%	124.96				
		664	Longitudinal		40.8%	126.91				
		665	Longitudinal		15.3%	126.99				
		No mode in range -> Bridge OK								
100	5.0 (No x-part considered)	19	Vertical	1 all	2.3%	2.19	TC2	CL1	0.199	0.021
							TC3	CL2	0.314	0.033
							TC4	CL3	0.762	0.079
		43	Vertical		51.4%	5.45				
		116	Lateral		30.9%	8.89				
		149	Lateral		29.4%	12.47				
		353	Vertical		5.6%	26.58				
		355	Vertical		5.0%	26.74				
		404	Lateral		8.1%	37.90				
		861	Longitudinal		6.3%	119.21				
		862	Longitudinal		17.0%	120.15				
		867	Longitudinal		48.6%	121.75				
		No mode in range -> Bridge OK								
100	10.0	1	Vertical		52.8%	3.70				
		25	Lateral		19.4%	15.35				
		27	Lateral		48.3%	16.28				
		53	Vertical		7.7%	25.00				
		209	Lateral		9.6%	72.10				
		376	Longitudinal		14.4%	109.12				
		377	Longitudinal		54.4%	109.18				
		No mode in range -> Bridge OK								
150	2.5	1	Lateral		64.1%	2.94				
		2	Vertical		60.0%	3.25				
		5	Lateral		15.5%	13.00				
		6	Vertical		14.9%	15.51				
		13	Lateral		5.4%	25.08				

Length	Width	Mode no.	Direction	Shape	Mass part. (%)	Eigenfreq. (Hz)	Traffic Class	Confort Level	Vertical Accel. Max (m/s ²)	Lateral Accel. Max (m/s ²)	
150	5.0	354	Longitudinal		70.0%	86.90					
		No mode in range -> Bridge OK									
		1	Vertical		60.1%	3.70					
		2	Lateral		65.1%	5.33					
		58	Vertical		7.9%	20.80					
		63	Lateral		8.8%	22.33					
		69	Lateral		7.2%	23.69					
		426	Longitudinal		27.4%	83.50					
		428	Longitudinal		28.0%	83.69					
		No mode in range -> Bridge OK									
150	10.0	1	Vertical		60.1%	3.21					
		8	Lateral		67.7%	8.28					
		24	Vertical		5.6%	13.05					
		37	Vertical		7.6%	20.77					
		95	Lateral		10.0%	37.74					
		325	Longitudinal		55.3%	77.52					
		No mode in range -> Bridge OK									
200	2.5	1	Lateral		64.2%	1.67					
		2	Vertical		60.6%	2.32					
		5	Lateral		15.6%	7.87					
		6	Vertical		15.0%	11.20					
		9	Lateral		6.9%	16.41					
		20	Vertical		6.9%	25.99					
		155	Longitudinal		70.8%	65.17					
		No mode in range -> Bridge OK									
200	5.0	1	Vertical		61.6%	2.66					
		2	Lateral		65.6%	3.08					
		7	Lateral		6.3%	12.55					
			Vertical		3.3%						
		8	Vertical		11.8%	12.88					
			Lateral		1.7%						
		9	Lateral		7.0%	14.85					
		17	Lateral		5.8%	25.01					
		148	Longitudinal		19.8%	61.91					
		154	Longitudinal		54.2%	63.62					
		No mode in range -> Bridge OK									
200	10.0	1	Vertical		58.7%	2.74					
		2	Lateral		11.4%	4.88					
		6	Lateral		55.3%	5.62					
		62	Vertical		10.4%	15.35					
		123	Lateral		6.0%	22.60					
		464	Longitudinal		67.3%	60.59					
No mode in range -> Bridge OK											
250	2.5	1	Lateral	1 all	60.8%	1.11	TC2	CL1	0.147	0.142	
							TC3	CL2	0.232	0.225	
							TC4	CL3	0.562	0.546	
		2	Vertical	1 all	58.0%	1.98	TC2	CL1	2.463	0.060	
							TC3	CL2	3.895	0.096	
							TC4	CL3	9.435	0.232	
		5	Lateral		15.8%	5.26					
		7	Vertical		15.9%	9.38					
		9	Lateral		7.4%	11.73					
		19	Vertical		7.4%	21.33					
		172	Longitudinal		69.2%	54.02					
		No mode in range -> Bridge OK									
		250	5.0	1	Lateral		62.3%	2.06			
2	Vertical			1 all	59.1%	2.25	TC2	CL1	0.586	0.049	
							TC3	CL2	0.926	0.077	
							TC4	CL3	2.244	0.186	
5	Lateral				16.2%	9.33					
6	Vertical				15.5%	10.65					
16	Lateral				7.4%	18.02					
175	Longitudinal				57.5%	52.42					
177	Longitudinal		10.9%	52.73							

Length	Width	Mode no.	Direction	Shape	Mass part. (%)	Eigenfreq. (Hz)	Traffic Class	Confort Level	Vertical Accel. Max (m/s ²)	Lateral Accel. Max (m/s ²)
250	10.0	1	Vertical	1 all	60.2%	2.29	TC2	CL1	0.121	0.003
							TC3	CL2	0.191	0.040
							TC4	CL3	0.462	0.010
		2	Lateral		65.4%	3.67				
		55	Vertical		9.5%	13.21				
65	Lateral		16.3%	15.33						
375	Longitudinal		70.7%	49.54						
300	2.5	1	Lateral	1 all	61.3%	0.77	TC2	CL1	0.393	0.204
							TC3	CL2	0.622	0.322
							TC4	CL3	1.506	0.780
		2	Vertical	1 all	58.6%	1.60	TC2	CL1	1.281	0.088
							TC3	CL2	2.026	0.139
							TC4	CL3	4.907	0.336
		4	Lateral		15.8%	3.70				
		7	Vertical		15.7%	7.63				
		8	Lateral		6.8%	8.36				
		13	Lateral		4.6%	14.14				
		18	Vertical		7.3%	17.48				
167	Longitudinal		32.4%	44.70						
168	Longitudinal		38.5%	44.87						
300	5.0	1	Lateral		65.0%	1.41				
		2	Vertical	1 all	61.9%	1.70	TC2	CL1	1.490	0.052
							TC3	CL2	2.356	0.082
							TC4	CL3	5.707	0.200
		5	Lateral		15.3%	6.71				
		6	Vertical		14.9%	8.25				
		13	Lateral		5.0%	14.02				
		21	Lateral		4.9%	18.09				
		23	Vertical		5.3%	18.78				
153	Longitudinal		64.9%	42.79						
300 (No x-part considered)	10.0	1	Vertical	1 all	59.2%	1.96	TC2	CL1	1.531	0.035
							TC3	CL2	2.420	0.056
							TC4	CL3	5.863	0.135
		2	Lateral		64.1%	2.69				
		60	Lateral		9.7%	11.02				
		81	Lateral		5.6%	14.50				
		177	Vertical		5.2%	22.54				
		410	Longitudinal		21.8%	42.36				
411	Longitudinal		43.4%	42.41						

APPENDIX D Accelerations plots

